Using inhibitory precursor cell transplantation to investigate the role of inhibition in noise-induced pathology of the inferior colliculus

by

Maryanna Stephanie Owoc

BS, Worcester State University, 2014

Submitted to the Graduate Faculty of the

School of Medicine in partial fulfillment

of the requirements for the degree of

Doctor of Philosophy

University of Pittsburgh

2022

UNIVERSITY OF PITTSBURGH

SCHOOL OF MEDICINE

This dissertation was presented

by

Maryanna Stephanie Owoc

It was defended on

February 28, 2022

and approved by

Srivatsun Sadagopan, Ph.D., Assistant Professor, Dept of Neurobiology, Dept of Bioengineering, and Dept of Otolaryngology, University of Pittsburgh

Gerald Brandacher, M.D., Professor, Dept of Plastic and Reconstructive Surgery and Dept of Surgery, Johns Hopkins University

Sandra Kuhlman, Ph.D., Associate Professor, Dept of Biological Sciences and Dept of Biomedical Engineering, Carnegie Mellon University

Sarah Ross, Ph.D., Associate Professor, Dept of Neurobiology, University of Pittsburgh

Rebecca Seal, Ph.D., Associate Professor, Dept of Neurobiology, University of Pittsburgh

Dissertation Director: Karl Kandler, Ph.D., Professor, Dept of Neurobiology, Dept of Bioengineering, and Dept of Otolaryngology, University of Pittsburgh

Using inhibitory precursor cell transplantation to investigate the role of inhibition in noise-induced pathology of the inferior colliculus

Maryanna Stephanie Owoc, PhD

University of Pittsburgh, 2022

The inferior colliculus (IC) is a nexus of auditory processing in the midbrain, in that it receives and integrates ascending, descending, commissural, and multimodal inputs. As such, the IC has been implicated in refining the response to auditory stimulation and multimodal integration.

The IC consists of a central nucleus (CNIC) and surrounding cortex (CtxIC) – ascending inputs primarily innervate the CNIC, whereas descending and multimodal inputs target the CtxIC. The distinct nature of inputs to CNIC and CtxIC neurons predicts distinct response properties in these IC subdivisions. However, distinguishing neurons from the CNIC and CtxIC based on response properties alone has remained challenging. In chapter 2, using in-vivo electrophysiological recordings in anesthetized mice, we show that CNIC and CtxIC neurons exhibit small but significant differences in receptive field parameters. When combined using machine-learning models, we show that neural recordings can be localized to the CNIC or CtxIC solely based on response properties. The methods developed here would also allow us to better target interventions to functionally-defined IC regions and to characterize response properties in future experiments that employ the circuit manipulations outlined below.

Neural response properties in the IC arise from the convergence of excitatory and inhibitory inputs. Noise exposure can lead to decreased inhibition in the IC and has been implicated in the development of central auditory pathologies. In chapters 3 and 4 we investigate whether transplantation of inhibitory precursor cells derived from the medial ganglionic eminence (MGE)

can mitigate the effects of noise exposure. We found that transplanted MGE cells survive, migrate, and differentiate into primarily inhibitory neurons in the IC (chapter 3). Critically, we found that transplantation of MGE cells into the IC of noise-exposed mice mitigated the noise induced shifts in auditory function as measured by the acoustic startle response (chapter 4).

Our data provide the first evidence that local increases in inhibition may be useful in mitigating a behavioral effect of noise exposure. Future research using these techniques could provide insight into the mechanisms underlying the development of noise induced pathology and the response properties that contribute to auditory processing in the normal and pathologic states.

Table of Contents

List of Tables

List of Figures

Preface

The work presented herein is based on several manuscripts that are in preparation.

Chapter 2 is a modified version of:

Owoc, M., Johnson, A., Kandler, K., Sadagopan, S. (2022) Distinguishing between inferior colliculus central nucleus and cortex neurons based on spontaneous and sound-evoked response properties. *In preparation.*

Chapter 3 is a modified version of:

Owoc, M., Rubio, M., Brockway, B., Sadagopan, S., Kandler, K. (2022) Embryonic medial ganglionic eminence cells survive and integrate into the inferior colliculus of adult mice. *In preparation.*

Acknowledgements

This dissertation would not have been possible without the combined efforts and support of the people who helped me during my graduate training. First and foremost, I would like to thank my dissertation advisors, Drs. Karl Kandler and Srivatsun Sadagopan, who encouraged me to follow my ideas and where the data took me. Their support and patience gave me the freedom to explore my interests and helped me to grow as a scientist.

Next, I'd like to thank my committee members – Drs. Gerald Brandacher, Sandra Kuhlman, Sarah Ross, and Rebecca Seal, who took time out of their busy schedules to provide advice and encouragement throughout my training. Drs. Kuhlman, Ross, and Seal were a part of my advising team since the very beginning. Their thoughtful comments, suggestions, and support helped to shape my dissertation research into the final projects included here. I would also like to thank Dr. Seal for coordinating the collaboration with Dr. Basbaum, without which I would not have been able to perform the surgeries needed for these experiments. Finally, I'd like to thank Dr. Brandacher for serving as my external examiner and for providing his valuable insight as a surgeon scientist.

I would also like to thank all of the past and present members of the Kandler and Area 41 (Sadagopan) labs for their support, expertise, and friendship. I would especially like to thank all of our former lab techs, Hannah Roos, Anna Flynn, and Kacey Womeldorf who spent countless hours performing experiments, keeping the mouse colony in order, and always providing a sympathetic ear. I would also like to thank Brian Brockway, who's advice was critical for mouse breeding and developing the immunohistochemistry protocols necessary for these experiments.

Finally, I would like to thank my family and friends for their unwavering love and support during not only my graduate training, but throughout my entire MD/PhD journey. My Mom and Dad have always supported my scientific and medical interests, and without them I would not be where I am today. I would also like to thank my friends, who provided a shoulder to cry on, a family when mine was far away, and who made me laugh even when I thought I couldn't. To my pets – Tiana, who's steadfast companionship comforted me when nothing else could, Charlotte, who's love knows no bounds, and Potato, who bravely walked across my face every morning to make sure I was up on time, thank you. Lastly, I would like to thank my boyfriend Phil. I don't know what the probability of us meeting on a BST-3 elevator was, but I know it was significant.

1.0 General Introduction

1.1 Subdivisions of the inferior colliculus

The inferior colliculus (IC) is a major subcortical auditory integration center, receiving ascending input from most auditory brainstem nuclei (Frisina et al., 1998), commissural input from the contralateral IC (Chandrasekaran et al., 2013; Ito and Oliver, 2014; Malmierca et al., 2003, 1995; Rees and Orton, 2019; Saldaña and Merchán, 1992), descending input from the auditory cortex (Saldaña et al., 1996; Winer, 2006), and contains a vast intrinsic network (Ito and Oliver, 2014; Malmierca et al., 1995; Miller et al., 2005; Oliver et al., 1991; Saldaña and Merchán, 1992; Sturm et al., 2014, 2017; Wallace et al., 2012) (Figure 1). In addition to its role in auditory integration, the IC is a nexus for multimodal integration, receiving input from somatosensory and visual centers (Coleman and Clerici, 1987; Faye-Lund, 1985; Li and Mizuno, 1997; Wise and Jones, 1977). The IC is divided into the central nucleus of the IC (CNIC) and the cortex of the IC (CtxIC). Each of these subdivisions receives unique inputs and are expected to play a distinct role in auditory processing and integration.

The CNIC is the most well studied region of the IC. The CNIC receives exclusively auditory inputs (Aitkin et al., 1994), primarily ascending input from lower brainstem nuclei (Beyerl, 1978; Coleman and Clerici, 1987; Shneiderman et al., 1988), and is essential for normal hearing (Jenkins and Masterton, 1982). The primary source of inputs to the IC is from the superior olivary complex (SOC) and lateral lemniscus (LL); which receive their inputs from the cochlear nucleus (CN) (Cant, 2005). The projections from the SOC are mixed (Oliver et al., 1995) while the projections from the LL are largely inhibitory (Riquelme et al., 2001) (Figure 1). Additionally,

the CNIC receives direct input from all CN subdivisions and a variety of cell types, including fusiform cells in dorsal cochlear nucleus (DCN), round and oval cells in anteroventral cochlear nucleus (AVCN), and round, oval, fusiform, and multipolar cells in the posteroventral cochlear nucleus (PVCN) (Coleman and Clerici, 1987; Ryugo et al., 1981; Warr, 1972). Inputs from the CN to the CNIC are excitatory (Oliver, 1987) and account for the primary source of excitatory input to the IC (Oliver, 2005) (Figure 1). Input to the CNIC is therefore mixed, with excitatory inputs slightly outnumbering inhibitory ones (60% excitatory vs 40% inhibitory) (Oliver, 2005).

Less well studied is the CtxIC, which can be further divided into the lateral and dorsal cortices. The lateral cortex is a three layered structure that receives multimodal input from somatosensory, visual, and auditory centers (Coleman and Clerici, 1987; Faye-Lund, 1985; Li and Mizuno, 1997; Wise and Jones, 1977). Each layer of the lateral cortex receives distinct inputs. Auditory inputs from the CNIC and auditory cortex terminate in all three layers of the lateral cortex (Lesicko et al., 2016), however layer three, the deepest layer, also receives inputs from the CN (Brunso-Bechtold et al., 1981; Cant and Benson, 2003; Coleman and Clerici, 1987; Oliver et al., 1999, 1997). Projections from the CN to the lateral CtxIC are more restricted than those to the CNIC. The CtxIC receives inputs from fusiform cells in DCN and multipolar cells in PVCN (Coleman and Clerici, 1987). Layer two of the lateral cortex contains neurochemical modules which are the primary target of somatosensory inputs (Lesicko et al., 2016). Due to inconsistent parcellation of the layers of the lateral cortex between species and the tendency to combine observations from all three layers, it has been difficult to elucidate the role of the lateral cortex (Oliver, 2005). However, based on the diversity of inputs, it is clear that the lateral cortex has a role in multimodal integration (Oliver, 2005).

The dorsal cortex is the primary recipient of excitatory inputs from the auditory cortex and also receives both excitatory and inhibitory commissural inputs from the contralateral IC (Oliver, 2005) and ascending inputs from the CN and the dorsal nucleus of the LL (Coleman and Clerici, 1987; Druga et al., 1997; Druga and Syka, 1984; Faye-Lund, 1985). The dorsal cortex is a four layered structure, with layer three of the dorsal cortex continuous with the commissure of the IC (Oliver, 2005). While the boundary of the dorsal cortex can be identified anatomically using NADPH-diaphorase immunohistochemistry (Druga and Syka, 1993), identifying the transition from the CNIC to the dorsal cortex experimentally has remained challenging. Despite differences in the intrinsic properties of neurons in the dorsal cortex and CNIC (Y. Li et al., 1998; Smith, 1992), there appears to be no clear functional border between these regions (Oliver, 2005). However, given that the dorsal cortex is the primary target of auditory corticocollicular projections (Oliver, 2005), it is likely that the dorsal cortex plays a role in modulating ascending input.

In summary, the IC is a complex structure and nexus of auditory and multimodal integration in the midbrain. The extrinsic inputs to the IC broadly target different subdivisions, with ascending inputs primarily innervating the CNIC while descending and multimodal inputs primarily innervate the CtxIC. While the majority of research has focused on the ascending pathway and CNIC, the CtxIC has a pivotal role in multimodal integration and top-down modulation of activity in the IC through commissural and intrinsic connections.

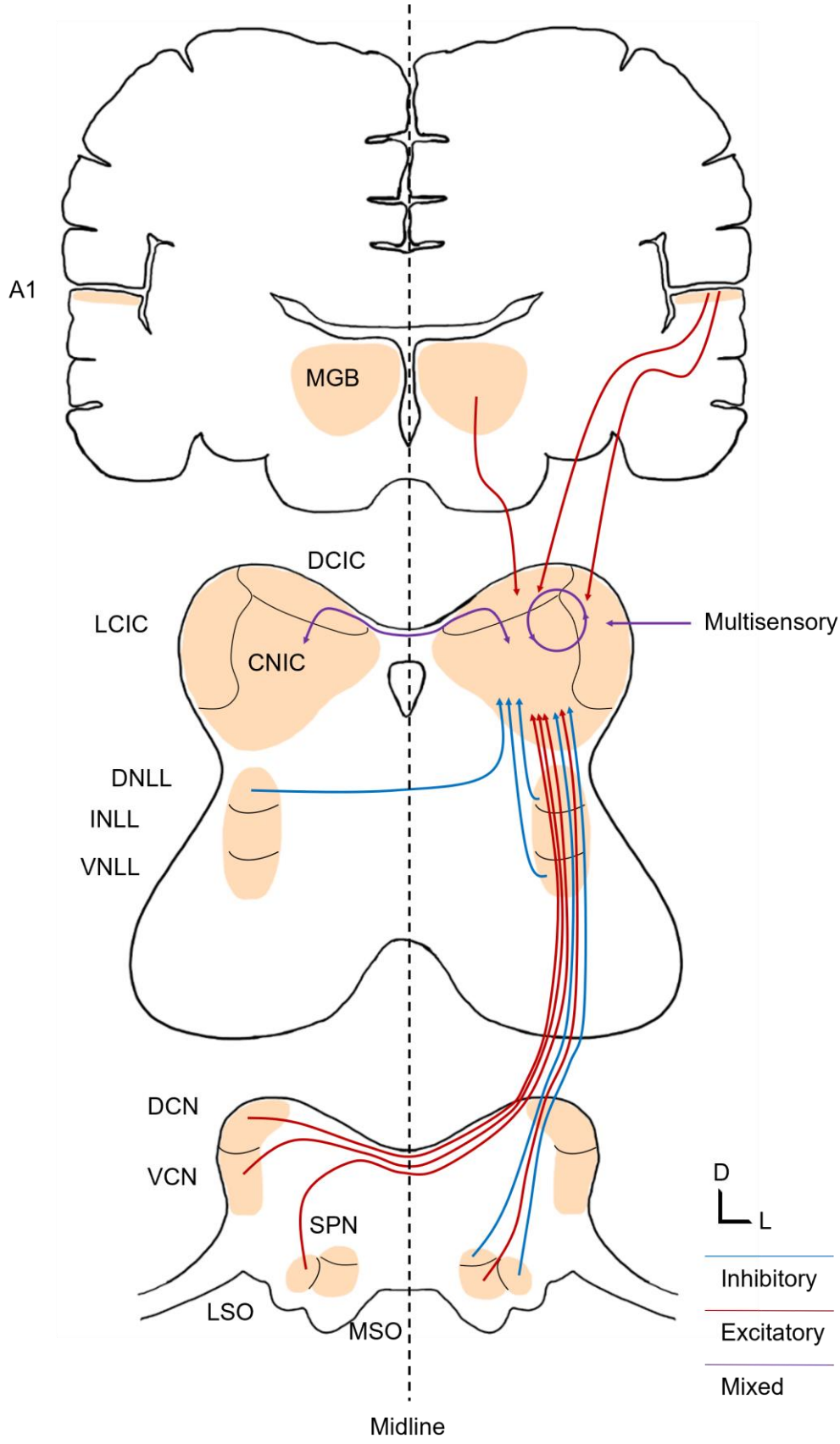
A1
MGB
DCIC
LCIC
CNIC
Multisensory
DNLL
INLL
VNLL
DCN
VCN
SPN
LSO
MSO
D
L
Inhibitory
Excitatory
Mixed
Midline

Figure 1. The subdivisions of the inferior colliculus receive inputs from distinct sources.

The central nucleus of the inferior colliculus (CNIC) is the primary target of ascending auditory projections. Contralateral excitatory inputs (red) arise from the dorsal and lateral cochlear nucleus (DCN and LCN, respectively) and the lateral superior olive (LSO). Contralateral inhibitory inputs (blue) arise from the contralateral dorsal nucleus of the lateral lemniscus (DNLL). Ipsilateral excitatory inputs arise from the medial superior olive (MSO). Ipsilateral inhibitory inputs arise from the superior paraolivary nucleus (SPN), the LSO, DNLL, and ventral nucleus of the lateral lemniscus (VNLL).

The dorsal cortex of the IC is the primary target of excitatory projections from the auditory cortex (A1) and medial geniculate body (MGB).

The lateral cortex of the IC is the primary target of multisensory inputs and receives input from A1.

All three subdivisions interact via intrinsic connections (mixed, purple).

The bilateral IC interact via commissural connections that primarily arise from the CNIC and dorsal cortex (mixed).

Inputs to only one IC are shown for simplicity, orientation is such that dorsal (D) is up and lateral (L) is to the left and right of midline (dashed line).

1.2 Commissural and intrinsic connections in the IC

The majority of IC synapses are actually derived from commissural and intrinsic connections (Saldaña and Merchán, 1992). The rat IC contains an astonishing 350,000 neurons, five times that of any auditory subcollicular nuclei or the medial geniculate body of the thalamus (Kulesza et al., 2002). Almost all of the neurons in the IC form intrinsic connections, suggesting that the extensive processing and integration that occurs in the IC is largely the result of these monosynaptic intracollicular connections (Saldana and Merchan, 2005).

The cytoarchitecture of the IC is most well studied in the CNIC. Neurons of the CNIC have been categorized into disc and stellate shaped (Malmierca et al., 1993; Meininger et al., 1986;

Oliver et al., 1991; Oliver and Morest, 1984). Disc shape neurons have flat dendritic trees that are parallel to each other and their axons, forming fibrodendritic laminae (Oliver et al., 1991). Stellate shaped neurons have dendritic trees that are unoriented or are oriented orthogonal to the fibrodendritic lamina, their axons can cross several laminae and contain thousands of terminal boutons (Oliver et al., 1991). Thus, disc shaped neurons are likely to influence the activity of neurons within their own fibrodendritic lamina while stellate cells have the potential to influence the activity in neurons across laminae. Both cell types are believed to contribute to the extensive intrinsic networks (Saldana and Merchan, 2005). Most commissural connections, however, appear to be derived from stellate cells (Saldana and Merchan, 2005).

The disc and stellate cells contributing to the vast intrinsic and commissural network of the IC are heterogenous in both form and distribution (Saldana and Merchan, 2005). Indeed, both excitatory (glutamatergic) and inhibitory (GABAergic) neurons contribute to intrinsic and commissural connections in the IC (Ito et al., 2009; Ono et al., 2005; Sturm et al., 2017). Intrinsic connections are found in all IC subdivisions (Saldana and Merchan, 2005) while the CNIC and dorsal cortex of the IC account for an extensive portion of the projections to the commissure (Rees and Orton, 2019) (Figure 1). Most IC neurons that form commissural inputs also have local collaterals (Saldana and Merchan, 2005), suggesting that they can modify activity in both the ipsilateral and contralateral IC.

Approximately 20-30% of IC neurons are GABAergic (Ito et al., 2018; Merchán et al., 2005; Oliver et al., 1994). GABAergic cells of the IC have been subdivided based on their synaptic organization and projection targets (Beebe et al., 2016; Foster et al., 2014; Ito et al., 2018) and their electrophysiological response properties (Sturm et al., 2017). Large GABAergic neurons (LG) possess the largest cell bodies in the IC and receive dense VGLUT-2 positive axosomatic

synapses (Ito et al., 2018). Conversely, small GABAergic (SG) neurons are similar in size to glutamatergic neurons in the IC (Ito et al., 2018). These categories are further classified based on the presence of perineuronal nets (Beebe et al., 2016; Foster et al., 2014; Ito et al., 2018), which stabilize synapses and inhibit structural plasticity (Karetko and Skangiel-Kramska, 2009; Morawski et al., 2012). Perineuronal nets have been found primarily surrounding most, but not all LG neurons (Ito et al., 2018). Additionally, GABAergic neurons in the IC can be discriminated based on their excitatory and inhibitory input maps (Sturm et al., 2017). Type 1 GABAergic neurons receive both excitatory and inhibitory inputs, with a slight bias towards inhibitory inputs; while Type 2 GABAergic neurons receive primarily excitatory inputs (Sturm et al., 2017). It has been suggested that Type 1 and 2 GABAergic neurons correspond to SG and LG neurons, respectively (Sturm et al., 2017).

The heterogenous nature of intrinsic and commissural connections suggests multiple roles in sound processing and integration, including binaural integration and regulating top-down modulation. Indeed, CNIC neurons that contribute to the commissure may also receive ascending input from the lateral lemniscus (Moore et al., 1998; Reetz and Ehret, 1999), suggesting a role in binaural hearing cues such as interaural level and time differences, which are important in sound localization. Furthermore, the auditory cortex and medial geniculate body of the thalamus modulate IC activity through direct synapses onto IC neurons and indirectly via intracollicular connections (Patel et al., 2017; Saldana and Merchan, 2005; Winer, 2005; Winer et al., 2002). Corticofugal projections are largely excitatory (Feliciano and Potashner, 1995; Saldana and Merchan, 2005; Winer, 2005) and are tonotopically matched (i.e. project to neurons with a similar best frequency) (Andersen et al., 1980; Saldaña et al., 1996; Saldana and Merchan, 2005). As such, corticofugal activity would be expected to lead to facilitation. However, both facilitation and

inhibition have been observed following corticofugal activation (Saldana and Merchan, 2005; Suga et al., 2000). Corticofugal mediated facilitation appears to be highly focused and targets tonotopically matched IC neurons (Zhang and Suga, 1997). Conversely, corticofugal mediated inhibition appears to be more widespread and effects unmatched IC neurons (Zhang and Suga, 1997). The inhibitory effects of corticofugal activation likely result from the activation of intrinsic circuits. Thus, the intrinsic and commissural connections in the IC are important in shaping responses within the IC as well as regulating and modulating the effects of extrinsic inputs to the IC.

Intrinsic and commissural connections within the IC are also crucial to the structure and organization of the IC (Saldana and Merchan, 2005). The IC is organized along several factors, including best frequency (i.e. tonotopy), onset latency, and periodicity (Biebel and Langner, 2002; Hattori and Suga, 1997; Schreiner and Langner, 1988; Walton et al., 1998). This organization results from the cumulative effects of the cytoarchitecture of the IC, lemniscal projections, and the intrinsic and commissural connections. Intrinsic and commissural connections are critical for the formation of the fibrocellular laminae of the IC (Saldana and Merchan, 2005) and may increase specificity by forming excitatory connections with neurons with similar response properties in the same, or contra, region, and inhibitory connections with those with different response preferences. The most prominent and well-studied of these topographic organizations is tonotopy.

1.3 Tonotopic organization of the inferior colliculus

A defining feature of the auditory system is that the nuclei are organized according to best frequency, or tonotopy. This feature originates in the cochlea, where spectral decomposition of

acoustic stimuli occurs. The location of basilar membrane motion provides information regarding the frequency composition of the stimuli, a phenomenon known as place coding (Zwislocki and Nguyen, 1999), and provides the foundation for tonotopy in central auditory structures. Extrinsic inputs to the IC are topographically matched (Andersen et al., 1980; Oliver and Morest, 1984; Saldaña et al., 1996; Saldana and Merchan, 2005; Stiebler and Ehret, 1985), preserving the tonotopic relationship which is then reinforced and shaped by inhibitory inputs (Egorova et al., 2001).

Each fibrodendritic lamina of the IC contains neurons who share a similar best frequency, creating an isofrequency band (Oliver and Morest, 1984; Stiebler and Ehret, 1985). The isofrequency axis (i.e. the direction along which neurons share a similar best frequency) is orthogonal to the tonotopic axis of the IC (Steibler 1985, Romand 1990). The tonotopic axis of the IC is organized such that low frequencies are represented dorsolaterally and high frequencies ventromedially (Stiebler and Ehret, 1985).

This tonotopic organization is preserved across the boundaries between the CNIC and DCIC (Stiebler and Ehret, 1985). While discontinuities in the tonotopic bands of the CNIC and LCIC have been reported (Stiebler and Ehret, 1985), it appears that the tonotopic organization of the ventral portion of the LCIC is actually a reflection of that in the IC, albeit one that runs nearly perpendicular to the tonotopic axis in the CNIC (Loftus et al., 2008) (Figure 2). Thus, electrophysiological recordings in the LCIC demonstrate a similar progression of best frequencies (with low frequencies dorsal and high frequencies ventral). This is unique from other auditory nuclei, where tonotopy is reversed at the boundary, and allowing for electrophysiological identification of the boundary (e.g. auditory cortex) (Guo et al., 2012). As a result of its continuous

tonotopic organization, distinguishing the CNIC from the CtxIC based on electrophysiological response properties has remained challenging.

The studies that have attempted to identify differences in the response properties of neurons in the CNIC and CtxIC have largely been in the anesthetized cat (Aitkin et al., 1994, 1981, 1978). These studies demonstrate that neurons in the CNIC have sharper frequency tuning, lower thresholds, shorter onset latencies, and may prefer simple stimuli (Aitkin et al., 1994, 1981, 1978). While a few studies have characterized the response properties of neurons in the CNIC and CtxIC of the mouse using two-photon calcium imaging (Barnstedt et al., 2015; Wong and Borst, 2019), the majority of the research has focused on the CNIC (Egorova et al., 2006, 2001, 2020; Lee et al., 2019) or evaluated the combined response properties the IC, disregarding the location of the recording (Galazyuk et al., 2017; Ono and Oliver, 2014; Portfors and Felix, 2005; Tan et al., 2007; Walton et al., 1997). Given the distinct sources of inputs to the CNIC and CtxIC, it is likely that these neurons have a unique role in auditory processing and thus may exhibit different response properties. The genetic tractability of the mouse has made it one of the most commonly used models for auditory neuroscience. Understanding the differences in the response properties of these neurons may further our understanding of their role in auditory processing under normal and pathologic conditions. In chapter 2 we aim to characterize the response properties of neurons in the CNIC and CtxIC and determine whether we can train machine learning algorithms to reliably classify neurons as CNIC or CtxIC.

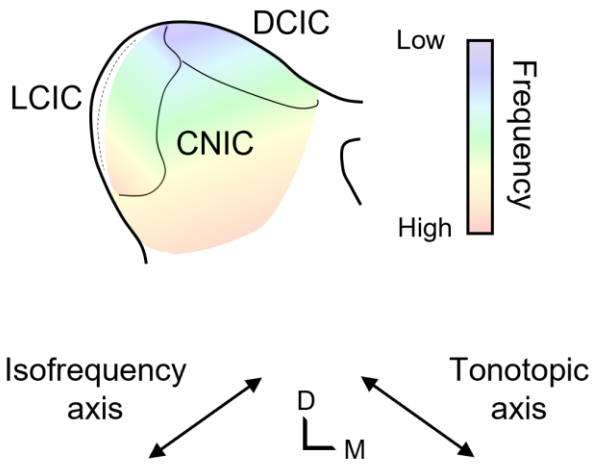

Figure 2. Tonotopic organization of the inferior colliculus

The inferior colliculus is organized according to best frequency, or tonotopically. Neurons that share a similar best frequency form an isofrequency band. The tonotopic axis runs orthogonal to the isofrequency axis, with low frequencies (purple) represented dorsolaterally and high frequencies (red) ventromedially. This organization is continuous across the boundaries separating the central nucleus of the IC (CNIC) from the dorsal and lateral cortices (DCIC and LCIC, respectively).

In this schematic, frequencies are represented as a color gradient with high frequencies red and low frequencies purple. The schematic is oriented such that dorsal is up and medial is to the left.

1.4 Efferent projections from the IC

In addition to shaping auditory information through commissural and intrinsic connections, the IC plays a role in modulating auditory processing at lower brainstem nuclei via efferent inputs. Indeed, the IC has efferent projections to nearly every nucleus that projects to it, including the dorsal nucleus of the LL, the SOC, and the CN (Figure 3) (Thompson, 2005). Thus, the IC has an important role in shaping ascending auditory information through direct and indirect feedback loops.

The most well studied of these descending projections is from the CNIC to the dorsal CN (Thompson, 2005). The CNIC and dorsal CtxIC are the primary source of IC projections to the dorsal CN (Caicedo and Herbert, 1993; Schofield, 2001). These projections are bilateral, with a preference for the ipsilateral CN (Caicedo and Herbert, 1993; Kane and Conlee, 1979; Schofield, 2001), and are likely mixed, with at least one inhibitory component (Thompson, 2005). Projections from the IC target several cell types in the CN, including granule cells, fusiform cells, and giant cells. Granule cells are the target of both auditory and non-auditory inputs, making them an important site of integration for multi-modal inputs. In addition to efferent projections from the IC, granule cells receive auditory input from the auditory cortex, medial olivocochlear (MOC) neurons, and auditory nerve fibers (Thompson, 2005). Non-auditory inputs arise from the vestibular and somatosensory systems (Wright and Ryugo, 1996), pontine gray (Ohlrogge et al., 2001), and the brainstem serotonergic system (Hurley and Thompson, 2001). Thus, the IC modulates the multimodal processing that occurs in CN neurons. Projections from the IC to fusiform and giant cells of the dorsal CN create a direct feedback loop, as these cell types project to the contralateral IC (Thompson, 2005).

Efferent projections from the IC are also involved in shaping auditory input at the level of the cochlea through modulation of basilar membrane motion and auditory nerve sensitivity via the MOC reflex (Guinan, 2006). Efferent projections from the IC to the SOC primarily target the periolivary regions which contain the MOC neurons (Warr, 1980). The MOC neurons in turn make cholinergic synapses onto outer hair cells in the contralateral cochlea (Art et al., 1984; Goutman et al., 2015; Guinan, 2006; Rasmussen, 1953). Projections from the IC to MOC neurons are glutamatergic (Saint Marie, 1996). Thus, increased MOC activity leads to decreased outer hair cell activity, the net effect of which is decreased basilar membrane motion and decreased auditory

nerve sensitivity (Guinan, 2006). Since the primary source of incoming auditory information to the IC originates in the contralateral cochlea, the ICs influence on MOC cells creates an indirect feedback loop in which the IC can modulate the incoming acoustic information.

Efferent projections from the IC are thus another way in which the IC modulates and shapes acoustic information. As such, it is unsurprising that the IC plays a fundamental role in a variety of tasks, including sound localization (Wenstrup et al., 1986), temporal processing (Turner et al., 2006), and sensorimotor gating (Koch and Schnitzler, 1997; L. Li et al., 1998).

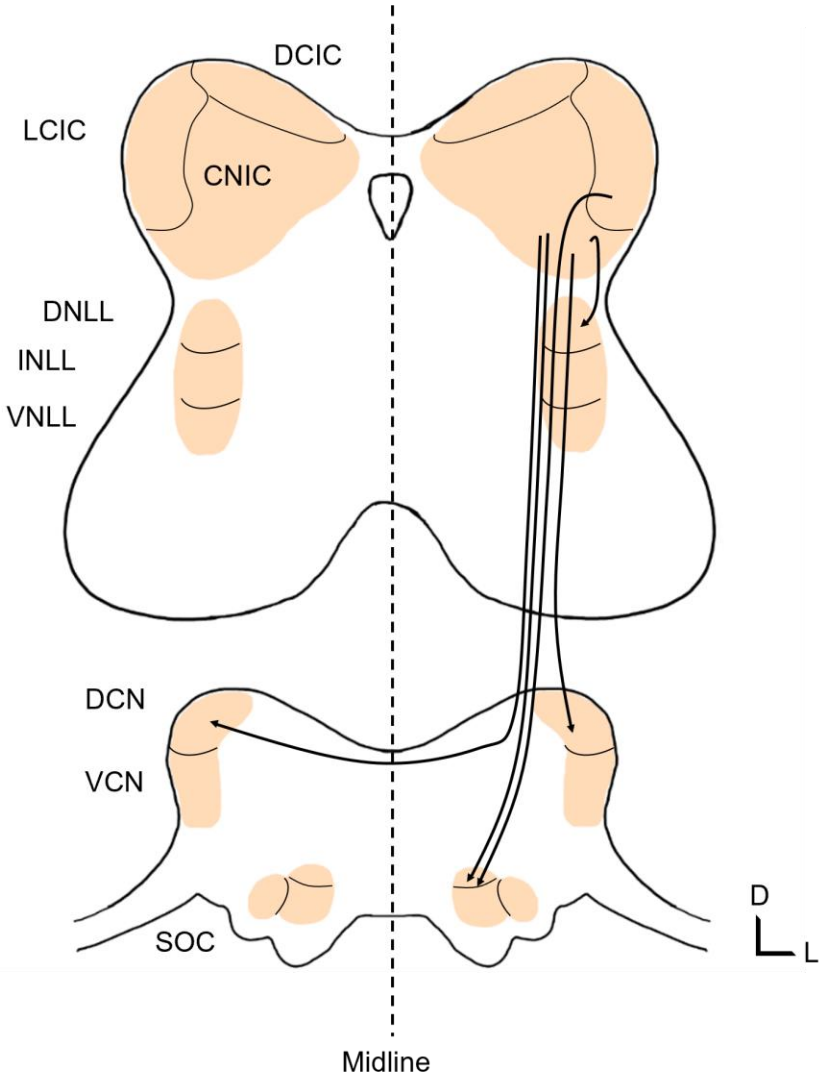

Figure 3. Efferent projections from the inferior colliculus

The central nucleus of the inferior colliculus (CNIC) has efferent projections that target the dorsal nucleus of the lateral lemniscus (DNLL) ipsilaterally, the dorsal cochlear nucleus (DCN) bilaterally, and the superior olivary complex (SOC) ipsilaterally.

The dorsal cortex has efferent projections that target the ipsilateral SOC.

Inputs to only one IC are shown for simplicity, orientation is such that dorsal (D) is up and lateral (L) is to the left and right of midline (dashed line).

1.5 The role of inhibition shaping in shaping IC response properties

The convergence of inputs to the IC leads to the development of *de novo* response properties as well as the refinement of response properties inherited from lower nuclei (Pollak et al., 2011). Extrinsic inputs to the IC arise from excitatory (glutamatergic) and inhibitory (either GABAergic or glycinergic) sources. Similarly, intrinsic and commissural connections in the IC are also mixed (glutamatergic and GABAergic). Thus, the electrophysiological response properties of neurons in the IC result from the interaction of excitatory and inhibitory inputs. However, the dominant influence appears to be inhibition. Indeed, blocking inhibition in the CNIC alters the response properties of these neurons to simple and complex stimuli and appears to be critical in shaping their tuning curves and increasing specificity in the CNIC (Pollak et al., 2011).

The frequency response areas of IC neurons have been characterized using the two-tone inhibition paradigm, which utilizes simultaneous presentation of both the characteristic frequency of the neuron as well as a second tone of variable frequency (Egorova et al., 2001). Two-tone stimuli revealed inhibitory receptive fields in every neuron that was recorded from, with inhibitory receptive fields flanking the excitatory field in almost all neurons (82%) (Egorova et al., 2001). Consistent with this, blocking inhibition in the IC has been shown to increase frequency tuning bandwidth (LeBeau et al., 2001; Peggy Shadduck Palombi and Caspary, 1996; Xie et al., 2005; Yang et al., 1992). Together, these finding suggests that inhibitory inputs onto CNIC neurons arise from a broader spectral range than that of excitatory inputs (Egorova et al., 2001; LeBeau et al., 2001; Peggy S. Palombi and Caspary, 1996; Xie et al., 2005; Yang et al., 1992). Since extrinsic inputs map to tonotopically matched regions within the IC, this inhibitory shaping may arise from the inhibitory intrinsic connections in the IC. Consistent with this, the developmental refinement of intrinsic input maps results in an inhibitory input map that is overlapping, but larger than the

excitatory input map (Sturm et al., 2014). Thus, intrinsic inhibitory inputs are believed to have a critical role in shaping the receptive fields of neurons in the IC.

Selectivity in the CNIC, however, extends beyond the frequency receptive field. Indeed, neurons within an isofrequency laminae can be separated into "functional zones" with distinct binaural response properties and periodicity preferences (Loftus et al., 2010; Schreiner and Langner, 1988; Wenstrup et al., 1986). Like tonotopy, the response properties of neurons within a functional zone are likely inherited from their extrinsic inputs and shaped by intrinsic and commissural connections within the IC. Consistent with this, ascending projections to the IC terminate within functional zones of an isofrequency band according to their input source (Aitkin and Schuck, 1985; Loftus et al., 2004; Maffi and Aitkin, 1987; Oliver et al., 1997; Shneiderman and Henkel, 1987) and blocking inhibition locally decreases neural selectivity (Pollak et al., 2011).

This functional organization is believed to contribute to call type selectivity. For example, some neurons will respond to a particular call while other neurons are unresponsive, despite the call containing energy in the frequency response profile of the unresponsive neuron (Klug et al., 2002; Pollak et al., 2011; Xie et al., 2005). The selectivity of these neurons is believed to be the result of inhibition, as blocking inhibition leads to decreased selectivity (Klug et al., 2002; Pollak et al., 2011; Xie et al., 2005). Frequency modulated sweeps within a call are likely one of the features accounting for neural selectivity in the IC (Pollak et al., 2011). Blocking inhibition abolishes directional selectivity in CNIC neurons suggesting that inhibition plays an important role in shaping the response (Andoni et al., 2007; Fuzessery and Hall, 1996; Pollak et al., 2011).

Spectro-temporal receptive fields (STRFs) have been used in an attempt to understand the relationship between the spectral (i.e. frequency) and temporal response of CNIC neurons (Andoni et al., 2007; Brimijoin and O'Neill, 2005; Chen et al., 2012). The majority of IC neurons however

appear to integrate inputs in a non-linear fashion, meaning that their response to complex sounds such as FM sweeps is not merely a sum of the response to each component frequency (Andoni et al., 2007; Brimijoin and O'Neill, 2005; Pollak et al., 2011). Most of this research, however, has been done in bats and there is evidence that neurons in the IC may be preferentially selective for sweeps most relevant to species specific communication (Pollak et al., 2011). Thus, these findings might be applicable to humans but difficult to study in less vocally communicative animal models, such as rodents. However, the neural mechanisms underlying processing of complex sounds in the IC of rodents appears to be similar to those found in the bat (Portfors and Felix, 2005). Thus, inhibition appears to be critical in the response profile of neurons to both simple and complex stimuli across mammalian species.

Auditory perception, however, relies on more than frequency coding. Temporal cues provide important stimulus information and contribute to auditory processing, including pitch perception, sound localization, and speech discrimination (Rees and Langner, 2005). These tasks rely on reliable encoding of stimulus onset and offset as well as the sound envelope (Rees and Langner, 2005). The temporal response profiles of IC neurons are encoded through several mechanisms, including the response pattern and periodicity preferences.

Broadly speaking, response patterns in the IC can be characterized as onset, sustained, and offset responses (Berger et al., 2014; Rees and Langner, 2005). The response type of neurons in the IC is not fixed and can vary with stimulus frequency and level (Rees and Langner, 2005). One mechanism by which response type is mediated is through inhibition. Response patterns appear to be shaped by inhibitory currents that precede excitatory ones (Covey et al., 1996; Nelson and Erulkar, 1963; Pedemonte et al., 1997; Rees and Langner, 2005). Blocking this inhibition leads to increases in the firing rate and can result in changes in the response pattern, most frequently toward

a sustained response type (Le Beau et al., 1996). Noise exposure, which is also known to lead to hyper-excitable response properties (Berger et al., 2014; Coomber et al., 2014; Longenecker and Galazyuk, 2016; Ma et al., 2006; Mulders and Robertson, 2013, 2009), has also been shown to affect the distribution of response patterns. Interestingly, noise exposure increases the number of onset responders (Berger et al., 2014). These differences could be the result of methodological differences, or they could represent the effects of variable degrees of decreased inhibition on response patterns. Regardless, inhibition plays an important role in mediating neural response type.

Periodicity coding in the IC occurs through two mechanisms: temporal synchronization to the stimulus envelope (temporal modulation) and rate modulation (increasing firing rate for preferred modulation frequencies) (Goldberg and Brown, 1969; Langner and Schreiner, 1988; Liang et al., 2002). Temporal modulation appears to be the preferred method for lower modulation frequencies while rate modulation encodes information at higher modulation frequencies (Rees and Langner, 2005). Periodicity coding can arise from monaural and binaural inputs and are organized into a periodic map that is orthogonal to the tonotopic map (Schreiner and Langner, 1988). Monaural periodicity cues are important in speech discrimination. Neural selectivity for directionally oriented changes in amplitude modulated tones and duration tuning emerges in the IC (Rees and Langner, 2005). Inhibitory inputs are believed to play a critical role in the generation and spatial representation of these response properties (Rees and Langner, 2005). Binaural cues, such as interaural timing differences (ITD), contribute to sound localization. The neural basis of envelope ITD encoding begins with the auditory nerve, which is well synchronized to sounds in our AM range (Joris et al., 2004). In the IC, neurons that are sensitive to ITD show changes in their firing rate based on whether the contralateral envelope precedes or follows the ipsilateral envelope (Ono et al., 2020). The lateral SOC receives binaural inputs and it is likely that the

interaction of excitatory and inhibitory inputs here contributes to ITD sensitivity in IC neurons (Ono et al., 2020).

Neural response properties in the IC arise from the convergence of excitatory and inhibitory inputs from ascending, descending, intrinsic, and commissural sources. The net effect of these inputs, however, appears to be inhibitory. Loss of inhibition in the IC leads to decreased specificity for spectral and temporal cues. As a result, any change in the excitatory and inhibitory balance of the IC could have a detrimental effect on auditory processing.

1.6 The effects of hearing loss on the IC

Noise exposure can lead to permanent or temporary auditory threshold shifts. Permanent threshold shifts are believed to result from the loss of inner hair cells (Liberman and Dodds, 1984; Lim, 1976) while temporary threshold shifts result from the loss of afferent nerve terminals and delayed degeneration of the auditory nerve fibers (Kujawa and Liberman, 2009). The basal cochlea is particularly vulnerable to acoustic trauma, leading to a preferential loss of high frequency inputs (Lim, 1976). The resulting imbalance in afferent inputs leads to plasticity in central auditory structures, including the IC, and changes the response properties of neurons in response to lower frequency sounds (Willott, 2005).

Changes in the response properties of IC neurons following noise exposure are time dependent. Immediately following noise exposure, the spontaneous firing rates of neurons in the IC are unchanged (Dong et al., 2010; Gröschel et al., 2014; Palmer and Berger, 2018; Wang et al., 1996) or, in some cases, decreased (Niu et al., 2013; Palmer and Berger, 2018). Significant increases in spontaneous firing rates are evident across a board range of frequencies by twelve

hours post noise exposure (Mulders and Robertson, 2013). Over time, however, increases in the spontaneous firing rate are most prevalent in the tonotopic regions that correspond to the region of hearing loss (Manzoor et al., 2013; Mulders and Robertson, 2013; Vogler et al., 2014). While the exact time course of circuit changes in the IC is debated (likely due to methodologic differences), it is clear that the IC experiences both short- and long-term changes following noise exposure (Palmer and Berger, 2018). Currently, it is thought that the immediate changes observed in the IC following noise exposure are due to loss of peripheral input (Salvi et al., 2000). Consistent with this, cochlear ablation or severing the auditory nerve soon after acoustic trauma prevents the formation of hyper-excitable activity patterns in higher auditory structures, including the IC (Mulders and Robertson, 2009). However, this approach is unsuccessful at later time points (Mulders and Robertson, 2011), suggesting that while circuit reorganization following noise exposure may initially depend on peripheral input it is, in the long-term, maintained intrinsically.

The long-term sequelae of hearing loss are summarized by the central gain model. The central gain model hypothesizes that noise exposure reduces neural activity at the level of the auditory nerve while paradoxically increasing spontaneous and sound evoked responses in the midbrain, thalamus, and auditory cortex (Asokan et al., 2018; Auerbach et al., 2019, 2014; Mulders and Robertson, 2009). Interestingly, increased excitation in these central auditory structures has been observed with and without concomitant hearing loss, suggesting that both temporary and permanent threshold shifts may lead to circuit reorganization in higher auditory structures. Thus, even in the absence auditory threshold shifts, noise exposure may have a significant effect on auditory processing.

Consistent with the central gain model, neurons in the IC demonstrate hyper-excitable response properties following noise exposure. These include: increased spontaneous firing rates

(SFRs) and bursting activity (Berger et al., 2014; Coomber et al., 2014; Longenecker and Galazyuk, 2016; Ma et al., 2006; Mulders and Robertson, 2013, 2009), increased tuning broadness (Ma et al., 2006), and increased neural gap detection thresholds (Berger et al., 2014). Hyper-excitable response properties in the IC following hearing loss are believed to be the result of decreased GABAergic signaling (Bledsoe et al., 1995; Dong et al., 2009; Milbrandt et al., 2000; Mossop et al., 2000; Sturm et al., 2017). Given the extensive and varied inputs to the IC, long-term changes in the response properties of IC neurons are likely mediated by changes in the response properties of both extrinsic inputs as well as reorganization of local IC circuits.

Synaptic reorganization of local IC circuits has been observed following mild hearing loss and affects both excitatory and inhibitory neurons (Sturm et al., 2017). Interestingly, the resulting reorganization appears to be variable and correlated with gap detection deficits (Sturm et al., 2017), which are commonly used as an indicator of tinnitus in animal models (Berger et al., 2014; Chen et al., 2013; Hayes et al., 2014; Sturm et al., 2017; Turner et al., 2006). In animals without gap detection deficits, synaptic reorganization is observed but the net excitatory/inhibitory balance is maintained at a level similar to that of control subjects (Sturm et al., 2017). In animals with gap detection deficits however, synaptic reorganization led to a net increase in excitation, primarily due to the loss of excitatory inputs onto type 1 GABAergic neurons, which are believed to correspond to local GABAergic neurons (Sturm et al., 2017). Given that hyperexcitable response properties of IC neurons have been identified in animals with and without tinnitus (Berger et al., 2014; Coomber et al., 2014), the finding that synaptic reorganization varies between these two populations could suggest that hyperexcitable response properties in non-tinnitus animals may be the result of extrinsic increases in excitation while tinnitus animals experience both extrinsic and intrinsic increases in excitation.

The central gain model may also explain the presence of auditory processing deficits in patients with clinically normal hearing thresholds, such as difficulty understanding speech in noise (Grant et al., 2021). Indeed, recent research in gerbils suggests that even in the absence of auditory threshold shifts, noise exposure can degrade the neural representation of speech in background noise in the IC at high sound levels (Monaghan et al., 2020). Interestingly, the neural representation was improved at moderate sound levels (Monaghan et al., 2020). A model that combined damage to high-threshold auditory nerve fibers with increased central auditory gain reproduced these electrophysiological findings (Monaghan et al., 2020). These findings are consistent with the central gain model and implicate the combined effects of peripheral damage and central gain in auditory processing deficits in the setting of normal auditory thresholds following noise exposure.

The loss of peripheral input leads to changes in the spontaneous and sound evoked activity of central auditory neurons and circuit reorganization. Even in the absence of auditory threshold shifts, auditory processing deficits related to acoustic overexposure can occur, suggesting subtle but clinically significant changes in hearing (Grant et al., 2021; Gu et al., 2010; Roberts et al., 2010; Weisz et al., 2006). The finding that the degree and type of synaptic reorganization varies between animals with and without gap detection deficits suggests that local changes in the IC may be responsible, at least in part, for the generation and maintenance of noise induced pathology.

1.7 Clinical consequences of noise exposure: Tinnitus and hyperacusis

Exposure to dangerously loud sounds is an unfortunately common occurrence that can lead to not only hearing loss, but also pathologies such as tinnitus (Coomber et al., 2014; Middleton et al., 2011; Sturm et al., 2017; Wang et al., 2009; Yang et al., 2011) and hyperacusis (Knipper et al.,

2013; Manohar et al., 2017). Tinnitus, often described as “ringing in the ears,” and hyperacusis, increased sound sensitivity and decreased sound level tolerance, have been reported by patients with (Aazh and Moore, 2018; König et al., 2006; Sheldrake et al., 2015) and without (Aazh and Moore, 2018; Gu et al., 2010; Schaette and McAlpine, 2011; Sheldrake et al., 2015) concomitant hearing loss. Even in the absence of hearing loss, these symptoms can have a detrimental effect on quality of life (Ayodele et al., 2020; Bartels et al., 2008; Reynolds et al., 2004; Weidt et al., 2016). Interestingly, many patients co-report tinnitus and hyperacusis, suggesting a common etiology (Aazh and Moore, 2018; Cederroth et al., 2020; Fournier and Hébert, 2013; Katzenell and Segal, 2001; Schecklmann et al., 2014).

Despite ongoing research efforts, the etiology of tinnitus and hyperacusis remains unknown. While originally thought to originate within the cochlea, the finding that cochlear or auditory nerve ablation does not resolve tinnitus symptoms points to a central mechanism in the development and maintenance of tinnitus (Soleymani et al., 2011; Zacharek et al., 2002). Consistent with this, there is evidence that hyper-excitability in central auditory structures, including the IC, may contribute to the subtle changes in auditory processing and mediate the development of tinnitus an hyperacusis (Auerbach et al., 2019; Coomber et al., 2014; Ma et al., 2006; Middleton et al., 2011; Mulders and Robertson, 2013, 2009; Pedemonte et al., 1997; Resnik and Polley, 2017; Richardson et al., 2012; Sturm et al., 2017; Wang et al., 2009; Yang et al., 2011). As a result, researchers have turned to behavioral models to better understand the relationship between hyper-excitable response properties in central auditory centers and the perceptual experience of tinnitus and hyperacusis.

1.8 The acoustic startle response

The subjective nature of tinnitus and hyperacusis makes them difficult to study in animal models. As a result, much work has been done to create behavioral methods to identify these pathologies (Hayes et al., 2014). Behavioral methods to determine whether an animal is experiencing tinnitus and/or hyperacusis have relied on operant conditioning tasks and, more recently, the acoustic startle response (ASR) (Hayes et al., 2014). Unlike operant conditioning tasks, the ASR is an innate reflexive response to loud sounds (Davis et al., 1982; Yeomans et al., 2002), and thus requires no training. Additionally, since there is no risk of extinction of the behavior, the ASR can be repeated over long durations. The advantages of the ASR have made it one of the most popular behavioral paradigms for tinnitus and hyperacusis (Hayes et al., 2014).

The ASR became a viable tool for studying tinnitus when it was discovered that a silent gap inserted in a continuous background sound suppresses the ASR in naïve mice, but fails to do so in a subset of noise exposed animals (Turner et al., 2006). Animals with gap detection deficits (i.e. who do not experience gap induced inhibition of the ASR) are believed to have tinnitus based on the assumption that the tinnitus percept fills the silent gap (Turner et al., 2006). In support of this hypothesis, the emergence of hyper-excitable response properties of neurons in the IC following noise exposure is associated with the development of gap-detection deficits (Berger et al., 2014; Chen et al., 2013; Hayes et al., 2014; Sturm et al., 2017; Turner et al., 2006). As a result, gap detection tasks have become an attractive model to identify tinnitus in animal models (Berger et al., 2014; Chen et al., 2013; Hayes et al., 2014; Sturm et al., 2017; Turner et al., 2006). However, the absence of gap detection deficits in human subjects (Campolo et al., 2013) has led to some debate as to whether gap detection deficits in animals are truly indicative of tinnitus or are instead representative of hyperacusis (Chen et al., 2013; Hickox and Liberman, 2014).

Behavioral paradigms for hyperacusis have also relied on the ASR. When used to evaluate for hyperacusis, the ASR is evaluated at multiple startle stimulus amplitudes (amplitude varied ASR, AmpVar-ASR). The ASR is small in response to lower amplitude startle stimuli and increases with increasing amplitude. It is assumed that animals with hyperacusis will have an elevated ASR in response to moderate to loud sounds, indicating decreased sound level tolerance (Berger and Coomber, 2015; Chen et al., 2013; Coomber et al., 2014; Hickox and Liberman, 2014; Sturm et al., 2017). However, the effects of noise exposure on the ASR are highly variable and appear to be dependent on the noise exposure conditions, subsequent degree of hearing loss, and time since noise exposure (Salloum et al., 2014). Therefore, it is important to consider all these variables when considering the effects of noise exposure on the ASR.

The ASR has also been used to assess sensorimotor gating using pre-pulse inhibition (PPI). PPI occurs when the presence of a pre-pulse (a tone-pip or noise pulse of moderate intensity) results in inhibition of the ASR (Carlson and Willott, 1996). The IC is critical for PPI, as lesioning the IC abolishes this behavior in naïve mice (Koch and Schnitzler, 1997; L. Li et al., 1998). In noise exposed mice, changes in PPI are correlated with the degree of hearing loss and resulting IC plasticity (Carlson and Willott, 1996; Willott and Turner, 2000). Thus, it is important to consider the PPI in conjunction with hearing thresholds.

As previously mentioned, there is some debate as to whether the effects of noise exposure on the ASR are due to tinnitus or hyperacusis. Given that many patients co-report tinnitus and hyperacusis (Aazh and Moore, 2018; Cederroth et al., 2020; Fournier and Hébert, 2013; Katzenell and Segal, 2001; Schecklmann et al., 2014), it is possible that animals similarly experience some combination of symptoms following noise exposure. Unless we are able to create objective measures for tinnitus and hyperacusis, it is unlikely that we will be able to determine the exact

psychoacoustic experience of an animal subject. Nonetheless, the ASR remains a useful tool in identifying disruptions in auditory function following noise exposure and provides a means to evaluate interventions.

1.9 Treating tinnitus: Current options and future directions

Despite ongoing research efforts, the etiology of tinnitus remains unknowns, making it difficult to provide treatment. To date, there are no FDA approved drugs for the treatment of tinnitus. While there has been some success in treating secondary symptoms of tinnitus, such as anxiety and depression, there has been little success in treating tinnitus itself (Czornik et al., 2022; Parnes, 1997; Salvi et al., 2009). Attempts to treat tinnitus pharmacologically have employed a variety of drug classes, including those that increase GABAergic transmission, tri-cyclic antidepressants (TCAs), selective serotonin reuptake inhibitors (SSRIs), non-steroidal anti-inflammatory drugs, and diuretics, to name a few (Czornik et al., 2022; Parnes, 1997; Salvi et al., 2009). While there is evidence that TCAs and SSRIs may provide some symptomatic relief, the beneficial effects were associated with concomitant anxiety and depression, suggesting that they are treating these secondary symptoms rather than the tinnitus itself (Czornik et al., 2022; Parnes, 1997; Salvi et al., 2009). Similarly, treatments such as cognitive behavioral therapy demonstrate some improvement compared to placebo; however, the effects are largely in treating the secondary symptoms of tinnitus and do not provide sustained relief (Czornik et al., 2022).

Unlike the other drug classes mentioned, those that increase GABAergic tone have the potential to treat a known underlying cause of tinnitus. While there has been some success in treating tinnitus in animal models using drugs that systemically increase inhibition (Brozoski et

al., 2010, 2007; Yang et al., 2011), there has been no clear clinical efficacy in humans (Bauer and Brozoski, 2006; Czornik et al., 2022; Parnes, 1997; Piccirillo et al., 2007; Salvi et al., 2009). Furthermore, systemically increasing GABAergic transmission can result in undesirable side effects including somnolence, confusion, bradypnea, and difficulty concentrating, among others. The side effect profile of these drugs, combined with the lack of clear clinical efficacy, render them suboptimal. Rather than increasing inhibition systemically, we wonder whether a more targeted approach could provide more consistent results while minimizing off-target side-effects. The IC is a nexus of auditory processing and integration, is critical for PPI (Koch and Schnitzler, 1997; L. Li et al., 1998), and experiences local circuit reorganization that has been implicated in the emergence of behavioral gap detection deficits (Sturm et al., 2017). As such, the IC is a particularly apt target to explore the effects of local increases in inhibition on auditory behavior.

In Chapters 3 and 4 we describe a series of experiments in which we test the hypothesis that local increases in inhibition in the IC are sufficient to mitigate the effects of noise exposure. To locally increase inhibition in the IC, we transplanted inhibitory precursor cells derived from the embryonic medial ganglionic eminence (MGE) into the IC of naïve and noise exposed mice. The MGE is the birthplace of cortical inhibitory interneurons (Lavdas et al., 1999), and while naturally destined for the cerebral cortex, these inhibitory precursor cells are capable of surviving in a variety of cortical and subcortical structures (Alvarez-Dolado et al., 2006; Baraban et al., 2009; Bráz et al., 2012; Hammad et al., 2015; Martínez-Cerdeño et al., 2010; Derek G Southwell et al., 2010; Southwell et al., 2014; Wichterle et al., 1999; Yang et al., 2016). However, the fate of transplanted MGE cells in auditory and brainstem structures had not been previously characterized. In Chapter 3 we characterize the migration, differentiation, and integration of MGE cells in the IC;

and in Chapter 4 we investigate whether transplantation of MGE cells into the IC of noise exposed mice is sufficient to mitigate the behavioral effects of noise exposure.

1.10 Summary of dissertation research

The aims of this dissertation are twofold, 1) to characterize the spontaneous and sound evoked response properties of neurons in the CNIC and CtxIC in mice, and 2) to investigate the role of inhibition in mitigating the effects of noise exposure. In chapter 2, we characterize the electrophysiological response properties of neurons in the CNIC and CtxIC and test whether these populations can be reliably separated using three different machine learning models. We found that there are subtle, but significant, differences in the frequency response properties of neurons in the CNIC and CtxIC and that robust, reliable discrimination can be achieved. In chapters 3 and 4 we investigate whether transplanted MGE cells will functionally integrate into the IC of adult mice and mitigate the behavioral effects of noise exposure. In chapter 3, we demonstrate that transplanted MGE cells survive and integrate into the adult IC, with similar viability in the non-noise exposed and noise exposed IC. In chapter 4, we demonstrate that increased inhibition in the IC is sufficient to mitigate at least some of the behavioral effects of noise exposure. Together, our data suggest that local increases in inhibition may be useful in mitigating the effects of noise exposure.

2.0 Distinguishing between inferior colliculus central nucleus and cortex neurons based on spontaneous and sound-evoked response properties

2.1 Introduction

The inferior colliculus (IC) is a major auditory brainstem nucleus that receives ascending (Frisina et al., 1998), descending (Saldaña et al., 1996; Winer, 2006), commissural (Chandrasekaran et al., 2013; Ito and Oliver, 2014; Malmierca et al., 2003, 1995; Rees and Orton, 2019; Saldaña and Merchán, 1992), and intrinsic inputs (Ito and Oliver, 2014; Malmierca et al., 1995; Miller et al., 2005; Oliver et al., 1991; Saldaña and Merchán, 1992; Sturm et al., 2014, 2017; Wallace et al., 2012). The IC consists of a 'core' or central nucleus (CNIC) surrounded by a 'shell', or cortex (CtxIC). The CNIC receives primarily ascending input from lower brainstem nuclei (Beyerl, 1978; Coleman and Clerici, 1987; Shneiderman et al., 1988) and accounts for an extensive portion of the projections to the commissure (Rees and Orton, 2019). The CtxIC can be subdivided into the lateral and dorsal cortices. The lateral cortex receives multimodal input from somatosensory, visual, and auditory centers (Coleman and Clerici, 1987; Faye-Lund, 1985; Lesicko et al., 2016; Li and Mizuno, 1997; Wise and Jones, 1977). The dorsal cortex receives inputs from the auditory cortex, cochlear nucleus, and the dorsal nucleus of the lateral lemniscus (Coleman and Clerici, 1987; Druga et al., 1997; Druga and Syka, 1984; Faye-Lund, 1985). Thus, the CNIC and individual cortices are believed to play distinct roles in sound processing and integration.

Despite being well defined anatomically, distinguishing neurons of the CNIC and CtxIC based on their electrophysiological response properties alone has remained elusive. A few studies

have attempted to differentiate the response properties of CNIC and CtxIC neurons in the cat (Aitkin et al., 1994, 1981, 1978) and guinea pig (Syka et al., 2000). While a few studies have characterized the response properties of neurons in the CNIC and CtxIC of the mouse using two-photon calcium imaging (Barnstedt et al., 2015; Wong and Borst, 2019), the majority of the research has focused on the CNIC (Egorova et al., 2006, 2001, 2020; Lee et al., 2019) or evaluated the combined response properties the IC, disregarding the location of the recording (Galazyuk et al., 2017; Ono and Oliver, 2014; Portfors and Felix, 2005; Tan et al., 2007; Walton et al., 1997). The genetic tractability of the mouse has made it one of the most prevalent models in auditory neuroscience. While there is some evidence that the neural mechanisms underlying IC function is preserved across mammalian species (Portfors and Felix, 2005), some of the features of the response properties of IC neurons, such as selectivity, appear to be species specific (Pollak et al., 2011). Thus, better understanding of the response properties of neurons in the CNIC and CtxIC may provide important insight and aid in the interpretation and understanding of the role the IC plays in auditory processing and integration. At the same time, exploring methods of determining neuron location from electrophysiological responses would be highly beneficial for experiments in other species where the IC is not close to the surface and cannot be stereotactically accessed (for example, in non-human primates) (Rocchi and Ramachandran, 2018; Slee and Young, 2011; Wang et al., 2022).

The goal of the present study is to 1) comprehensively characterize the response properties of neurons in the CNIC versus CtxIC, and 2) test whether these populations can be classified based on these response properties alone. To accomplish this, we obtained responses of CNIC and CtxIC neurons to a stimulus battery that included pure tones, two-tones, amplitude-modulated tones, and dynamic random cords. We then applied logistic regression (LR), support vector machine (SVM),

and random forest (RF) classifiers on response parameters derived from pure-tone responses to determine if neurons from the CNIC and CtxIC could be reliably separated based on simple response properties. We found that the response properties of CNIC and CtxIC neurons subtly differed in their pure-tone responses and that all three types of models could result in robust, reliable classification of anatomical location. However, in anesthetized mice, these differences did not translate to significant differences in neural responses to other stimulus types.

2.2 Methods

Experimental procedures were performed in accordance with National Institutes of Health guidelines and were approved by the Institutional Animal Care and Use Committee at the University of Pittsburgh. All experiments were performed in CBA/CaJ mice (Jax 000654).

2.2.1 Surgical procedures

Adult CBA/CaJ mice (6-11 weeks old) of either sex were sedated with an IP injection of dexmedetomidine (IP, 0.5mg/kg) to facilitate maintenance of the anesthetic state at low doses of general anesthetic. Ten minutes after dexmedetomidine injection, general anesthesia was induced with vaporized isoflurane (2.5-3% for surgery). When subjects no longer exhibited a toe pinch reflex, they were transferred to the stereotaxic apparatus and the isoflurane lowered to a maintenance dose (2-2.5%). Body temperature was monitored and maintained at 36.5-38.5˚C (FHC DC temperature controller). The IC were located using stereotaxic coordinates (-5.3mm caudal and +/- 1.3mm lateral from bregma). A 1.4mm burr hole was drilled into the skull using a

high speed stereotax-mounted drill (Model 1474, Kopf). The craniotomies were covered with 1% agarose. A custom head post was affixed to the anterior skull using dental acrylic (Metabond) and allowed to set for at least 15min before transfer to the recording chamber.

2.2.2 Acoustic stimuli

All stimuli were generated in Matlab (Mathworks) at a sampling rate of 100kHz, converted to analog (National Instruments), attenuated (TDT), power amplified (TDT) and delivered through a speaker (MF1, Multifield Magnetic Speaker, TDT) located approximately 10cm from the subject on the contralateral side. Stimuli included pure tones (4-32kHz), amplitude-modulated tones, two-tone complexes, and a 1-minute-long segment dynamic random chords (10 repetitions) to estimate spectrotemporal receptive fields (STRFs).

2.2.3 Electrophysiology

All recordings were conducted in a double-walled sound-attenuating booth (IAC), the walls of which were lined with anechoic foam (Pinta Acoustics). Subjects were headfixed to a vibration-isolation tabletop. Isoflurane concentration was lowered to 0.5-1.5% for recordings, and body temperature maintained at 36.5-38.5˚C (FHC DC temperature controller). Single units were recorded using a 64-channel silicon probe (64D sharp, fabricated by IDAX Microelectronics) (Du et al., 2011) with individual sites electroplated to achieve an impedance of ~2-3MΩ. The electrode was dipped in DiI before recordings to allow for post-hoc verification of the recording site. The agarose was removed from the craniotomies and the probe positioned above the IC at a 15˚ angle,

pointed rostrally, and lowered to a depth of 1.5mm using a hydraulic microdrive (FHC Inc.). Mineral oil was placed over the craniotomy sites to prevent the tissue from drying. Electrophysiological signals were digitized and amplified using a low-noise amplifier (Ripple Neuro) and visualized using Trellis suite software (Ripple, Inc.). The data was sorted off-line to isolate single unit clusters using JRClust (Jun et al., 2017). Cluster quality was assessed using a range of metrics (e.g. signal-to-noise ratio of spike waveform, ISI histogram, stability of cluster over recording duration). Only well isolated single unit clusters (SNR $\geq$ 5) were considered for analysis. Post-hoc reconstruction of the probe track was used to obtain the location of recorded single units in the IC (Figure 4B).

2.2.4 Post-hoc verification of probe location

At the end of the recording session, we performed histochemistry for cytochrome oxidase to delineate the borders of the CNIC anatomically (Cant and Benson, 2005; Ito et al., 2018) and used the DiI staining to register the probe trajectory to the underlying IC anatomy. Subjects were transcardially perfused with 0.1M phosphate buffer saline (PBS) followed by 4% paraformaldehyde (PFA) in 0.1M PBS. The brains were extracted and post fixed in 4% PFA overnight at 4˚C. Following post fixation, the brains were cryoprotected in 30% sucrose in 0.1M PBS for 48 hours at 4˚C. Coronal sections (50μm in thickness) were cut using a freezing microtome.

Sections were washed in 0.1M PBS then incubated at room temperature in a solution containing 10mg diaminobenzidine (Sigma D5905), 20mL 0.1M PBS, 5mg cytochrome oxidase (Sigma C2037), and 0.8g sucrose. Sections were incubated at room temperature until the CNIC

appeared well differentiated (typically 4 hours). Sections were washed three times in 0.1M PBS and mounted onto superfrost plus microscope slides (Fisherbrand).

Light and fluorescent microscopy was performed to visualize the CO (Figure 4A) and DiI, respectively. Digitized images of coronal sections were obtained (Axio Imager, Zeiss) and overlaid in imageJ.

2.2.5 Data analysis

The frequency response area (FRA) was characterized by acquiring responses to 100ms pure tones ranging from 4 to 32kHz (12steps/oct) at various sound levels (30-70dB SPL, 5dB spacing). The spontaneous firing rate was determined during the interstimulus interval (100ms). The best frequency (BF) was defined as the frequency that elicited the highest firing rate at any sound level. Threshold was defined as the lowest sound level to evoke a response significantly different from baseline. The characteristic frequency (CF) was defined as the frequency that elicited the highest firing rate at threshold. Onset latency was determined using the peristimulus time histogram (PSTH, 1ms bins) of the most active trials (90^{th} percentile or higher). The earliest time bin that displayed spike counts significantly greater than spontaneous rate for three consecutive bins was taken to be the onset latency. For cases in which the spontaneous rate was zero, the threshold was set to 1 spike/sec. The bandwidth at each level was estimated using a rectangular fit of the tuning curve at that level (Sadagopan and Wang, 2008). For each neuron, a linear fit of the bandwidth in octaves was estimated for the data between 0 and 15dB relative to threshold and 15 to 35dB relative to threshold (Figure 5H). The difference in slope was used to determine if the bandwidth increased linearly with increasing amplitude (difference = 0) or if the

bandwidth increased more (difference >0) or less (difference <0) rapidly at higher amplitudes. A similar analysis was performed for the firing rate. Q, defined as the best frequency divided by the bandwidth in hertz, was calculated at each level relative to threshold and fit with an exponential decay function (Figure 5K). Tau of Q was determined for each neuron and outliers were identified using the ROUT method and excluded. Linear and exponential decay functions were fit using GraphPad Prism software.

Gap detection was evaluated at a range of pure tone frequencies with gaps (0-100ms, log steps) embedded 500ms after tone onset. Note that because exact neuron BFs were only determined offline (see Discussion), the best frequency of each single unit for gap detection was approximated as the frequency that elicited the highest firing rate in the absence of a gap (i.e. gap length = 0ms). The frequency corresponding to the minimum gap detection threshold was also noted. The difference in octaves from the estimated best frequency and minimum gap detection frequency was calculated. The gap threshold was defined as the gap length required for the firing rate during the gap to be significantly modulated (ANOVA) compared to the firing rate in an equal-length response bin immediately preceding or following the gap. Single unit responses were classified as onset, sustained, offset, or other (based on Berger et al., 2014). The onset window was defined as the first 30ms after stimulus onset plus the estimated onset latency (5ms). The sustained window was defined as the 30ms following the onset window. The offset window was defined as the first 30ms following stimulus offset. The response in each response window was considered significant if it was greater than the spontaneous firing rate plus two standard deviations. Single units that had a significant response in only the onset window were classified as onset responders. Units with a significant response in the onset and sustained windows were considered sustained responders.

Units with a significant response in only the offset window were considered offset responders. Single units that did not fit into one of these categories were classified as other.

Amplitude-modulated tones (500ms in length, AM frequencies 2-256 Hz, log steps) were presented at a range of pure tone frequencies, based on LFP responses. For the reasons stated above, the best frequency of each unit was estimated as the frequency that elicited the highest overall firing rate. The rate-based best modulation frequency (rBMF) and discharge synchrony-based best modulation frequency (tBMF) were calculated using previously described methods (Liang et al., 2002).

Spectrotemporal receptive fields (STRFs) were estimated using NEMS (Pennington and David, 2020; Thorson et al., 2015) and previously described methods (Montes-Lourido et al., 2021). Briefly, the actual peristimulus time histogram (PSTH) of unit responses to dynamic random chords was computed in 5ms bins, averaged over 10 repetitions. Nested cross-validation, where 90% of the data was used to fit the model and the remaining 10% was used to test the model, was repeated 10 times using non-overlapping segments to yield 10 STRF estimates which were then averaged to result in a mean receptive field. A significance mask was calculated using a permutation test (Montes-Lourido et al., 2021), and non-significant STRF weights were set to zero. The correlation coefficient between the predicted responses to the test data sets and actual responses (r-test) was used as a metric of goodness of fit. STRFs with an r-test <0.3 were excluded from further analysis. The performance of three STRF models, with 17, 29, or 365 parameters, were compared. The temporal and frequency response profiles of the average full-rank STRF estimate for each neuron were estimated using a Gaussian fit (Matlab, MathWorks). Sideband

inhibition was further investigated using a second order analysis in which the stimulus frames containing frequency content in the excitatory frequency range (F_0= peak excitatory frequency +/- 1 standard deviation) were extracted. The average response rate of the neuron was then plotted based on the additional frequency content (F_i) contained in the stimulus bins. For comparison, stimulus bins that did not contain F_0 were extracted and plotted according to F_i. Units were considered to be inhibited if the response to $F_0 + F_i$ was less than the response at F_i.

Lateral suppression was determined using simultaneous presentation of tone-pairs. In each stimulus set, one tone was presented at a fixed frequency (F1) and a simultaneously presented second tone was varied in frequency (F2; +/- 1 octaves rel. F1; 10 steps/oct). This was repeated for a number of F1 frequencies. Best frequency for each unit for this paradigm was approximated as the frequency in which the peak response was at F1=F2. The maximal percent suppression and the area under the curve from -0.5 to 0.5 oct and -1 to 1 oct was calculated.

Logistic regression (LR), linear support vector machine (SVM), and random forest classifiers (RF) were trained on pure-tone responses (used to derive the FRA) to determine whether CNIC (n= 107 single units) and CtxIC (n= 86 single units) responses could be reliably separated based on simple response properties. Missing values were estimated using SimpleImputer (Scikit-learn toolbox in Python). Anatomical probe location ground-truth, determined using DiI and cytochrome oxidase labeling, was used to create a binary target variable. Further details of data used for classification are shown in Table 1. Monte-Carlo cross validation, where 80% of the data was randomly selected and used to fit the model and the remaining 20% was used to test the model, was repeated 100 times. Models were trained and evaluated using scikit-learn (Pedregosa et al.,

2011). The LR algorithm was implemented with the "liblinear" solver. The SVM algorithm used a linear kernel. The RF algorithm was implemented with an "entropy" scoring criterion and an ensemble size of 50. Model performance was evaluated based on accuracy, whether the model correctly classified the units, and area under the receiver operating characteristic (ROC) curve, a measure of discrimination. Average accuracy and area under the ROC curve were calculated across the 100 runs for each type of model.

Table 1. Data Used to train classification models

	CNIC	CtxIC
	107 Samples	86 Samples
Variable	*Missing Data*	*Missing Data*
Spontaneous firing rate (mean)	0	0
Spontaneous firing rate (standard deviation)	0	0
Threshold	0	0
Onset latency	0	0
Change in slope of bandwidth (oct)	44	13
Tau of Q	37	19
Change in slope of firing rate	44	13
Characteristic frequency – best frequency	0	0

Statistical analysis was performed using GraphPad Prism software. Data were evaluated for normal distribution using a one sample Kolmogorov-Smirnov (K-S) test. Two sample t-tests or Mann Whitney tests were used to compare two independent groups with either normally or non-normally distributed data, respectively. Kruskal-Wallis tests were used to compare three or more groups, multiple comparisons were corrected for using the Dunn pairwise method. Two-way ANOVA was used for comparisons in which there were two independent variables, multiple comparisons were made using Tukey's test. Cumulative frequency distributions were compared using the two-sample

K-S test. Statistical significance for all tests was set to $p<0.05$ and corrected for in cases of multiple comparisons.

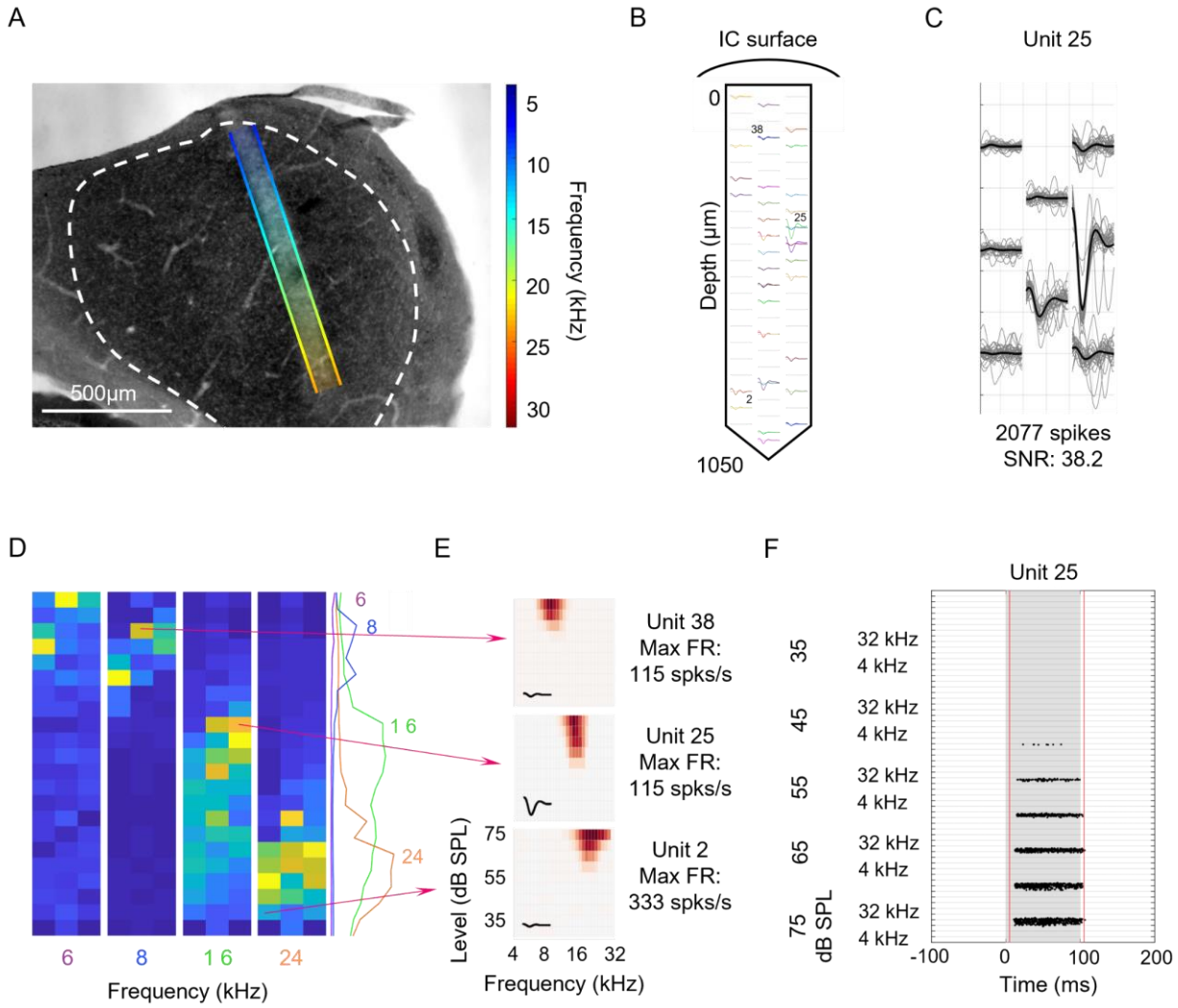

Figure 4. Identifying probe location and mapping single units

A. Cytochrome oxidase was used to identify the central nucleus of the inferior colliculus (dashed white line). The probe location (overlaid gradient) was confirmed using DiI (not pictured). Multiunit activity was used to estimate the tonotopic axis (overlaid gradient: purple – low frequencies, red – high frequencies).

B. Post-hoc reconstruction of the 64-channel silicon probe and the location of identified single units. Single units 2, 25, and 38 are labeled and referenced in C (unit 25), E (units 2, 25, and 38), and F (unit 25).

C. Spike waveforms were isolated, clustered, and visualized in JRClust. Voltage fluctuations were observed on multiple channels. Waveforms with consistent shapes and timing were combined to form single unit clusters. The spike waveform for unit 25 at its primary and neighboring electrode channels is shown here. Unit 25 was a cluster of 2077 spikes with a signal-to-noise ratio (SNR) of 38.2.

D. Heat maps of the average multiunit activity (MUA), defined as the envelope of the band-pass filtered (350-3500Hz) and rectified raw signal, at each contact in response to pure tones of different frequencies (6, 8, 16, and 24kHz). The average MUA (mV) at each contact was normalized to the peak MUA across all channels and frequencies. The colormap corresponds to the normalized average MUA, dark blue indicates no response and yellow indicates the highest response. Colored lines on the right margin correspond to MUA depth profiles, averaged over three closely spaced contacts, to 6 (purple), 8 (blue), 16 (green), and 24 (orange) kHz.

E. Frequency response areas from isolated single units 2 (bottom), 25 (middle), and 38 (top) show responses that are consistent with the expected tonotopic gradient of the IC as well as the MUA map. The color map corresponds to the firing rate (FR), the maximum FR (right margin) is dark red, spontaneous firing rate is white. Insets: spike waveforms.

F. Raster plot for unit 25. The grey shading indicates stimulus duration, black dots correspond to spike times. Red lines indicate the response window, assuming a 5ms latency.

2.3 Results

Recordings were performed in 5 subjects (n=7 IC). Four tracks were confirmed to be in the CNIC (n=3 mice) and three were in the CtxIC (n=2 mice).

2.3.1 CNIC and CtxIC units exhibit subtle but significant differences in spontaneous and pure-tone evoked response parameters

The FRAs of CNIC and CtxIC units were similar in shape, with subtle but significant differences in their response properties. In both the CNIC and CtxIC, the majority of units demonstrated “V” shaped tuning (Figure 5A) (Ramachandran et al., 1999). We isolated 107 CNIC and 86 CtxIC units that responded to pure tones, with BFs ranging from 4 to 32kHz (Figure 5B). There was no significant difference between the cumulative probability distributions of the BF of

CNIC or CtxIC units (p=0.66), suggesting that observed differences are not due to systematic differences in sampling.

Unlike previous studies (Syka et al., 2000), we found that units in the CNIC had lower spontaneous firing rates, higher onset latencies, and higher thresholds than units in the CtxIC. Indeed, the spontaneous firing rate of units in the CNIC (median=0.024 spks/s, IQR=0.16) was significantly lower than that of units in the CtxIC (median=0.084 spks/s, IQR=0.56, p=0.006, Figure 5D) The standard deviation of spontaneous firing rates of units in the CNIC (median=0.49 spks/sec, IQR=1.12) was also significantly lower than that of CtxIC units (median=1.03 spks/s, IQR=2.61, p=0.001, Figure 5E). The distribution of spontaneous firing rates was not Poisson distributed (i.e. the mean was not equal to the standard deviation) in either the CNIC or CtxIC. Thus, the increased variability in the spontaneous firing rates in the CtxIC is not likely related to the increased mean. The median onset latency of CNIC units (8ms, IQR=2) was significantly higher than the median onset latency of CtxIC units (7ms, IQR=2, p=0.0006, Figure 5F). Finally, the median threshold of CNIC units was 55dB SPL (IQR=10), significantly higher than that of CtxIC units (median=40dB SPL, IQR=15, p<0.0001, Figure 5G). In summary, units in the CNIC exhibit lower and less variable spontaneous firing rates, are slower to respond to pure tone stimuli, and have higher thresholds than units in the CtxIC.

In addition to pure tone thresholds, we further characterized the shape of the FRA in terms of tuning asymmetry and change in bandwidth with increasing stimulus level. We found that CNIC units exhibited narrower tuning whose bandwidth increased linearly with increasing stimulus amplitude without changes to frequency eliciting peak firing rate at each level (i.e. BF=CF, median difference=0 oct, IQR=0.4), while CtxIC units demonstrated a low-frequency tail, with a higher CF than BF (median difference=0.2 oct, IQR=0.9, p<0.0001, Figure 5C). To determine whether

the BW increased linearly with increasing stimulus level, we plotted the BW in octaves at each level relative to threshold and fit the data with two lines, one from 0-15dB relative to threshold and the second from 15-35dB relative to threshold (Figure 5H). Units that did not have enough data to fit both lines were excluded from analysis. The median change in slope of BW was negative in the CNIC (n = 66; median=-0.014 oct/dB relative to threshold, IQR=0.029) and CtxIC (n = 75; -0.046 oct/dB relative to threshold, IQR=0.054), indicating that in both populations the BW increased less rapidly with increasing amplitude (Figure 5I). However, the change in slope of the BW was significantly lower in the CtxIC compared to the CNIC ($p<0.0001$). Additionally, units in the CNIC had, on average, narrower tuning at levels above threshold compared to units in the CtxIC (Figure 5H). Consistent with our BW data, we found that, on average, units in the CNIC had Q values that were higher at almost every level above threshold compared to units in the CtxIC (Figure 5K). Moreover, the Tau of Q was significantly higher in the CNIC (median=5.69, IQR=5.44, n=72) compared to the CtxIC (median=4.34, IQR=4.34, n=69, $p=0.042$, Figure 5L). Together, these data suggest that compared to CtxIC units, units in the CNIC are more consistently and narrowly tuned, with relatively linear increases in BW with level.

Finally, we examined the change in the slope of the firing rate (FR) with increasing stimulus level using a similar analysis as described above. Using this analysis, we expect that units with monotonic rate-level functions will have a change in slope equal to zero. Consistent with previous studies (Aitkin et al., 1994; Syka et al., 2000), we found that units in the CNIC were more likely to have non-monotonic rate-level functions compared to CtxIC units. This was reflected in our analysis, in which we found that the median change in slope of the FR was significantly lower in the CNIC (median=-1.3 spks/sec/dB relative to threshold, IQR=7.08, n=63) compared to the

cortex of the IC (median=-0.264 spks/sec/dB relative to threshold, IQR=2.13, n=73, p=0.013, Figure 5J).

To summarize, compared to the CtxIC, units in the CNIC have lower and less variable spontaneous firing rates, slightly delayed onset, higher thresholds, are more consistently and selectively tuned, and have a higher prevalence of non-monotonic rate-level functions. As a result, the FRAs of units in the CNIC are narrower and have more consistent growth in their bandwidth with increasing level compared to those in the cortex of the IC (Figure 5M). Because we sampled a similar range of BFs in CNIC and CtxIC, these differences in the response properties of units in the CNIC and CtxIC are not due to systematic sampling biases and represent true underlying differences.

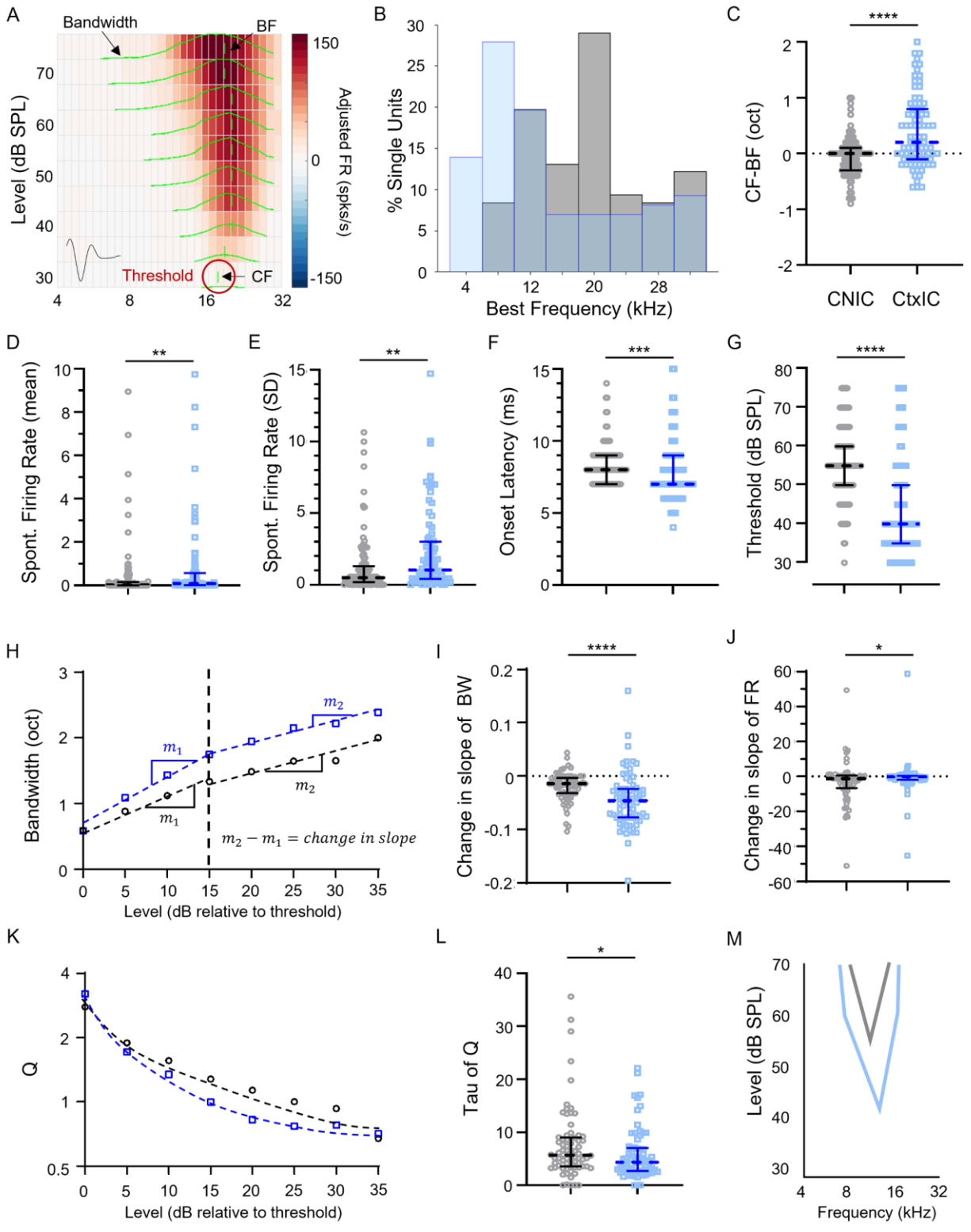

Figure 5. Units in the CNIC have lower and less variable spontaneous firing rates, delayed onset, higher thresholds, are more consistently and selectively tuned, and have non-monotonic rate-level functions

A. A representative frequency response area (FRA). The majority of the FRAs demonstrated “V” shaped tuning. The best frequency (BF) was defined as the frequency that elicited the highest response rate while the characteristic frequency (CF) was defined as the frequency that elicited the highest response at threshold. Green curves are frequency tuning curves at each sound level, and vertical green lines denote the frequency that elicited the highest response at each level. Threshold was defined as the lowest amplitude to elicit a significant response (red circle). The color map corresponds to the firing rate minus the spontaneous firing rate. Red: increase in the FR over the spontaneous FR (dark red- max firing rate). White: FR equal to the spontaneous FR. Blue: decrease in the FR, below spontaneous FR (dark blue- max inhibition).

B. The distributions of BFs of single units in the central nucleus of the IC (CNIC, grey) and cortex of the IC (CtxIC, blue) were not significantly different ($p=0.66$, Kolmogorov-Smirnov test).

C-G, I, J, L: Plots show data from individual units (CNIC=grey circles, CtxIC= blue squares) with median (dashed horizontal line) and interquartile range (error bars). Asterisks denote statistical significance (*$p<0.05$, **$p<0.01$, ***$p<0.001$, ****$p<0.0001$).

C. FRA asymmetry, quantified as the difference in octaves between the CF and BF. Units in the CtxIC demonstrated a low-frequency tail (median=0.2 oct) while units in the CNIC demonstrated symmetric tuning (median=0 oct, $p<0.0001$, Mann-Whitney test).

D. Mean spontaneous firing rates of units in the CNIC and CtxIC. The spontaneous firing rate of units in the CNIC (median=0.024 spks/sec) was significantly lower than that of units in the CtxIC (median=0.084 spks/sec, $p=0.006$, Mann-Whitney test).

E. The standard deviation of the spontaneous firing rates of units in the CNIC and CtxIC. The standard deviation of spontaneous firing rates was significantly higher in the CtxIC (median= 1.026) compared to the CNIC (median=0.491, $p=0.001$, Mann-Whitney test).

F. Onset latency of units in the CNIC and CtxIC. The onset latency was higher in the CNIC (median=8 ms) compared to CtxIC (median=7 ms, $p=0.0006$, Mann-Whitney test).

G. Thresholds of CNIC and CtxIC units. units in the CNIC had a higher threshold (median=55 dB SPL) compared to units in the CtxIC (median=40dB SPL, $p<0.0001$, Mann-Whitney text).

H. Schematic representation of the analysis used in I. The bandwidth (BW) in octaves was plotted at each level relative to threshold. The data plotted here are the mean BW at each level relative to threshold. A line was then fit to the data

between 0 and 15dB relative to threshold and 15 to 35 dB relative to threshold. The change in slope of the BW in octaves was then calculated A change in slope of BW of zero indicates a linear increase in BW with increasing level. A negative change in slope of BW indicates that the BW increases less rapidly at higher amplitudes while a positive change in slope indicates that the BW increases more rapidly at higher amplitudes. A similar analysis was performed for the firing rate in J.

I. The change in slope of the BW. The median change in slope of BW was negative for both CNIC (median=-0.014 oct/dB relative to threshold) and CtxIC (median=-0.046 oct/dB relative to threshold), indicating that the BW increased less rapidly with increasing amplitude. The change in the slope of the BW was significantly lower in the CtxIC compared to the CNIC ($p<0.0001$, Mann-Whitney test). Therefore, units in the CNIC demonstrate a more linear increase in BW with increasing stimulus level than units in the CtxIC.

J. Change in the slope of the firing rate (FR). No change in the slope of the FR indicates a monotonic rate-level function. The change in slope of the FR was significantly lower in the CNIC (median=-1.3 spks/sec/dB relative to threshold) compared to the CtxIC (median=-0.264 spks/sec/dB relative to threshold, $p=0.013$, Mann-Whitney test). Thus, units in the CNIC have a higher incidence of non-monotonic rate-level functions, with a decrease in FR with increasing stimulus level.

K. Schematic representation of the analysis used in L. The Q at each level relative to threshold was plotted and fit with an exponential decay function. The data plotted here are the mean Q at each level relative to threshold. The Tau of Q was calculated for each single unit. Outliers were identified using the ROUT method.

L. The Tau of Q was significantly higher in the CNIC (median=5.69) compared to the CtxIC (median=4.34, $p=0.042$, Mann-Whitney test).

M. Schematic summary. Together, these data demonstrate that the FRAs of single units in the CNIC (grey) have a higher threshold, are more narrowly tuned, and have a more consistent growth in their bandwidth with increasing level compared to those in the CtxIC (blue).

2.3.2 CNIC units exhibit a narrower frequency response profile and sustained temporal response profile than CtxIC units

Presenting single pure-tones does not engage known mechanisms such as side-band suppression. Additionally, by presenting single tones at fixed inter-stimulus intervals, it is difficult to characterize the temporal response profiles of units. To reveal putative side-band interactions and the temporal response profile of units, we used dynamic random chord (DRC) stimuli (Figure 6B) to evoke responses, and fit linear-nonlinear models to the responses using the Neural Encoding Model System (NEMS) (Pennington and David, 2020; Thorson et al., 2015). For each recorded unit, the encoding model estimated a set of 360 linear weights (36 frequencies x 10 time bins, called the spectrotemporal receptive field or STRF, Figure 6C) and the parameters (n=5) of a level-shifted double-exponential point nonlinearity. Neural responses to the DRC stimulus were predicted using this model with nested cross-validation (see Methods), and the correlation coefficient between the predicted PSTH and the actual PSTH (r-test) was computed. STRFs with low r-test values (r-test<0.3) were excluded from further analysis (Figure 6A). The median r-test of the included STRFs was 0.7 (IQR=0.3, n=94) for CNIC units and 0.6 (IQR=0.2, n=95) for CtxIC units, indicating that there were no systematic differences in the STRF estimation procedure between the two regions.

From the STRF, by fitting Gaussians to the positive and negative STRF weights averaged separately along the frequency and time axes, we extracted four 'tuning curves' corresponding to the excitatory (E) and inhibitory (I) spectral and temporal response profiles (Figure 6C). Eight parameters were extracted to quantify these tuning curves – the peak E and I position in frequency and time (corresponding to the mean of the Gaussian fits), and the width of E and I in frequency

and time (corresponding to the standard deviation of the Gaussian fits). Response profiles with peak positions that fell out of the range of STRF frequency and time extents were excluded from analysis. Most units exhibited co-tuned E and I frequency tuning curves, regardless of their location in the IC. The median difference between the peak E and I frequencies was 0 oct (IQR=0.02, n=81) for CNIC units and 0.01 oct (IQR=0.48, n=72) for CtxIC units (Figure 6E). Consistent with results from the FRA analysis described above, E and I frequency tuning widths were significantly different between CNIC and CtxIC units ($H=33.09$, $p<0.0001$, Table 2; E width $p=0.04$, I width $p=0.03$, Figure 6F). In both the CNIC and CtxIC, the E width was significantly higher than the I width (CNIC $p=0.009$, CtxIC $p=0.03$, Figure 6F). Together, these data confirm that units in the CNIC are more narrowly tuned than the CtxIC. Surprisingly, we did not see clear lateral inhibition in the STRFs of CNIC or CtxIC units, although this may be due to the low spontaneous firing rate and the use of anesthesia (Figure 5D).

Because we used a spectrotemporally varying stimulus (DRC), these data also allowed us to characterize the time course of E and I responses. Most STRFs exhibited a pattern of excitation followed by a period of inhibition. The peak I response occurred later in CNIC units compared to CtxIC units (Figure 6G). Indeed, the difference in the peak E and I timing was 13.7ms in the CNIC and 10.3ms in the CtxIC (Figure 6G; $p<0.0001$). Additionally, E and I widths were also different between CNIC and CtxIC units ($H=109$, $p<0.0001$, Table 3). Excitatory temporal response profiles were generally wider than the inhibitory temporal profiles (CNIC $p<0.0001$, CtxIC $p<0.0001$). The excitatory temporal response profile of CNIC units was wider than CtxIC units ($p=0.0004$). These data reveal that CNIC units exhibit sustained excitation in time compared to units in the CtxIC, suggesting differences in temporal processing between the two regions.

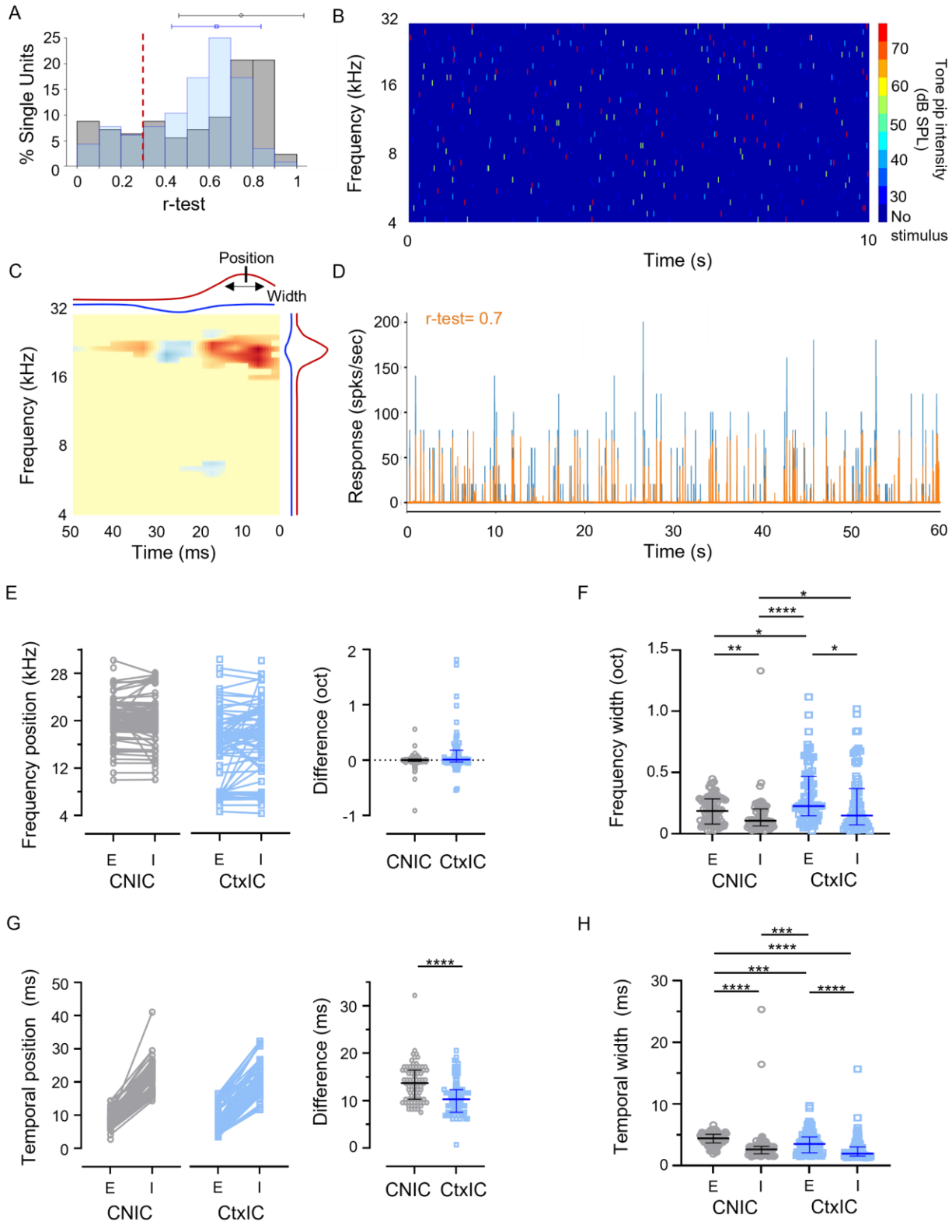

Figure 6. CNIC units have a narrower frequency response profile and sustained excitatory response compared to CtxIC units

A. Distribution of the correlation values (r-test) between the predicted and actual PSTH. Single units with a r-test less than 0.3 (dashed red line) were excluded from further analysis. The median and interquartile range for each distribution, after excluding r<0.3, are plotted above. CNIC is grey, CtxIC is blue.

B. A 10 second segment of the STRF stimulus, a dynamic random chord. Colors correspond to tone pip intensity (right margin: colormap scale, dark blue – no stimulus, red – 75 dB SPL).

C. Representative STRF showing a frequency-tuned period of excitation (red) followed by a period of inhibition (blue). The frequency (right) and temporal (top) response profiles for both the excitatory (red) and inhibitory (blue) response are shown along the margins. The position (mean) and width (standard deviation) of the response profiles were derived from Gaussian fits.

D. Actual response PSTH (blue) and the predicted response PSTH (orange) using the STRF shown in C. The correlation coefficient between the predicted and the actual response (r-test) was 0.7, indicating that the STRF had high predictive value.

E-H. Quantification of STRF response profiles for CNIC (gray) and CtxIC (blue) units. Individual values are plotted together with medians and interquartile ranges. Asterisks indicate statistically significant differences (*p<0.05, **p<0.01, ***p<0.001, ****p<0.0001).

E. The position of E and I frequency response peaks, with lines connecting E and I peak position values (left). The difference between E and I response peaks is plotted on the right. The majority of single units exhibited overlapping E and I frequency response profiles (CNIC median=0, CtxIC=0.01, p=0.053, Mann-Whitney test).

F. E and I frequency tuning widths of CNIC (gray) and CtxIC (blue) units. Compared to CtxIC units, CNIC units exhibited narrower tuning (E width p=0.0351, I width p=0.0313). In both regions, the E frequency tuning width was wider than the I frequency tuning width (CNIC p=0.0093, CtxIC p=0.0280). Kruskal-Wallis test and post-hoc Dunn's multiple comparisons test.

G. The position of E and I temporal response peaks, with lines connecting the E and I temporal peak position values (left). The difference between E and I temporal response peak position (in ms) is plotted on the right. The temporal difference between the E and I peaks was greater in CNIC units (13.70ms) compared to CtxIC units (10.27ms, p<0.0001, Mann-Whitney test).

H. E and I temporal tuning widths of CNIC (gray) and CtxIC (blue) units. Compared to CtxIC units, CNIC units showed wider temporal E widths (p=0.0004). Temporal E widths were generally wider than temporal I widths (CNIC p<0.0001, CtxIC p<0.0001). Kruskal-Wallis test and post-hoc Dunn's multiple comparisons test.

Table 2. STRF frequency response profile widths of CNIC and CtxIC units

Descriptive statistics

	Median (oct.)	IQR (oct.)	n
CNIC: excitatory	0.19	0.2	91
CNIC: inhibitory	0.11	0.14	83
CtxIC: excitatory	0.23	0.32	78
CtxIC: inhibitory	0.15	0.3	74

Kruskal-Wallis table

Kruskal-Wallis H	33.09
degrees of freedom	3
p value	<0.0001

Dunn's multiple comparison test

	Mean rank 1	Mean rank 2	Mean rank diff.	Adjusted P Value
CNIC: excitatory vs CNIC: inhibitory	166.2	120.9	45.29	0.009
CNIC: excitatory vs CtxIC: excitatory	166.2	206.2	-40.08	0.04
CNIC: excitatory vs CtxIC: inhibitory	166.2	163	3.19	>1
CNIC: inhibitory vs CtxIC: excitatory	120.9	206.2	-85.36	<0.0001
CNIC: inhibitory vs CtxIC: inhibitory	120.9	163	-42.09	0.03
CtxIC excitatory vs CtxIC: inhibitory	206.2	163	43.27	0.03

Red p-values indicate statistical significance.

Table 3. STRF temporal response profile widths of CNIC and CtxIC units

Descriptive statistics

	Median (ms)	IQR (ms)	n
CNIC: excitatory	4.44	1.41	94
CNIC: inhibitory	2.64	1.22	85
CtxIC: excitatory	3.52	2.57	95
CtxIC: inhibitory	1.94	1.48	92

Kruskal-Wallis table

Kruskal-Wallis H	109
degrees of freedom	3
p value	<0.0001

Dunn's multiple comparison test

	Mean rank 1	Mean rank 2	Mean rank diff.	Adjusted P Value
CNIC: excitatory vs CNIC: inhibitory	265.3	143.7	121.6	<0.0001
CNIC: excitatory vs CtxIC: excitatory	265.3	203.5	61.9	0.0004
CNIC: excitatory vs CtxIC: inhibitory	265.3	116.1	149.2	<0.0001
CNIC: inhibitory vs CtxIC: excitatory	143.7	203.5	-59.8	0.0009
CNIC: inhibitory vs CtxIC: inhibitory	143.7	116.1	27.6	0.5
CtxIC excitatory vs CtxIC: inhibitory	203.5	116.1	87.4	<0.0001

Red p-values indicate statistical significance.

2.3.3 Narrow STRF tuning widths might suggest the presence of unrevealed side-band suppression

In both CNIC and CtxIC, E frequency tuning widths were substantially and significantly narrower than bandwidths computed from the FRA, both when matched for stimulus power (Fig.

7A) and at each tested sound level relative to threshold (Fig. 7B; Mann-Whitney tests with multiple-comparisons corrected p-value significance threshold of p=0.006). Consistent with observed differences between CNIC and CtxIC, both the probe location (CNIC vs CtxIC) and stimulus type (FRA vs STRF) had significant, independent effects on the bandwidth (Table 4). Additionally, consistent with our observation that the E frequency width of the STRF was more significantly reduced compared to the FRA in the CtxIC than in the CNIC, we observed a significant interaction between the probe location and stimulus type (Table 4; two-way ANOVA). These results suggest that the denser DRC stimulus might reveal the presence of side-band suppression, which was not activated when presenting single tones. This is likely because the very low spontaneous rates in our preparation hampered our ability to observe further suppression.

To directly investigate if the narrower STRF frequency tuning widths could be recapitulated using traditional paradigms, we examined the effects of two simultaneously presented pure tones on response rate. By positioning one tone at the best frequency, we reasoned that we could drive units robustly so that suppression by a second frequency could be observed. Because of our array recording set up, the exact best frequencies of units could not be estimated until units were sorted offline after the experiment. Therefore, during the experiment, we presented two tones by fixing on of tone frequencies (F1) at one of few values that spanned the range of frequencies observed in a given track. The second tone frequency (F2) was roved in a +/- 1 octave range around F1. For analysis, the best frequency of each unit was approximated to be the frequency that elicited the highest response when the two frequencies were equal (F1=F2). If the strongest response rate was not at F1=F2, it was likely that we did not accurately position F1 at the best frequency during the experiment, and these data were not used. A subset of units (CNIC n=20/129 and CtxIC n=11/129) demonstrated a response that was greatest at F1=F2. In both CNIC

and CtxIC units, we saw a variety of responses, including units with sustained side-band suppression (Figure 7C, left) and those with variable suppression (Figure 7C, right). On average, units demonstrated a maximum firing rate suppression of 68% in the CNIC (SD=26.3) and 75% in the CtxIC (SD=10.7). There was no significant difference in the maximal percent reduction between the two populations (p=0.40). Next, we quantified total suppression as the area under the curve from -0.5 to 0.5 oct and -1 to 1 oct (Figure 7E). This analysis can differentiate between sustained suppression and variable or narrow suppression, even if two units exhibited the same maximal suppression. We did not observe significant differences in the area under the curve between -0.5 and 0.5 oct (CNIC mean=0.47, SD=0.24; CtxIC mean=0.37, SD=0.12; p=0.21, unpaired t test) or -1 and 1 oct (CNIC median=0.95, IQR=0.68; CtxIC median=0.90, IQR=0.4; p=0.68, Figure 7E). Together, these data suggest that while both CNIC and CtxIC units are indeed influenced by side-band suppression, they exhibit similar degrees of suppression. We note that these analyses are constrained by our array recording methodology, in that we could not present stimuli with one tone precisely at the BFs of recorded units. Because we approximated BF as the frequency at which the maximal response was observed at F1 = F2, this precluded us from being able to observe any two-tone facilitation.

Our two-tone data suggest that a small percentage of units in the CNIC and CtxIC demonstrate lateral suppression, with similar results between the two populations. However, our analysis assumed that the best frequency was when the peak response occurred at F1=F2, which excludes the possibility of facilitation. Furthermore, using two-tone responses to understand the increase in selectivity that we observed in the STRF is indirect. To address these limitations, we performed a second-order STRF analysis in which we compared the response rate of units to stimulus bins that contained the frequencies within the excitatory response profile to those that did

not. We found a few examples of lateral suppression, in which the response rate of units to stimulus bins that contained frequencies in the excitatory response profile as well as those in the sidebands was lower than that of the response to just sideband stimulation (Figure 8A). However, we also saw units that maintained higher response rates when the stimulus contained frequencies within the excitatory response profile, regardless of the presence of sideband frequencies (Figure 8B). In both response types, we also saw regions of facilitation, where stimuli that contained frequencies in the excitatory response profile and sideband elicited a stronger response than those that contained only frequencies in the excitatory response profile. These data suggest that neurons in the IC may experience inhibition, facilitation, or both in the presence of sideband stimulation. These complex interactions and their contribution to increased selectivity warrants further investigation.

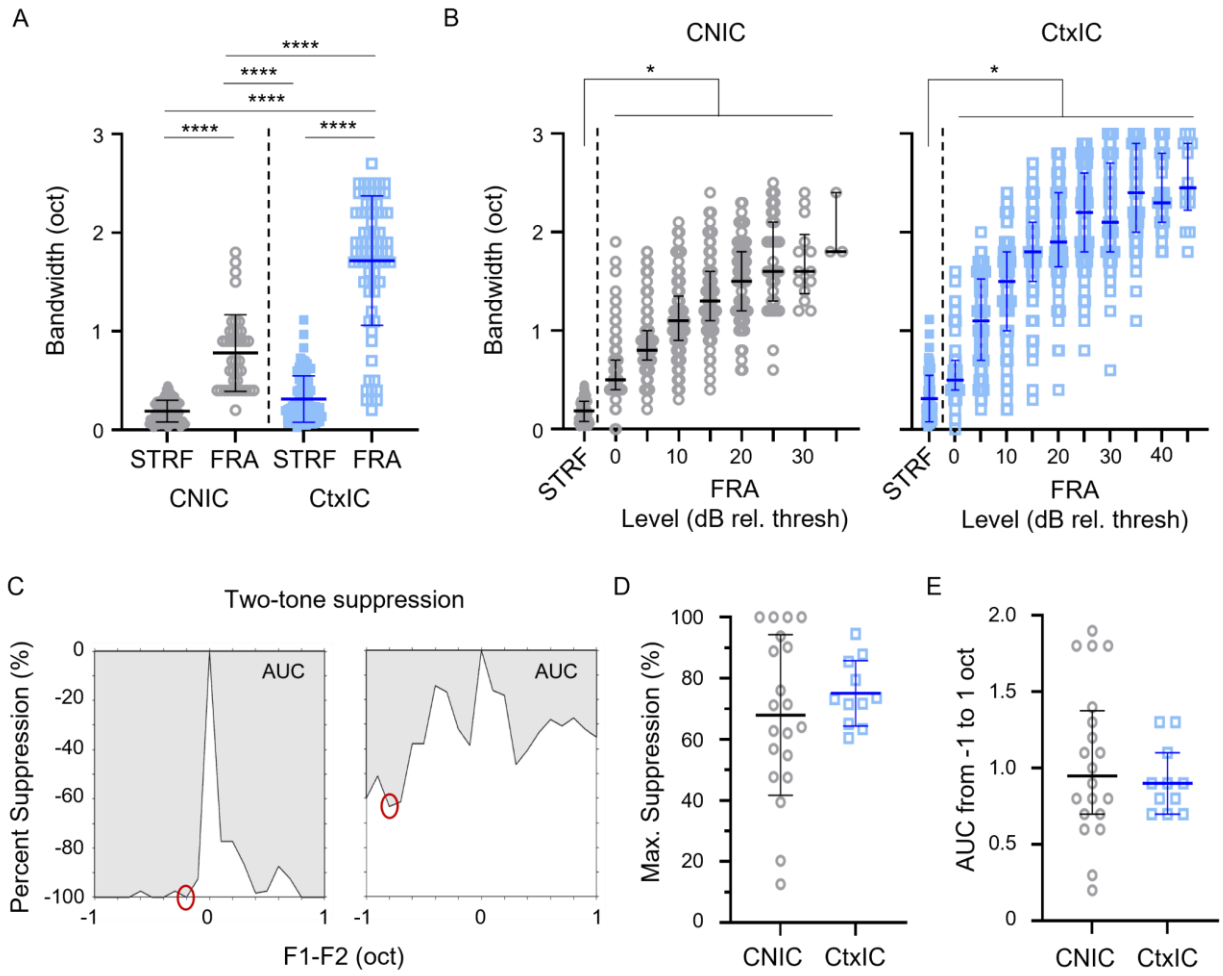

Figure 7. Single units in the CNIC and CtxIC exhibit side-band suppression

A, B, D, and E. Individual data points are plotted with mean and standard deviation in A and D and median and interquartile range in B and E. Asterisks indicate statistically significant differences (*p<0.05, **p<0.01, ***p<0.001, ****p<0.0001).

A. The effects of recording site (CNIC vs. CtxIC) and stimulus type (dynamic random chord vs. tone pip) on the frequency bandwidth of the receptive field (STRF and FRA). STRF bandwidth corresponds to the standard deviation of the Gaussian fit to the E frequency response profile. FRA bandwidth corresponds to the bandwidth of pure-tone responses calculated at stimulus-power-matched levels. STRF bandwidth was narrower than FRA bandwidth for both CNIC (STRF mean=0.19oct, FRA mean=0.78oct, p<0.0001) and CtxIC (STRF mean=0.31oct, FRA mean=1.72oct, p<0.0001)., CNIC FRA bandwidths were narrower than CtxIC FRA bandwidths (p<0.0001). Two-way ANOVA with post hoc Tukey's multiple comparisons test.

B. STRF E bandwidth was narrower than FRA bandwidths at all tested levels relative to threshold in both CNIC and CtxIC units (Multiple Mann-Whitney tests with $p<0.006$ considered significant).

C. Representative two-tone suppression responses from two units from the CNIC (left) and CtxIC (right). Best frequency was approximated as the frequency at which the peak response occurred when F1=F2. The left example illustrates sharply tuned, strong sideband suppression while the right example shows more variable suppression with multiple peaks and valleys (right). From the two-tone suppression plots, we extracted the maximal percent suppression (red circles), and area under the curve (AUC, shaded region).

D. The degree of maximal percent suppression was similar between CNIC and CtxIC units. The average maximal suppression was 68% in the CNIC and 75% in the CtxIC. There was no significant difference between the populations ($p=0.40$, Unpaired t test).

E. Total sideband suppression (AUC) from -1 to 1 oct was similar between CNIC (median=0.95) and CtxIC (median=0.90) units ($p=0.68$, Mann-Whitney test).

Table 4. The effects of probe location and stimulus type on the bandwidth of the STRF and power matched FRA

Two-way ANOVA table

	SS (Type III)	DF	MS	F (DFn, DFd)	P value
Interaction	10.62	1	10.62	F (1, 278) = 69.84	<0.0001
Probe location	17.91	1	17.91	F (1, 278) = 117.8	<0.0001
Stimulus type	63.49	1	63.49	F (1, 278) = 417.6	<0.0001
Residual	42.27	278	0.15		

Tukey's multiple comparisons test

	Mean 1 (oct)	Mean 2 (oct)	Mean Diff.	95% CI of diff.	Adjusted P value
CNIC: FRA vs CNIC: STRF	0.78	0.19	0.59	0.40 to 0.78	<0.0001
CNIC: FRA vs CtxIC: FRA	0.78	1.72	-0.94	-1.14 to -0.74	<0.0001
CNIC: FRA vs CtxIC: STRF	0.78	0.31	0.47	0.27 to 0.66	<0.0001
CNIC: STRF vs CtxIC: FRA	0.19	1.72	-1.53	-1.68 to -1.37	<0.0001
CNIC: STRF vs CtxIC: STRF	0.19	0.31	-0.12	-0.28 to 0.03	0.18
CtxIC: FRA vs CtxIC: STRF	1.72	0.31	1.40	1.24 to 1.57	<0.0001

Red p-values indicate statistical significance

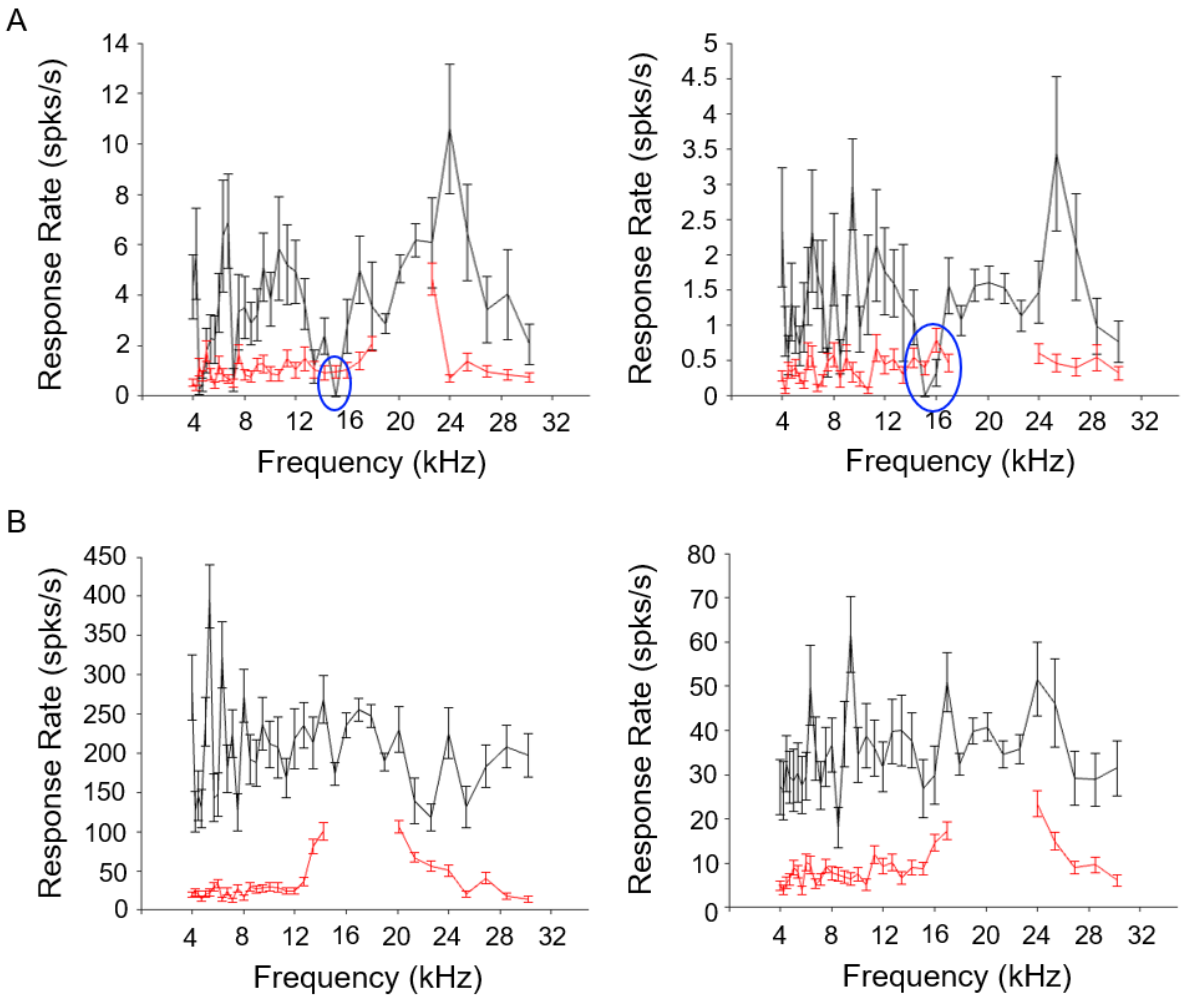

Figure 8. Single units in the IC may exhibit inhibition, facilitation, or both in the presence of sideband stimulation

Response pofiles were similar between CNIC and CtxIC units. A and B depict the response rates of representative CNIC units to stimulus bins that contained the frequencies within the excitatory response profile (black lines, mean and SEM) and to those that did not (red lines, mean and SEM).

A. Example of a single unit with lateral suppression, where the response rate to a stimulus bin that contained frequencies in the excitatory response profile as well as those in the sidebands was lower than that of the response to just sideband stimulation (blue circles).

B. Example of a single unit that maintained higher response rates when the stimulus contained frequencies within the excitatory response profile, regardless of the presence of sideband frequencies.

In all examples, there is also evidence of facilitation, where the response rate in the sideband is higher than that of the response to bins containing only the excitatory frequencies.

Together, these data suggest that neurons in the IC may experience inhibition, facilitation, or both in the presence of sideband stimulation.

2.3.4 The majority of IC single units are gap detecting, with similar gap detection thresholds in CNIC and CtxIC units

Having established these basic differences in tuning properties between CNIC and CtxIC units, we presented a series of stimuli to further probe the temporal integration properties of these units. First, we presented pure tones with embedded gaps to determine neural response types and gap detection thresholds. We classified single units according to three main response types: onset, sustained, and offset (Figure 9A). Units that did not fit into these three categories were classified as other. The response type was determined based on an approximation to the best frequency, which we estimated as the frequency that elicited the highest firing rate in the absence of a gap. We acknowledge that this strategy might bias our analyses in favor of onset and sustained responders. In addition to characterizing the response type using the objective measures described in the methods section, each response was also manually inspected and only one unit displayed an offset response. The percentage of single units in the onset, sustained, and other categories were roughly equal in both the CNIC and CtxIC (Figure 9B, bottom). Single units classified as "other" responders typically had inconsistent response types that varied between trials, typically between onset and sustained response types. These data suggest that both the CNIC and CtxIC have units with heterogenous gap-response types with no significant difference between the two populations.

Single units in the CNIC and CtxIC were similar in their gap detection responses. The majority of units (CNIC= 65%, CtxIC=73%) detected gaps at one or more tested frequencies (Figure 9B, top). At the estimated BF, the distribution of gap detection thresholds of units in the CNIC and CtxIC were relatively uniform, with gap detection thresholds distributed across all gap lengths (Figure 9C). There was no difference in the cumulative distributions of gap detection thresholds between the two groups ($p=0.81$). While 59% (60/102 single units) of CNIC units exhibited a minimum gap detection threshold at the estimated best frequency, 41% (42/102 single units) had minimum gap detection thresholds in the sidebands. In the CtxIC, 37% (41/112 single units) of single units exhibited a minim gap detection threshold at the estimated best frequency while 63% (71/112 single units) had minimum gap detection thresholds in the sidebands. However, there was no difference in the cumulative distributions of CNIC and cortex of IC ($p=0.42$). While the frequencies tested here are too far apart to truly characterize gap detection in the sideband, these data suggest that a subset of IC neurons may have improved gap detection in the sideband and warrants further investigation. In summary, our data indicate that neurons in the CNIC and CtxIC have similar gap detection capabilities, with the majority of neurons responding to silent gaps in pure tones and similar distributions in their response types and gap detection thresholds.

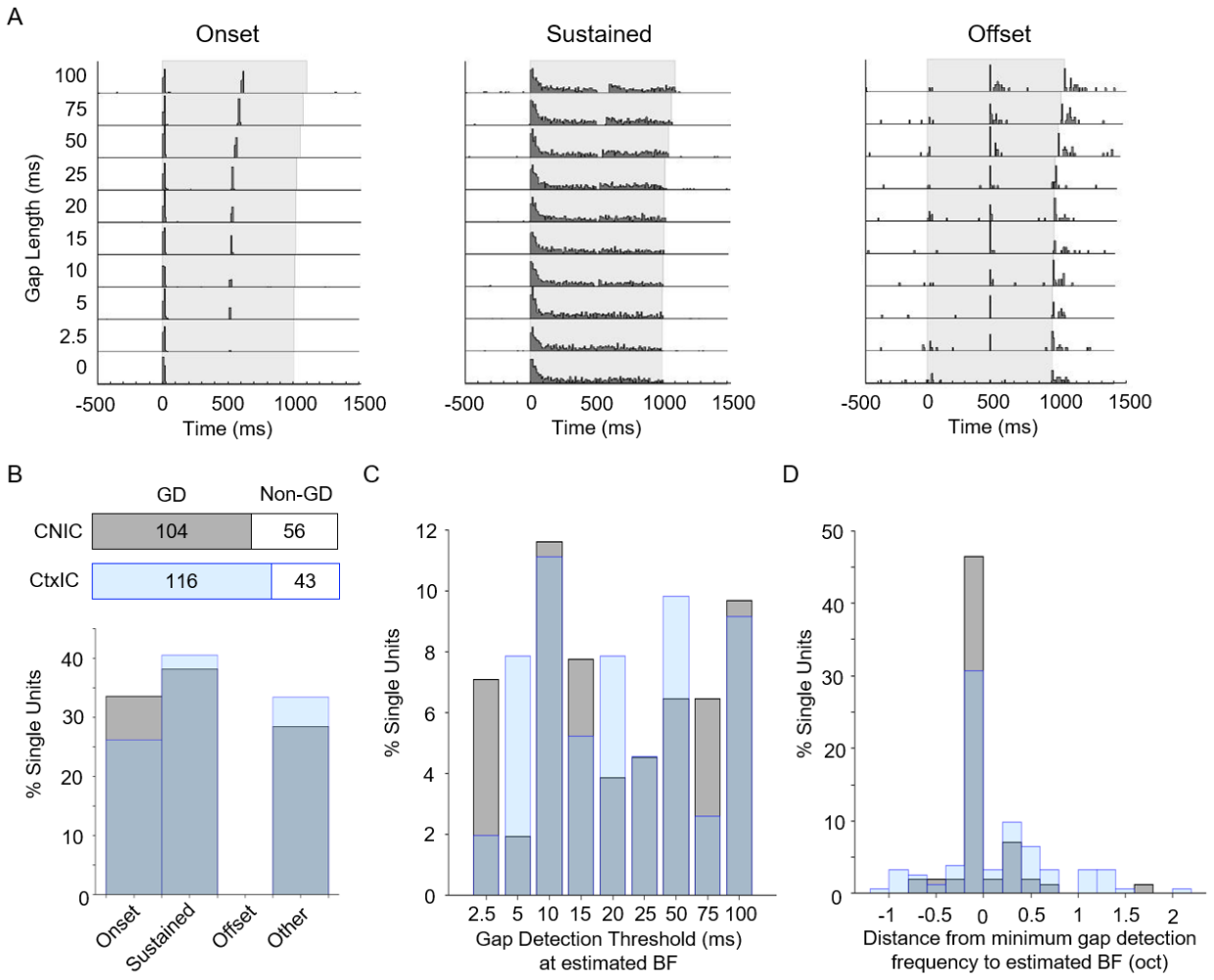

Figure 9. The majority of IC units exhibit gap detection, with similar distributions in response type and gap detection thresholds in units of the CNIC and CtxIC

A. Examples of single units showing onset (left), sustained (middle), and offset responses (right). One unit exhibited an offset response type but not at the estimated best frequency, which was defined as the frequency eliciting the highest firing rate when no gap was present.

B. In the CNIC, the majority, 65% (104/160), of single units exhibited gap detection (GD) at one or more frequency (top). Similarly, in the CtxIC, 73% of single units (116/159) exhibited gap detection (top). The distribution of response types at the estimated best frequency of units in the CNIC and CtxIC was similar (bottom).

C. Gap detection thresholds were distributed across all tested gap lengths in both the CNIC and CtxIC. There was no difference in the cumulative distributions of gap detection thresholds between the two groups (p=0.81, Kolmogorov-Smirnov test).

D. Distributions of from the difference (in octaves) between the minimum gap detection frequency and the estimated best frequency were indistinguishable between CNIC and CtxIC (p=0.42, Kolmogorov-Smirnov test). This analysis also reveals that not all single units exhibited a minimum gap detection threshold at the estimated best frequency.

2.3.5 The majority of single units in the CNIC and CtxIC responded to amplitude modulated tones, with the temporal best modulation frequency (tBMF) lower than the rate-based best modulation frequency (rBMF)

In addition to gap detection thresholds, we assessed temporal processing by characterizing responses to sinusoidal amplitude modulated (sAM) tones. The majority of single units responded to sAM tones, with similar responses in the CNIC and CtxIC. Synchrony, or temporal modulation of firing rate, was observed in 73% (97/133 single units) of CNIC units and 57% (90/158 single units) of CtxIC units at one or more carrier frequency (Figure 10A, top). The distribution of the tBMF was similar between CNIC and CtxIC units, with a median tBMF of 12Hz in both populations (Figure 10A, bottom). There was no significant difference in the cumulative distributions of the tBMF in CNIC or CtxIC (p=0.13). Modulation of response rate as a function of sAM frequency was observed in 89% (118/133 single units) of CNIC units and 84% (133/158 single units) of CtxIC units at one or more carrier frequency (Figure 10B, top). The distribution of the rBMF was skewed towards higher frequencies for both CNIC and CtxIC units, with a median rBMF of 64Hz in both populations. There was no significant difference in the cumulative distributions of the rBMF in CNIC and CtxIC (p=0.62). Together, these data suggest that while CNIC neurons demonstrate an increased propensity for synchronized responses, no significant differences could be observed between CNIC and CtxIC for sAM responses.

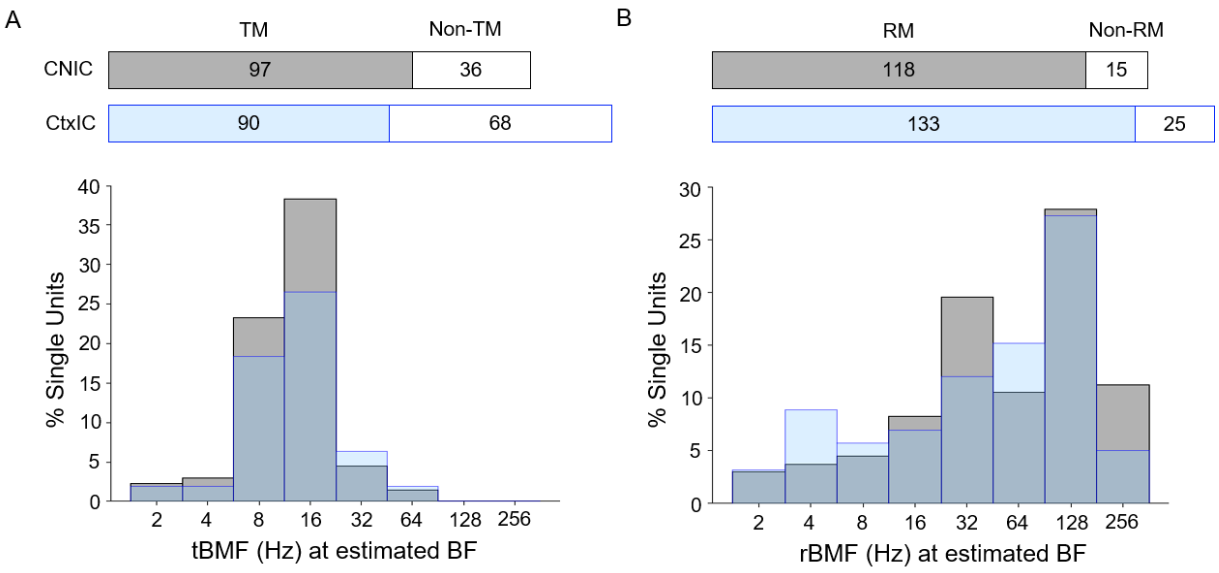

Figure 10. The majority of single units in the CNIC and CtxIC respond to amplitude modulated tones, with a temporal best modulation frequency (tBMF) lower than the rate-based best modulation frequency (rBMF)

A. The majority of single units temporally modulated their firing rates in response to sAM stimuli, with 73% (97/133 single units) of CNIC units and 57% (90/158 single units) of CtxIC units reaching a significant vector strength (Rayleigh statistic $\geq$ 13) at one or more carrier frequency. There was no significant difference in the cumulative distributions of the tBMF in CNIC and CtxIC (p=0.13, Kolmogorov-Smirnov test).

B. The majority of single units also exhibited changes to firing rate as a function of sAM frequency, with 89% (118/133 single units) of CNIC units and 84% (133/158 single units) of CtxIC units demonstrating significant rate modulation at one or more carrier frequency. There was no significant difference in the cumulative distributions of the rBMF in CNIC and IC cortex (p=0.62, Kolmogorov-Smirnov test).

2.3.6 Single units can be reliably classified as located in CNIC or CtxIC based on their responses to pure tone stimuli

In the previous sections, we have demonstrated that CNIC and CtxIC units differ significantly in their responses to pure-tone and STRF stimuli that confer subtly different tuning properties onto these units. We thus explored if these differences could be leveraged during an

experiment to determine recording location. We focused on responses to pure-tones because in contrast to STRF estimation, which is a more time-consuming and computationally intensive process, FRA parameters such as latencies, bandwidths etc. can be quickly estimated online. To determine if recording location could be ascertained from pure-tone responses, we used three machine learning algorithms (LR, SVM, and RF) with variables extracted from the FRA to train classification models (Table 1). All three model types provided robust classification, with an average area under the ROC curve of 0.8 when using the LR or SVM and 0.9 for the RF (Figure 11, Table 5). Thus, variables extracted from the FRA were sufficient for robust classification of recording location.

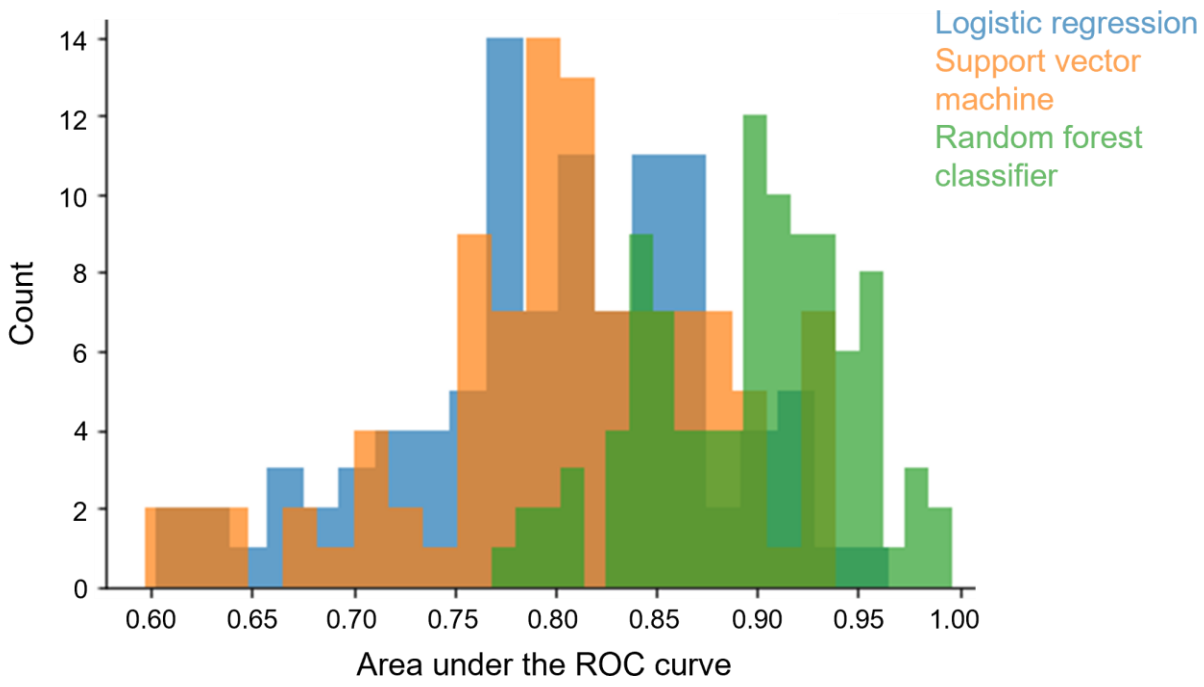

Figure 11. Single units can be reliable classified as CNIC or CtxIC units using factors derived from the FRA

Each histogram represents the area under ROC curve of the 100 iterations testing the performance of the logistic regression (blue), support vector machine (orange), and random forest classifiers (green). All three models performed well in terms of discrimination, with the random forest classifier achieving the highest performance. The average area under the ROC curve for each model was: logistic regression= 0.80 (0.006, variance), support vector machine= 0.81 (0.006), random forest classifier= 0.90 (0.002).

Table 5. Accuracy and area under the ROC curve of all three models

	Logistic Regression Mean (variance)	**Support Vector Machine** Mean (variance)	**Random Forest Classifier** Mean (variance)
Accuracy	0.76 (0.004)	0.78 (0.004)	0.84 (0.004)
Area under the ROC curve	0.80 (0.006)	0.81 (0.006)	0.90 (0.002)

2.4 Discussion

Using an extensive stimulus battery to characterize receptive field properties and to probe temporal and spectral integration, our experiments in anesthetized mice demonstrate subtle but significant differences between the response properties of CNIC and CtxIC neurons. In their STRFs, CNIC neurons showed narrower tuning and slower temporal response profiles than CtxIC neurons. Compared to CtxIC neurons, neurons in the CNIC had lower and less variable spontaneous firing rates, and in response to pure tones, showed longer onset latencies, higher thresholds, narrower and more symmetric tuning, and had a higher incidence of non-monotonic rate-level functions. However, in our preparation, these basic receptive field differences did not reliably translate to differences in responses to other commonly used stimuli, such as tones with embedded gaps and amplitude-modulated tones. Parameters derived from the FRA, when combined, could be reliably used to classify neurons as CNIC or CtxIC using machine learning methods, with non-linear methods (the RF classifier) achieving the highest performance. We can thus use these response property differences to determine recording location online during electrophysiological experiments. Online determination of location is critical in several experimental procedures, such as the injection of viral vectors or pharmacological agents, lesioning defined areas of interest, or microstimulation of functionally specific regions. Localization based on response properties alone would especially benefit targeting IC subdivisions in species where the IC is not close to the surface and is difficult to assess stereotactically (for example, in non-human primates) (Rocchi and Ramachandran, 2018; Slee and Young, 2011; Wang et al., 2022). Our results serve as proof-of-principle that such localization can be accomplished robustly and efficiently using responses to simple stimuli such as pure tones.

The differences we observed in the tuning bandwidth of neurons in the CNIC and CtxIC is consistent with previous reports in the cat and guinea pig (Aitkin et al., 1975; Syka et al., 2000) and may reflect the response properties of their inputs. The CNIC is the primary target of ascending projections from the cochlear nucleus (CN), superior olivary complex (SOC), and the lateral lemniscus (LL) (Beyerl, 1978; Cant, 2005; Coleman and Clerici, 1987; Oliver, 2005; Oliver et al., 1995; Riquelme et al., 2001; Shneiderman et al., 1988), while the CtxIC is the primary target of efferent and multimodal projections (Coleman and Clerici, 1987; Faye-Lund, 1985; Li and Mizuno, 1997; Oliver, 2005; Wise and Jones, 1977). The lateral CtxIC, however, receives some ascending input from the CN and sparse projections from the LL (Brunso-Bechtold et al., 1981; Cant and Benson, 2003; Coleman and Clerici, 1987; Oliver et al., 1999, 1997). The CNIC receives input from all CN subdivisions and a variety of cell types, including fusiform cells in dorsal cochlear nucleus (DCN), round and oval cells in anteroventral cochlear nucleus (AVCN), and round, oval, fusiform, and multipolar cells in the posteroventral cochlear nucleus (PVCN) (Coleman and Clerici, 1987). Conversely, the lateral CtxIC receives more restricted inputs from fusiform cells in DCN and multipolar cells in PVCN (Coleman and Clerici, 1987). While the CtxIC receives input from a limited number of CN subdivisions and cell types, they overlap with those that project to the CNIC, making it difficult to discern if these inputs contribute to the increased bandwidth we observed in CtxIC neurons compared to CNIC neurons. However, corticofugal projections from layer 5 the auditory cortex primarily target the CtxIC, and exhibit broad tuning (Williamson and Polley, 2019). Given the relative sparsity of ascending projections to the CtxIC, the tuning bandwidth of neurons in the CtxIC may be influenced primarily by efferent and intrinsic projections.

Interestingly, we observed increased onset latencies in the CNIC compared to the CtxIC, which is in opposition to what has been previously described in the guinea pig (Syka et al., 2000). The primary source of auditory inputs to the CtxIC is the ipsilateral CNIC and the auditory cortex (Morest and Oliver, 1984; Oliver, 2005), as such, we expected to find increased onset latencies in the CtxIC. One possibility is that onset latencies are inherited from ascending projections to the CNIC and CtxIC. As previously stated, the CN projects directly to the CNIC and CtxIC. However, the research on the response types in the CN appears to be either cell type (Cant and Benson, 2003) or region specific (Goldberg and Brownell, 1973), but not both. Furthermore, there is overlap in the CN subdivisions and cell types that project to the CNIC and CtxIC. Thus, further research is needed to investigate the response properties of neurons in the CN according to location, cell type, and projection target.

Our study must be interpreted keeping in mind two limitations. First, our data were acquired under anesthesia. The differences we observed in the frequency response properties of neurons in the CNIC and CtxIC may thus be due to distinct effects of anesthesia on these two populations. One potential source of variability is the effects of anesthesia on afferent and efferent pathways. While both the CNIC and CtxIC receive inputs from a variety of sources, the CNIC is the primary recipient of ascending auditory input (Beyerl, 1978; Coleman and Clerici, 1987; Shneiderman et al., 1988) while the CtxIC receives the majority of the efferent projections from the primary auditory cortex (Druga et al., 1997; Druga and Syka, 1984; Faye-Lund, 1985). Our observations differ from a previous study in guinea pigs, which showed that even in the anesthetized state, neurons in the CNIC have lower thresholds, shorter onset latency, and higher spontaneous firing rates than neurons in the CtxIC (Syka et al., 2000). Because the auditory cortex is especially suppressed under isoflurane anesthesia, and thus might have a strong effect on

descending inputs to the CtxIC, and because we did observe that CtxIC neurons exhibited a lower threshold, higher spontaneous rate, and shorter latency compared to CNIC neurons, we may have observed primarily the impact of other (i.e. non-corticocollicular) inputs to the CtxIC in our preparation, which may explain some of this discrepancy. Isoflurane anesthesia is also known to increase auditory brainstem response thresholds more than ketamine and xylazine (Cederholm et al., 2012), which may explain the higher thresholds we encountered in CNIC. However, a primary goal of our study was to localize region based on response properties alone in order to enable other procedures such as lesioning and viral vector injections that are typically carried out under anesthesia. Therefore, our ability to correctly localize CNIC and CtxIC neurons based on response properties is well suited to these applications.

A second limitation we encountered was methodological. While recording using high-density multielectrode arrays enabled us to simultaneously record the activity of a large number of neurons, we could reap the benefits of this technique only when using fixed stimulus sets. But when stimuli needed to be tailored to a specific neuron's preferences – for example, for choosing the carrier frequency for tone AM stimuli or for fixing one frequency at the BF for two-tone stimuli – array recordings were not optimal. In our experiments and analyses, we approximated the best frequency for two-tone, gap detection, and MTF analysis because we could not assess individual neuron BFs online. This may have affected our interpretation of results from the gap detection, amplitude modulation, and two-tone experiments. Indeed, this factor may have contributed to why we observed temporal receptive field differences between the STRFs of CNIC and CtxIC neurons that did not extend to gap-detection and two-tone stimulus sets.

In our preparation, the primary differences between the response properties of CNIC and CtxIC neurons were more apparent in their FRA response properties rather than in their temporal

response properties. Interestingly, in both the CNIC and CtxIC, we saw increased specificity in the STRF excitatory frequency response profile compared to the FRA. While we did not see evidence of side-band suppression in the STRF, we hypothesized that the increased specificity of STRFs may be the result of lateral inhibition, as previous research has shown that frequency tuning in the IC is shaped by inhibition (Egorova et al., 2001). Our two-tone suppression data confirmed that neurons in the IC are subject to strong side-band suppression (approximately 70% decrease in firing rate), which might reflect this underlying lateral inhibition. However, because of the second limitation outlined above, we could only test this in a smaller subset of neurons. As previously mentioned, this method also prevented us from observing two-tone facilitation (which is a rare occurrence in mice, see Egorova et al., 2001). Regardless, the neurons that met our inclusion criteria support the hypothesis that lateral inhibition may contribute to increased specificity in the STRF compared to the FRA.

The STRFs of CNIC and CtxIC neurons also showed differences in temporal integration, with CNIC neurons showing slower temporal modulation in the STRF than CtxIC neurons. But in our preparation, these differences did not translate to other commonly used measures of temporal processing, with CNIC and CtxIC neurons showing similar gap detection thresholds and temporal and rate-based modulation in response to AM tones. Interestingly, we did see that a higher fraction of CNIC neurons demonstrated temporally modulated responses to AM stimuli compared to CtxIC neurons. Previous research suggests that both the rate and temporal-based modulation in the CNIC is stimulus dependent and varies based on the carrier frequency and sound pressure level (Krishna and Semple, 2000). Of particular relevance to our study, however, was the finding that rate and temporal-based modulation was observed at multiple carrier frequencies (Krishna and Semple, 2000). Based on this, our observation that a higher number of CNIC neurons exhibit temporally

modulated responses to AM tones is likely indicative of a true difference and not an effect of the carrier frequencies. If further research confirms this finding, it could represent a functional difference in the role of the CNIC and CtxIC in sound processing. One such example could be in sound localization via interaural time differences (ITD). Both human and animal research suggests that ITD in the envelope may be used in sound localization (Bernstein and Trahiotis, 2012, 2008, 1994; Klein-Hennig et al., 2011; Li et al., 2019; McFadden and Pasanen, 1976; Nuetzel and Hafter, 1976; Ono et al., 2020). The neural basis of envelope ITD encoding begins with the auditory nerve, which is well synchronized to sounds in our AM range (Joris et al., 2004). Recent research suggests that the mouse IC is sensitive to ITD in the sound envelope (Ono et al., 2020). Thus, an increase in the number of temporal modulating cells in the CNIC may indicate that the CNIC contributes more to envelope ITDs than the CtxIC.

Regardless of whether differences were present to these more specific stimulus sets, we found that we could classify the location of CNIC and CtxIC neurons with high accuracy based on FRA parameters alone. Of the tested classifiers, the RF had the best average performance, which could reflect the features of the model itself or the structure and dimensionality of the training data. LR and linear SVM algorithms both construct a single classification model with a linear decision boundary from a training dataset, whereas the RF algorithm constructs an ensemble of decision tree models using random subsets of variables from a single training dataset (Breiman, 2001). The RF algorithm uses the aggregate outputs from the collection of trees (which are nonlinear classifiers) to classify a sample, and this reduces variance without increasing overall bias, resulting in lower error and improvements in predictive performance over single models (Hastie et al., 2009). The superior performance of the RF algorithm in differentiating CNIC and CtxIC neurons

may therefore be a result of the use of decision trees (which can better handle nonlinearities in data) and/or an ensemble approach.

While ensemble approaches typically increase performance, they usually do so at the expense of interpretability regarding variable interactions compared to single decision trees. However, one of the key benefits of the RF classifier is that it can rank variables by importance. Furthermore, the RF algorithm weights variables or combinations of variables for each group individually. Thus, it is possible that different variables or combinations of variables are significant for CNIC versus CtxIC. Given the small number of variables included in our modeling, we did not analyze the significance of each variable in classification. However, future research using this approach may provide insight into which response properties are the most salient and how neural characteristics interact to create the diverse range of responses seen in the IC.

The use of machine learning algorithms to understand the salience of neural responses is growing and has a number of applications. A recent study in the CtxIC demonstrated that the population response in this region is predictive of behavioral outcomes (Quass et al., 2022). Interestingly, the responses to hits and false alarms were divergent, suggesting that, on a population level, the CtxIC is integrating acoustic information, motor or pre-motor activity, and behavioral outcomes (Quass et al., 2022). This study is the first to demonstrate behaviorally relevant representations at the level of the IC (Quass et al., 2022) and encourages further research into the response properties at the single unit level that contribute to this population response.

To our knowledge, this study is the first to attempt to classify neurons as belonging to the CNIC or CtxIC based on their response properties. Our results suggest that the location of recorded neurons can be reliably identified using relatively simple stimuli and demonstrate the utility of appropriate machine learning techniques may be useful in characterizing neuron types in the IC.

In addition to their use in discriminating neurons from the CNIC and CtxIC, another application for machine learning models could be to distinguish between neural classes within a subdivision. Indeed, the cell types of the IC are largely heterogeneous, and it has been difficult to characterize neurons using neuromodulators and response properties alone. Machine learning methods may provide a means to discriminate between neural populations in the IC.

3.0 Embryonic medial ganglionic eminence cells survive and integrate into the inferior colliculus of adult mice

3.1 Introduction

Acoustic overexposure is a common problem that can lead to hearing loss as well as deficits in temporal processing (Phillips et al., 1994), tinnitus (Coomber et al., 2014; Middleton et al., 2011; Sturm et al., 2017; Wang et al., 2009; Yang et al., 2011), and hyperacusis (Knipper et al., 2013; Manohar et al., 2017). Even in the absence of auditory threshold shifts, auditory processing deficits related to acoustic overexposure can occur, suggesting subtle but clinically significant changes in hearing (Gu et al., 2010; Roberts et al., 2010; Weisz et al., 2006) which can have a detrimental effect on quality of life (Ayodele et al., 2020; Bartels et al., 2008; Reynolds et al., 2004; Weidt et al., 2016). Despite ongoing research efforts, the etiology of these otologic conditions remains elusive and as a result, few treatment options are available. The central gain model proposes that peripheral damage reduces neural activity at the level of the auditory nerve while paradoxically increasing spontaneous and sound evoked responses in the midbrain, thalamus, and auditory cortex (Asokan et al., 2018; Auerbach et al., 2019, 2014; Mulders and Robertson, 2009). As a result, decreased inhibition in central auditory circuits is hypothesized to mediate, at least in part, these subtle changes in auditory processing (Auerbach et al., 2019; Coomber et al., 2014; Ma et al., 2006; Middleton et al., 2011; Mulders and Robertson, 2013, 2009; Pedemonte et al., 1997; Resnik and Polley, 2017; Richardson et al., 2012; Sturm et al., 2017; Wang et al., 2009; Yang et al., 2011). Attempts to correct this hyper-excitable state in animal models have focused on increasing GABAergic inhibitory tone, with some success in mitigating

behavioral changes following noise exposure (Brozoski et al., 2010, 2007; Yang et al., 2011). Despite some success in animal models, there are currently no FDA approved drugs to treat tinnitus or hyperacusis. The use of gabapentin in humans has had mixed results, with one study showing partial relief from tinnitus in select patients with a history of acoustic trauma (Bauer and Brozoski, 2006) while another demonstrates no improvement compared to placebo (Piccirillo et al., 2007). These conflicting results and the side effect profile of these drugs, which impose limits on dose, duration, and safety of use, make them suboptimal. Rather than systemic administration, a more precise treatment that could locally increase inhibition in central auditory nuclei may allow for more consistent results while minimizing off-target side effects.

The inferior colliculus (IC) is a major subcortical auditory integration center, receiving ascending input from most auditory brainstem nuclei (Frisina et al., 1998), commissural input from the contralateral IC (Chandrasekaran et al., 2013; Ito and Oliver, 2014; Malmierca et al., 2003, 1995; Rees and Orton, 2019; Saldaña and Merchán, 1992), descending input from the auditory cortex (Saldaña et al., 1996; Winer, 2006), and a vast intrinsic network (Ito and Oliver, 2014; Malmierca et al., 1995; Miller et al., 2005; Oliver et al., 1991; Saldaña and Merchán, 1992; Sturm et al., 2014, 2017; Wallace et al., 2012). Acoustic overexposure leads to hyper-excitable changes in neural responses of IC neurons, including increased spontaneous firing rates (SFRs) and bursting activity (Berger et al., 2014; Coomber et al., 2014; Longenecker and Galazyuk, 2016; Ma et al., 2006; Mulders and Robertson, 2013, 2009), increased tuning broadness (Ma et al., 2006), and increased neural gap detection thresholds (Berger et al., 2014). The acoustic startle response (ASR), a reflexive behavior, has been exploited to determine the effects of noise exposure on central auditory gain, temporal processing, and sensorimotor gaiting. Indeed, hyper-excitability in the IC is associated with deficits in behavioral gap detection, a measure of temporal processing

that is commonly used as an animal model for tinnitus (Berger et al., 2014; Chen et al., 2013; Hayes et al., 2014; Sturm et al., 2017; Turner et al., 2006). Additionally, the IC appears to be critical for acoustic pre-pulse inhibition, a measure of sensorimotor gating, as lesioning the IC abolishes this behavior in naïve mice (Koch and Schnitzler, 1997; L. Li et al., 1998). Moreover, the magnitude of PPI is correlated with hearing loss and associated plasticity (Carlson and Willott, 1996; Willott and Turner, 2000). Together, this suggests that the IC plays an important role in mediating acoustic behaviors that are affected by acoustic overexposure. Thus, the IC is a particularly apt target to explore the effects of local increases in inhibition to restore normal auditory behavior.

One potential approach to locally increase inhibition is through transplantation of cells harvested from the embryonic medial ganglionic eminence (MGE), the birthplace of cortical inhibitory interneurons (Lavdas et al., 1999). While naturally destined for the cerebral cortex, these inhibitory neuron precursors survive, mature, and integrate into the post-natal cortex, striatum, hippocampus, amygdala, thalamus, and even the adult spinal cord (Alvarez-Dolado et al., 2006; Baraban et al., 2009; Bráz et al., 2012; Hammad et al., 2015; Martínez-Cerdeño et al., 2010; Derek G Southwell et al., 2010; Southwell et al., 2014; Wichterle et al., 1999; Yang et al., 2016). However, the fate of transplanted MGE cells in auditory structures and the brainstem remains unknown. Because survival, migration, and circuit integration of transplanted MGE cells is influenced by tissue environment (from 20% survival in the postnatal cortex (Alvarez-Dolado et al., 2006), to 1.3% survival in injured adult spinal cord (Bráz et al., 2012)), it is necessary to evaluate the fate of MGE cells in an auditory center to determine if this is a viable approach to locally increase inhibition following acoustic overexposure.

In the present study we characterized the migration, differentiation, and integration of transplanted MGE cell in the IC of non-noise exposed and noise exposed mice. Our results provide evidence that transplanted MGE cells survive, migrate, and differentiate into primarily inhibitory neurons in the IC of adult mice, with equal viability in non-noise exposed and noise exposed mice. Importantly, transplanted MGE cells integrate into the IC, forming synapses with and receiving synapses from endogenous IC neurons, and are active, with a high percentage of the MGE cells expressing c-fos in quiescent and stimulated conditions.

3.2 Methods

Experimental procedures were performed in accordance with National Institutes of Health guidelines and were approved by the Institutional Animal Care and Use Committee at the University of Pittsburgh.

3.2.1 Animal subjects

All experiments were performed in mice. Two types of donor mouse lines were used to harvest MGE cells. First, MGE cells were collected from homozygous Tg(act-EGFP)Y01Osb (green) mice (Jax #006567) which have widespread expression of green fluorescent protein (GFP) in all cells, with the exception of erythrocytes and hair. Alternatively, mouse lines were bred to create a second donor line, in which MGE cells could also provide information on neurotransmitter phenotype. A GABAergic phenotype was indicated by VGAT-driven expression of the fluorescent protein tdTomato. First, VGAT-ires-cre mice (Jax 016962, 129S6/SvEvTac background) were

crossed with the Ai9/tdTomato cre reporter line (Jax 007909, C57BL/6J background), to create a "VGAT-dT" line that is homozygous for both cre and dT. VGAT-dT was then crossed with the homozygous "Green" line. Resulting MGE cells carried a single gene of VGAT-ires-cre, tdTomato, and GFP. Host mice were either wild type C57 (Jax 000664) or CBA/CaJ mice (Jax 000654). C-fos expression in non-injected subjects was evaluated in non-noise exposed VGAT-dT mice and in noise exposed CBA/CaJ mice.

3.2.2 MGE cell collection

Collection and dissociation of MGE tissue explants was performed using previously described methods (Alvarez-Dolado et al., 2006). MGE tissue explants were collected between embryonic days 12 and 14 (E12-E14), with identification of the sperm plug representing E0. Briefly, pregnant dams were anesthetized with vaporized isoflurane and sacrificed via cervical dislocation. A "T" shaped incision was made along the abdomen and pelvis and the uterine horns were dissected out for collection of the embryos, which were placed in ice cold Hank's buffer. Embryos were collected from homozygous green mice or green mice crossed with VGAT-dT mice, to allow for determination of which transplanted cells were GABAergic (dT+). Embryos from green x VGAT-dT pairs were inspected for cre-recombination and discarded if RFP was observed outside the brain and spinal cord. The embryos were isolated and dissected individually in fresh, ice-cold Hank's buffer. After decapitation, the layer of cortical tissue was peeled back to expose the medial and lateral geniculate eminences (MGE and LGE respectively). The sulcus between the MGE and LGE was extended caudally to free the MGE. The MGE was then trimmed and collected in a sterile Eppendorf tube containing ice cold L-15 media. Once all the MGEs were collected the L-15 was removed and replaced with fresh L-15 media. The MGEs were

mechanically dissociated by withdrawing and returning the mixture 10-15 times through a 200 µL pipette tip. The suspension was then centrifuged at 2000 rpm for 3 minutes. The L-15 was removed and replaced with fresh L-15 media and the pellet of MGE cells was mechanically dissociated and centrifuged again in the same fashion. Finally, the cells were re-suspended in an appropriate volume of fresh L-15 to achieve a final concentration of approximately 100 cells/nL.

3.2.3 Stereotaxic injection

Intracranial injection of MGE cells into the IC was performed in mice aged between 5 and 9 weeks. Subjects were anesthetized with vaporized isoflurane anesthesia (3%) prior to being moved to the stereotaxic apparatus where the anesthesia was lowered to 2-2.5%. Body temperature was monitored and maintained at 36.5-38.5˚C (FHC DC temperature controller). The IC was targeted using stereotaxic coordinates (AP ~5.3mm posterior to bregma, ML ~1.3 mm from the midline). A 0.9-1.4mm burr hole was drilled into the skull using a stereotaxic mounted drill (Model 1474, Kopf). MGE cells were injected bilaterally into the IC of CBA/CaJ or C57 mice using pulled glass pipettes (~50um tip diameter). A total of 100-150nL of the MGE cell suspension was injected into either two sites spaced 1mm apart or ten sites spaced 0.1mm apart, at a rate of 1nL/sec (Nanoject III, Drummond).

3.2.4 Noise exposure

Mice of either sex (3.7-6.7 weeks old) were randomly selected for noise exposure (NE). NE consisted of bandpass-noise from 8-16kHz presented at 100dB SPL for 2 hours. The loudspeaker was a planar isodynamic tweeter (RT2H-A, HiVi, CA), with a relatively flat

frequency response (1.7-25kHz), and uniformly distributed sound energy. All NE was performed in a sound attenuating chamber (Medical Associates). Subjects were placed in a custom-built housing apparatus, constructed from a frame of Lego parts covered by a fine plastic mesh, designed to minimize changes in sound intensity due to changes in position (Clause et al., 2011). Sound intensity was calibrated to the center of the housing apparatus. Subjects were awake and allowed to move freely within the apparatus for the duration of the noise exposure.

3.2.5 C-fos experiments

C-fos experiments were performed in control (non-injected, non-NE), NE (non-injected, NE), MGE injected (non-NE and injected), and NE and MGE injected mice. Mice were randomly selected for exposure to 4 hours of quiet or 2 hours of quiet followed by 2 hours of 90dB SPL white noise pulses, 500ms in length delivered at 1 Hz. Following exposure to quiescence or sound stimulation, all mice were perfused and their brains processed for c-fos immunohistochemistry.

3.2.6 Immunohistochemistry

Host mice (1-22 weeks following MGE cell transplantation) were anesthetized through intraperitoneal injection of ketamine (100mg/kg) and xylazine (10mg/kg) and transcardially perfused with 0.1M PBS followed by 4% paraformaldehyde (PFA) in 0.1M PBS. The brains were dissected and post fixed in 4% PFA for 2 hours at room temperature or overnight at 4˚C. Following post fixation, the brains were cryoprotected in 30% sucrose in 0.1M PBS for 48 hours at 4˚C. Coronal sections (50um in thickness) were cut using a freezing microtome.

Immunohistochemistry for the VGAT protein was performed on tissue from host mice injected with GFP-expressing MGE cells. Sections were washed in 0.1M phosphate buffer saline (PBS) and blocked for 2 hours in PBS containing 5% donkey serum and 0.2% Triton X-100. Sections were then incubated in the primary antibody, polyclonal rabbit anti-VGAT (1:8,000; Chemicon AB5062P), diluted in 0.1M PBS containing 5% donkey serum and 0.2% Triton X-100 for 2 hours at room temperature and overnight at 4˚C. Sections were washed five times in 0.1M PBS and incubated in secondary antibodies (donkey anti-rabbit Alexa 594, 1:1,000; Thermo Fisher A21207) diluted in 0.1M PBS containing 5% donkey serum and 0.2% Triton X-100 for 2 hours at room temperature. Sections were washed three times in PBS, mounted onto superfrost plus microscope slides (Fisherbrand), and coverslipped with microscope cover glass (Fisherbrand).

C-fos expression in non-injected subjects was evaluated in non-NE VGAT-dT mice and in NE CBA/CaJ mice; for MGE injected subjects, MGE cells were harvested from green x VGAT-dT embryos and injected into CBA/CaJ mice. Primary antibodies included: polyclonal rabbit anti-human residues 4-17 of c-fos (1:10,000 Oncogene-PC38), polyclonal goat anti-tomato (1:500, Sicgen AB8181-200), and polyclonal chicken anti-GFP (1:500, Aves Labs GFP-1020). Secondary antibodies included: donkey anti-rabbit Alexa 647plus (1:1,000; Thermo Fisher), donkey anti-goat Alexa 568 (1:1,000; Thermo Fisher A11057), and donkey anti-chicken Alexa 488 (1:500; Jackson Immuno Research 703-545-155). Sections were washed in 0.1M PBS and blocked for 2 hours in 0.1M PBS containing 5% donkey serum and 0.25% Triton X-100. Sections were then incubated using the protocol described above. Sections were washed three times in 0.1M PBS, with the second wash containing DAPI (1:1,000). Sections were mounted onto superfrost plus microscope slides (Fisherbrand), and coverslipped with microscope cover glass (Fisherbrand).

3.2.7 Cell counts and quantification

Digitized images of coronal sections were obtained via a fluorescent microscope (Axio Imager, Zeiss or LAS X, Leica). Cells that remained aggregated at the injection site were excluded from analysis. Cells that migrated away from the injection site were counted from every other section, from the first section containing a transplanted MGE cell, and the final count multiplied by two to obtain the extrapolated count (Southwell et al., 2012). MGE survival rate was defined as the extrapolated number of GFP+ cells that migrated away from the injection site divided by the estimated number of injected MGE cells multiplied by 100. This is likely an underestimate of MGE cell survival, as it does not account for cell loss and/or death during the dissociation and injection process. However, this is the standard in the literature and was chosen to allow for comparisons of survival rate in the IC to other brain areas (Alvarez-Dolado et al., 2006; Bráz et al., 2012). The medial/lateral migration distance was defined as the distance from the edge of the injection site (i.e. the border of the clustered MGE cells) to the cell soma. Medial/lateral migration distance was therefore only calculated for cells in the same plane as the injection site. The rostral/caudal migration distance was defined as the number of sections the cell was from a section containing the injection site times the section thickness. Cells in the same plane as the injection site were therefore considered to have zero rostral/caudal migration. The percentage of MGE cells that mature into inhibitory neurons was defined as the number of RFP+ cells divided by the number of GFP+ cells.

Analysis of c-fos immunolabeling was performed in every other section of the IC from non-injected subjects. Analysis in injected subjects was performed in every other section from the first section to the last section containing a transplanted MGE cell. To determine the number of c-

fos positive cells, images were manually thresholded in imageJ. The watershed function was then used to separate touching objects. Finally, the analyze particles function was used to identify regions 20-250μm^2 in size. The identified regions were considered to represent c-fos+ cells and were saved as a ROI map. The number of transplanted MGE cells or VGAT-dT positive inhibitory cells was counted manually. A ROI map of the transplanted MGE cells or VGAT-dT positive inhibitory cells was created and combined with the c-fos map. The combined ROI map was placed over the raw images to visually confirm co-expression of c-fos, RFP, and, in the case of transplanted MGE cells, GFP.

3.2.8 Electron microscopy

The presence of synaptic connections was evaluated in non-NE CBA/CaJ mice at 10-19 weeks post-MGE cell transplantation. Subjects were anesthetized with ketamine (60 mg/kg) and xylazine (6.5 mg/kg) and transcardially perfused with 0.1M phosphate buffer (PB) pH=7.4, followed by 4% PFA and 0.5% glutaraldehyde in 0.1 M PB. Brains were then post-fixed for 90 minutes in the same fixative at 4°C. Following fixation, 80μm coronal sections were cut by vibratome in 0.1M PB and then cryoprotected with an ascendant gradient of glycerol in 0.1M PB. The glycerol gradient involved 30-minute incubations at 10%, 20%, and 30%, followed by an overnight incubation in 30% glycerol. Sections were frozen on dry ice and thawed in 0.1M PB. For the immunohistochemistry, sections were blocked with 10% normal goat serum for 1 hour at room temperature (RT) and incubated overnight at 4°C with a rabbit anti-GFP primary antibody (1:1000, Invitrogen A11122) in 0.1M PB. Sections were then incubated for 1hr at RT in a biotinylated secondary antibody goat anti-rabbit (1:700, Jackson Laboratories) in 0.1M PB. After, sections were incubated in avidin biotin peroxidase complex (ABC Elite, Vector

Laboratories, 60 min, RT), washed in 0.1M PB and developed with 3, 3-diaminobenzidine plus nickel (DAB; Vector Laboratories Kit; 2-5 min reaction). Sections were washed in 0.1M cacodylate buffer and postfixed with 1% osmium and 1.5% potassium ferrocyanide in cacodylate buffer for 1hr at RT. After, sections were dehydrated in an ascending gradient of ethanol (ETOH, 35%, 50%, 70%, 80%, 90%). Sections were blocked-stained with 3% uranyl acetate in 70% ETOH for 2hr at 4°C before proceeding to 80% ETOH. The final dehydration step was performed with 100% ETOH, and propylene oxide followed by infiltration with epoxy resin (EMBed-812, Electron Microscopy Science, PA USA). Sections were flat embedded between Aclar sheets and polymerized in an oven at 60°C for 48 hrs. Selected areas of the IC were trimmed and mounted on epoxy blocks and cut with a Leica EM UC7 ultramicrotome. Ultrathin sections (75-80nm in thickness) were collected on single slot cupper grids with formvar. Ultrathin sections were observed with a JEOL-1400 transmission electron microscope (JEOL Ltd., Akishima Tokyo, Japan) and images were captured with an Orius^{TM} SC200 CCD camera (Gatan Inc., Warrendale, PA, USA).

3.2.9 Statistical analysis

Statistical analysis was performed using GraphPad Prism software. Mann Whitney tests were used to compare two independent groups. Kruskal-Wallis tests were used to compare three or more groups, multiple comparisons were corrected for using the Dunn pairwise method. Two-way ANOVA was used for comparisons in which there were two independent variables, multiple comparisons were made using Tukey's test. Three-way ANOVA was used for comparisons in which there were three independent variables, multiple comparisons of groups that differed by one independent variable were made using Sidak's test. Frequency distributions and cumulative

distributions were generated for migration distance. Cumulative frequency distributions were compared using the two-sample Kolmogorov-Smirnov (K-S) test, multiple comparisons were accounted for using a Bonferroni adjusted p value. Correlations were evaluated using the Spearman correlation. Statistical significance for all tests was set to $p<0.05$ and corrected for in cases of multiple comparisons.

3.3 Results

3.3.1 Transplanted MGE cells survive, migrate, and differentiate into inhibitory neurons in the IC of non-noise exposed and noise exposed mice.

To determine if MGE cell transplantation is viable in the IC, we harvested MGE cells from E12-14 green mouse embryos and injected them bilaterally into the IC of adult C57 mice (Figure 12A). Previous studies suggested that MGE cell migration occurs in the first two weeks post transplantation and that maturation and stabilization occurs by four weeks post transplantation (Alvarez-Dolado et al., 2006; Yang et al., 2016). Therefore, we chose to investigate MGE cell appearance at one- and five-weeks post transplantation to confirm cell migration and maturation, respectively. At one-week post transplantation, most of the transplanted MGE cells were still aggregated in a cluster at the injection site, while some of the cells had begun to migrate radially (Figure 12B). The majority of the migrating cells had an immature morphology with a small, elongated soma and bipolar processes (Figure 12D, inset), characteristic of migrating cells and remained within the boundaries of the IC (Figure 12C, dashed white line). At five-weeks post transplantation, a cluster of injected MGE cells remained at the injection site (Figure 12E and F).

However, the MGE cells that did migrate appeared further away from the injection site than they did at 1-week post transplantation, with the number of cells per section decreasing with increasing distance from the center of the injection (Figure 12E-G, images 100µm apart). Additionally, the transplanted cells that migrated away from the injection site demonstrated a more mature morphology, with multiple branching processes (Figure 12F, insets), and boutons containing VGAT (Figure 12H-J, white arrowheads), suggesting that transplanted MGE cells form inhibitory synapses with host IC neurons.

To confirm that transplanted MGE cells mature into inhibitory neurons and to demonstrate long-term survival, we harvested MGE cells from E12-14 green x VGAT-dT mice and injected them bilaterally into the IC of adult CBA/CaJ mice (Figure 13A). At twenty weeks post transplantation, MGE cells had migrated away from the injection site and demonstrated a mature morphology with multiple branching processes (Figure 13B-D inset). The migrated MGE cells, and their processes, largely remained within the boundaries of the IC (Figure 13E-G, inset). Even in sections with relatively few transplanted MGE cell bodies, processes from transplanted MGE cells fill large portions of the IC (Figure 13H-J, inset). We observed MGE cells in the IC up to twenty-two weeks post transplantation, the latest timepoint evaluated, suggesting that long-term survival of MGE cells is achieved.

Next, we quantified MGE cell survival rate, differentiation, and migration distance in non-NE mice at five and after fourteen weeks post transplantation and in NE mice after fourteen weeks post transplantation. Survival rate was defined as the proportion of injected MGE cells that migrated away from the injection site, excluding MGE cells that remained clustered at the injection site. MGE cell survival rates were lower in both non-NE and NE subjects after 14 weeks post transplantation compared to non-NE subjects at 5 weeks post transplantation. The median MGE

cell survival rates were as follows: non-NE subjects at five weeks post transplantation (5w)=5.2%, non-NE subjects after 14 weeks post transplantation (14+w)=1.6%, and NE subjects after 14 weeks post transplantation (14+w, NE)=1.2% (Figure 14A, Table 6). The MGE cell survival rate was significantly lower in 14+w, NE subjects compared to non-NE subjects at 5w ($p=0.01$). There was no significant difference in the MGE cell survival rate of 5w and 14+w subjects ($p=0.12$). However, there was also no difference in the survival rate of 14+w and 14+w, NE subjects ($p=0.64$). Together, this suggests a trend towards decreased MGE cell survival between 5- and 14-weeks post transplantation.

To confirm that transplanted MGE cells differentiated into GABAergic cells, we harvested MGE cells from green x VGAT-dT mouse embryos, which allowed for identification of which transplanted cells (GFP+) are inhibitory (RFP+). After 14 weeks post transplantation, the vast majority of transplanted MGE cells expressed RFP, indicating GABAergic phenotype, in both non-NE (14w median=98%, IQR=5.3, n=15 IC) and NE subjects (14+w, NE median=97%, IQR=8.4, n=13 IC; $p=0.5$, Figure 14B).

In all three groups, the majority of MGE cells that migrated away from the injection site remained in the IC (5w median=94%, 14+w median=99%, 14+w, NE=99%). There was no significant difference in the percentage of MGE cells that remained in the IC between the three groups (Table 7). To determine whether MGE cells respect the boundaries of the IC or remain in the IC because of modest migration distances, we measured the medial/lateral (M/L) and rostral/caudal (R/C) migration distance of transplanted MGE cells (Figure 14C). At 5 weeks post transplantation the median M/L migration distance was 90.8µm (IQR=130.9, n=927 MGE cells). After 14 weeks post transplantation the median M/L migration distance increased slightly for both non-NE (median=150.4µm, IQR=189.6, n=1,777 MGE cells) and NE (median=143.4, IQR=190.4,

n=813 MGE cells) subjects. However, the distributions of M/L migration distances were not significantly different between 5w, 14+w, or 14+w, NE subjects (Figure 14D). The majority of transplanted MGE cells remained in the same R/C plane as the injection site at both 5 and after 14 weeks post transplantation, regardless of whether or not the host was NE (5w median=0µm, IQR=100, n=1,293 MGE cells; 14+w median=0µm, IQR=0, n=2,322 MGE cells; and 14+w, NE median=0µm, IQR=0, n=984 MGE cells, Figure 14E). These data could indicate that MGE cells remain in the IC due to modest migration distances. Additionally, these data provide evidence that MGE cell migration stabilizes by 5 weeks post transplantation and noise exposure has no effect on the ability of transplanted MGE cells to migrate in the IC.

While the vast majority of the transplanted MGE cells are GABAergic, a small percentage of non-inhibitory transplanted cells (non-NE=2%, NE=3%) were observed outside of the injection site. To determine whether these cell types have different migratory potentials, we analyzed the migration distance of non-inhibitory versus inhibitory transplanted cells 14+w and 14+w, NE subjects. Since the migration distance of transplanted MGE cells in these two groups was not significantly different, the data was combined and the migration distanced of cells based on their expression of VGAT-dT was evaluated. Both inhibitory (VGAT-dT+) and non-inhibitory MGE cells migrated similar distances in the M/L plane (p=1, Figure 14F). However, a portion of the inhibitory (VGAT-dT+) MGE cells migrated further from the injection site than non-inhibitory MGE cells in the R/C plane (p=0.04, Figure 14G).

These data indicate that transplanted MGE cells demonstrate long-term survival in the IC of non-NE and NE mice, with comparable survival rates between the two groups at 14+w post transplantation. Furthermore, MGE cells demonstrate similar migration distances and differentiate into GABAergic neurons at equal rates in both non-NE and NE subjects, indicating that

transplanted MGE cells are equally viable in the normal and pathologic IC. Additionally, MGE cells obtained a morphologically mature appearance by 5 weeks post transplantation, with complex, branching processes and axonal boutons containing the vesicular transporter VGAT, suggesting that MGE cells not only survive in the IC but form inhibitory synapses with host neurons.

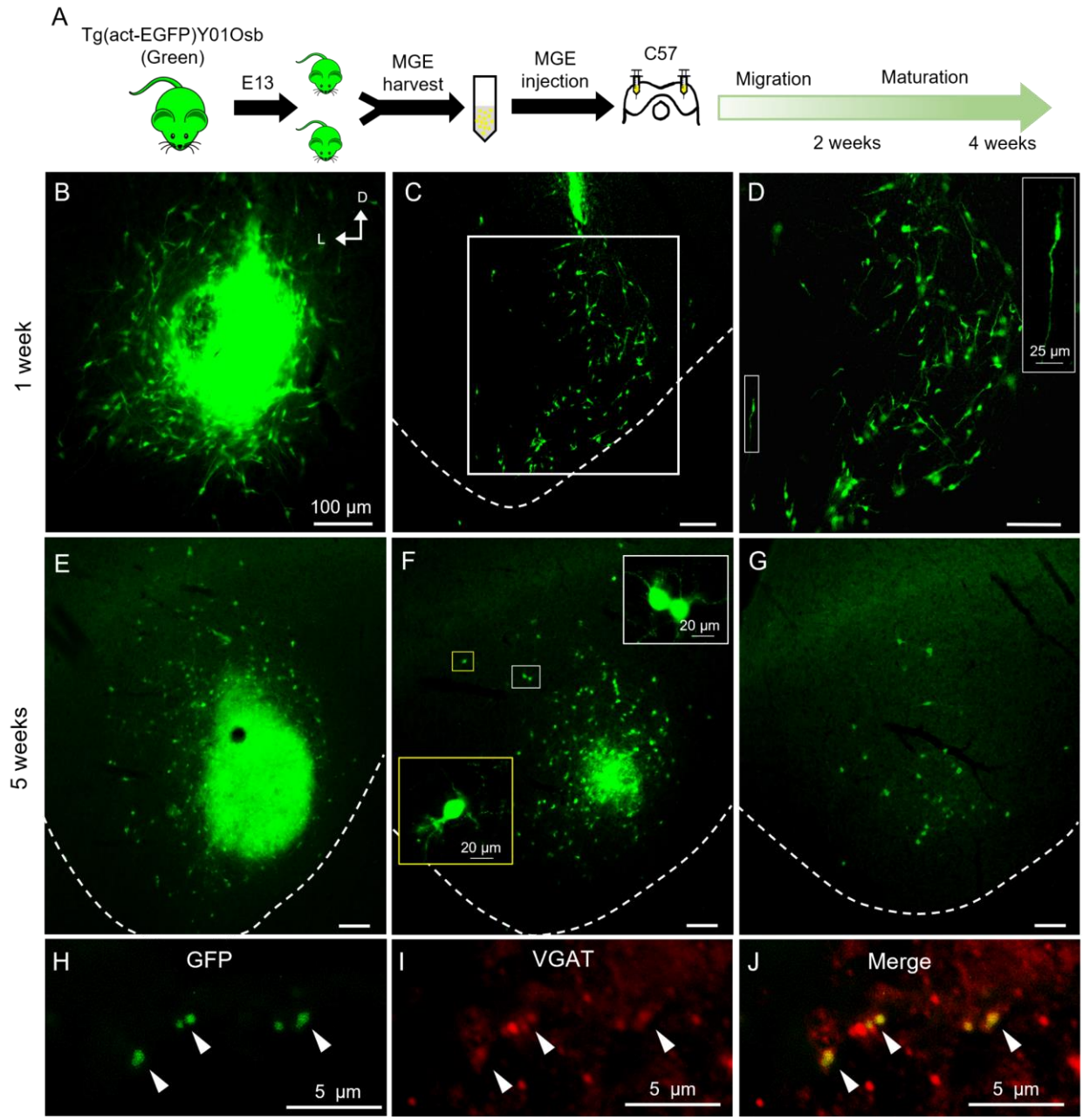

Figure 12. Transplanted MGE cells migrate and mature in the IC

A. Methods schematic: MGE cells were harvested on E13 from green mice (which ubiquitously express GFP) and injected bilaterally into the IC of adult C57 mice.

B-D. One-week post transplantation. The majority of transplanted MGE cells (GFP+) are clustered at the injection site (B), with individual cells migrating radially. The migrating cells appear to remain within the boundaries of the IC (C, dashed white line represents the border of the IC). D is a magnified image of the boxed region in C. MGE cells exhibit elongated soma and bipolar processes (D, inset), characteristic of migrating cells.

E-G. Five weeks post transplantation, images are from serial sections separated by 100um. The majority of the transplanted MGE cells remain clustered at the injection site (E, F). The MGE cells that have migrated appear to have traveled further than at one-week post transplantation, with the number of cells decreasing as the distance from the injection site increases (G). MGE cells have attained a mature morphology with multipolar processes (F, insets).

H-J. Boutons of MGE axons express VGAT. (H) Examples of GFP expressing boutons of MGE axons. (I) VGAT immunohistochemical labeling is reflecting the labelling of GABAergic boutons. (J) Overlay of H and I indicated that all boutons shown in H are VGAT+ MGE axonal boutons.

Scale bars are 100μm in length unless otherwise noted. Image orientation is noted in B with arrows pointing laterally (L) and dorsally (D).

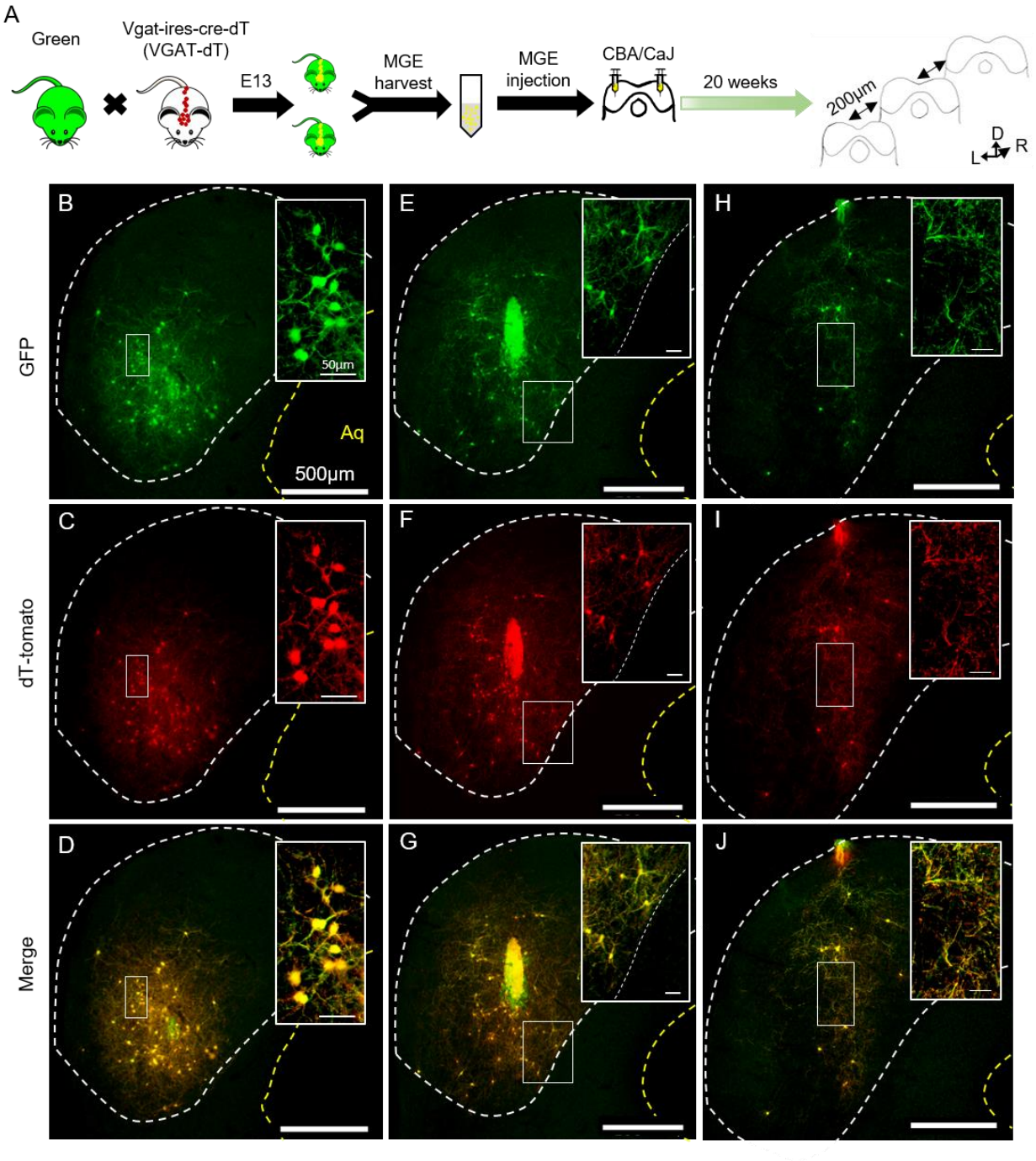

Figure 13. Long-term survival of transplanted MGE cells in the IC

A. Methods schematic: MGE cells were harvested on E13 from green (express GPF ubiquitously) x VGAT-dT (inhibitory cells express dT-tomato) mice and injected bilaterally into the IC of CBA/CaJ mice, with or without prior noise exposure. Images are from a non-noise exposed subject at 20 weeks post transplantation. Images were taken

from serial sections spaced 200μm apart, progressing from caudal (B-D) to rostral (H-J). Images are oriented such that dorsal is up and lateral is left.

B-J. Transplanted MGE cells express GFP (green, top row), and transplanted MGE cells that are GABAergic also express dT-tomato (red, middle row). The IC is outlined in white and the aqueduct is outlined in yellow. Scale bars are 500μm in length for the main images and 50μm in length for the insets.

B-D. Transplanted MGE cells migrated away from the injection site and demonstrate a mature morphology with multiple branching processes (inset). The majority of the transplanted cells appear to differentiate into inhibitory neurons, with extensive co-expression of GFP and dT-Tomato observed.

E-G. The migrated MGE cells, and their processes (inset), appear to largely remain within the boundaries of the IC (dashed white line). Co-expression of GFP and dT-tomato is observed in both the cell bodies and their processes.

H-J. In sections with few transplanted cell bodies, a dense plexus of processes from the transplanted cells is observed (inset).

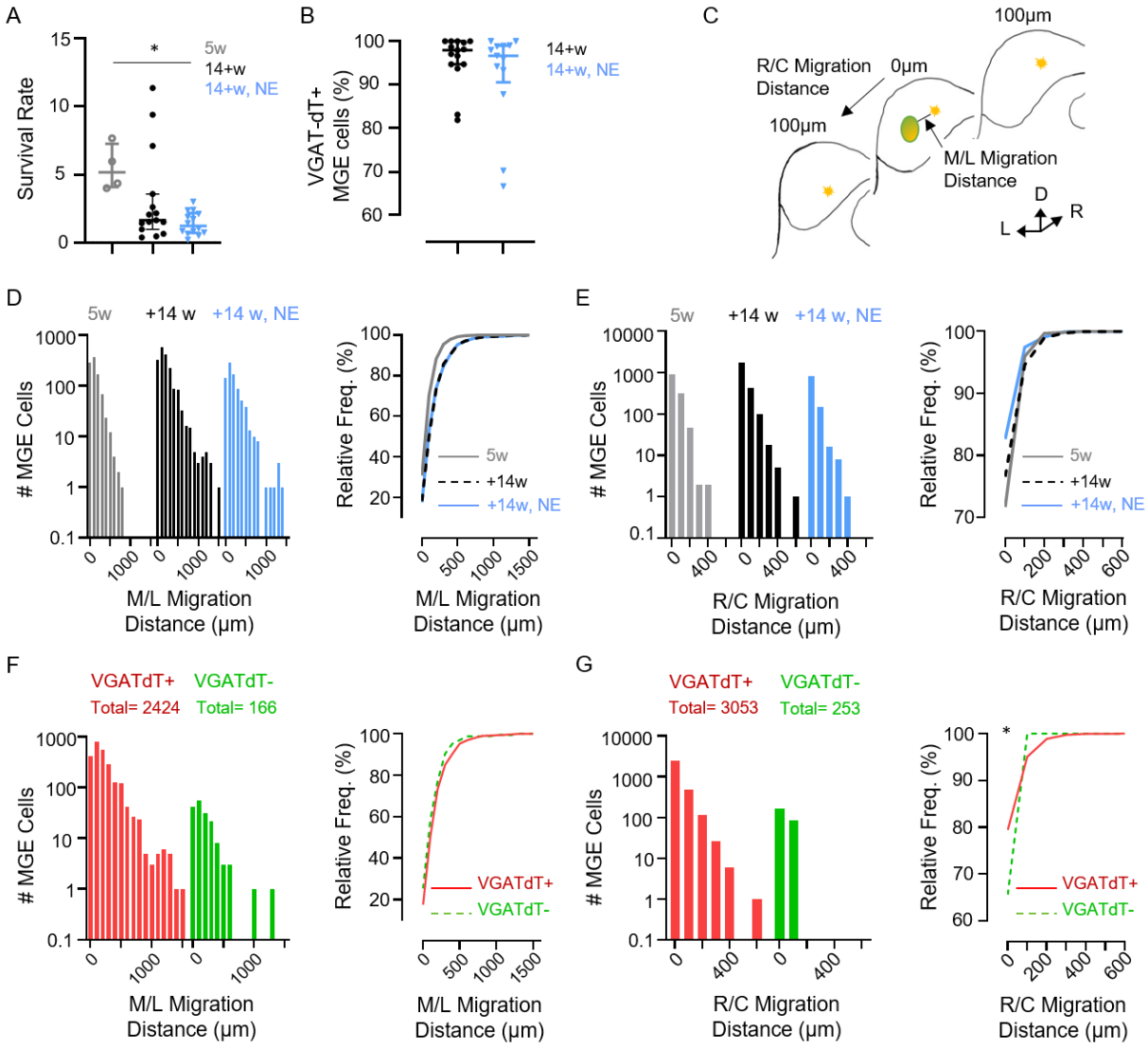

Figure 14. Transplanted MGE cells demonstrate similar long-term survival rates and migration distances in the non-noise exposed and noise exposed IC and primarily differentiate into inhibitory neurons

MGE survival, migration distance, and differentiation in non-noise exposed C57 mice at 5 weeks post transplantation (5w, grey open circles, n=4 IC), non-noise exposed CBA/CaJ mice after 14 weeks post transplantation (14+w, black closed circles, n=15 IC), and noise exposed CBA/CaJ mice at over 14 weeks post transplantation (14+w, NE, light blue inverted triangles, n=14 IC). A and B, individual data with median and interquartile range. Asterisks denotes statistical significance (*p<0.05).

A. The survival rate of transplanted MGE cells in 14+w, NE subjects (median=1.23%) was significantly less than the survival rate of 5w subjects (5.17%, $p<0.05$). There were no significant differences between 5w and 14+w subjects (1.64%, $p=0.12$) or +14w and +14, NE subjects ($p=0.64$, Kruskal-Wallis and Dunn's multiple comparison test).

B. Transplanted MGE cells primarily differentiated into inhibitory neurons (14+w=97.96%, 14+w, NE=96.67%). There was no significant difference between the groups in the percentage of transplanted MGE cells that expressed VGAT (Mann-Whitney test).

C. A schematic representation of the method used to measure migration distance. Medial/lateral (M/L) migration distance was calculated as the distance from the MGE soma to the edge of the injection site and as a result was only calculated for cells in the same plane as the injection site (i.e. in a section that contained an aggregate of injected cells). Rostral/Caudal (R/C) migration distance was calculated as the number of sections away a cell was from a section containing the injection site multiplied by section thickness. Therefore, cells in the same plane as the injection site had a R/C migration distance of 0, while cells two sections away had a R/C distance of 100µm. The sketched sections are oriented such that dorsal (D) is up, rostral (R) is diagonal, and lateral (L) is to the left.

D. Histograms of the M/L migration distance of cells at 5w, 14+w, and 14+w, NE (left to right). Comparisons of the cumulative distributions of the M/L migration distance between the three groups revealed no significant differences (far right, K-S test).

E. Histograms of the R/C migration distance of cells at 5w, 14+w, and 14+w, NE (left to right). Comparisons of the cumulative distributions revealed no significant differences in the R/C migration distance (far right, K-S test).

F and G. Since there was no difference in the M/L and R/C migration distance of cells in the +14w and +14w, NE groups, the migration distance of cells based on their expression of VGAT-dT was combined.

G. Histograms (left) and cumulative distributions (right) of the M/L migration distance of VGAT-dT positive (red, solid line) and negative (green, dashed line) cells. There was no significant difference in the M/L migration distance of these populations of cells (K-S test).

H. Histograms (left) and cumulative distributions (right) of the R/C migration distance of VGAT-dT positive (red, solid line) and negative (green, dashed line) cells. Comparison of the cumulative distributions revealed a significant difference in the R/C migration distance of these cell types, with greater migration potential observed in VGAT-dT+ cells ($p=0.04$, K-S test).

Table 6. MGE cell survival rates

Descriptive Statistics

	Median (%)	IQR	n (IC)
5 weeks post transplantation (5w)	5.17	3.17	4
14+ weeks post transplantation (+14w)	1.64	2.6	15
14+ weeks post transplantation, noise exposed (+14w, NE)	1.23	1.46	14

Kruskal-Wallis table

Kruskal-Wallis H	8.27
degrees of freedom	2
P value	0.02

Dunn's multiple comparisons test

	Mean rank 1	Mean rank 2	Mean rank diff.	Adjusted P Value
14+w vs. 14+w, NE	17.53	13.07	4.46	0.64
14+w vs. 5w	17.53	28.75	-11.22	0.12
14+w, NE vs. 5w	13.07	28.75	-15.8	0.013

Red p-values indicate statistical significance.

Table 7. MGE cell migration within the IC

Descriptive Statistics

	Median (%)	IQR	n (IC)
5 weeks post transplantation (5w)	94	13.9	4
14+ weeks post transplantation (+14w)	99	2.7	15
14+ weeks post transplantation, noise exposed (+14w, NE)	94	13.9	14

Kruskal-Wallis table

Kruskal-Wallis H	0.68
degrees of freedom	2
p value	0.71

Dunn's multiple comparisons test

	Mean rank 1	Mean rank 2	Mean rank diff.	Adjusted P Value
14+w vs. 14+w, NE	18.4	16.1	2.3	>1
14+w vs. 5w	18.4	14.8	3.7	>1
14+w, NE vs. 5w	16.1	14.8	1.4	>1

3.3.2 Transplanted MGE cells integrate into the host IC, forming synaptic connections with host neurons.

The experiments described in section 3.1 provide evidence of long-term survival of transplanted MGE cells in the non-NE and NE IC and suggest that MGE cells have the potential to form inhibitory synapses onto host dendrites. To confirm this, we used EM to obtain direct evidence of synaptic contacts between transplanted GFP+ MGE cells and endogenous neurons in the IC (Figure 15). Transplanted MGE cells made synaptic contact with the soma (Figure 15A and B) and dendrites (Figure 15D) of host IC neurons, which also received synaptic contacts from other host IC neurons (Figure 15A and C). The GFP+ presynaptic endings made symmetrical

contacts and contained small pleomorphic synaptic vesicles, characteristic of inhibitory endings. Additionally, the GPF+ MGE dendritic profiles received synaptic endings from host neurons. Indeed, we observed dendrites from transplanted GFP^+ MGE cells postsynaptic to both putative excitatory (Figure 15E-G) and inhibitory (Figure 15H and I) axonal endings derived from host neurons. Furthermore, mossy-like pre-synaptic endings, which make contacts with multiple dendrites, from host neurons contacted both transplanted GFP+ MGE dendritic profiles and those of host neurons (Figure 15E). The soma of GFP+ MGE cells were not observed receiving synaptic endings from either host neurons or from other GFP+ MGE cells. In addition to forming synaptic contacts, axons of transplanted GPP+ MGE cell could be surrounded by a thin layer of myelin (Figure 15J). Together, these data suggest that MGE cells integrate into the host IC, forming synapses with and receiving synaptic endings from host IC neurons. Additionally, we observed dendrites from endogenous IC neurons receiving synapses from both endogenous and transplanted MGE dendrites, suggesting that the MGE cells have the potential to modulate the activity of host IC neurons.

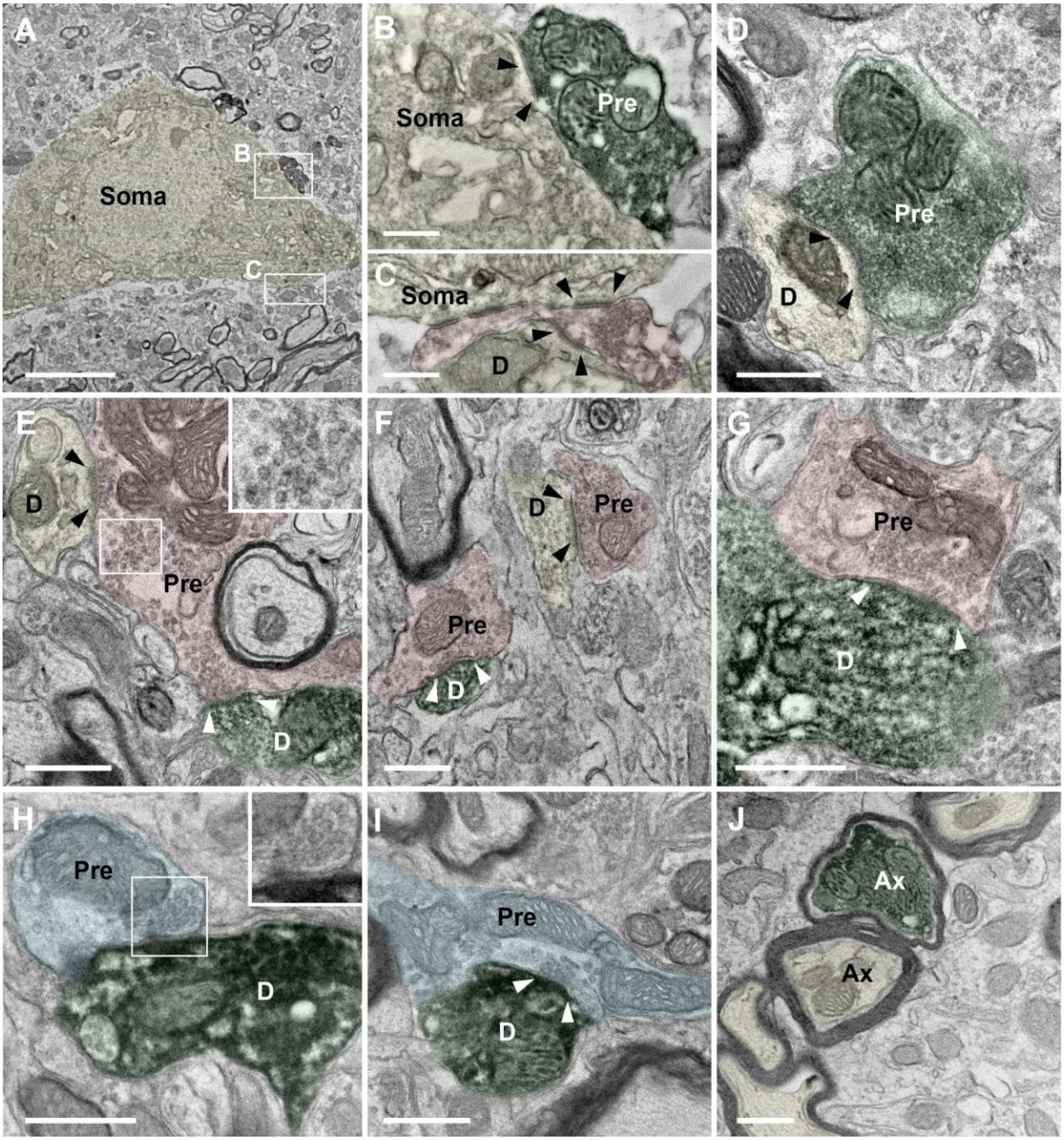

Figure 15. Transplanted MGE cells form synapses with and receive synaptic endings from endogenous IC neurons

The electron micrographs have been colored to help visualization. Green: GFP-positive (GFP+) electrondense profiles (dendrites, presynaptic endings and a myelinated axon); Yellow: GFP-negative profiles from IC host neurons (soma, dendrites and myelinated axons); Pink: GFP-negative profiles of putative excitatory endings; Blue: GFP-negative

profiles of putative inhibitory endings. D: dendrite; Pre: presynaptic ending; Ax: axon. The color font of the GFP+ profiles is white.

A. Unlabeled (GFP-negative) large cell body within the core of the IC. White boxes are shown in higher magnification in B and C. Scale bar: 5µm.

B-C. A GFP+ (B) and GFP-negative (C) presynaptic endings in apposition to the plasma membrane of the soma. Arrowheads point to a symmetric (B) and asymmetric (C) synaptic contact characteristic of inhibitory and excitatory synaptic endings, respectively. Scale bars: 0.5µm.

D. A GFP+ synaptic ending (Pre) makes a synaptic contact (arrowheads) with a GFP-negative dendrite. The GFP-positive presynaptic ending appears to have small and pleomorphic synaptic vesicles (SVs, inset) that are characteristic of inhibitory endings. Scale bar: 0.5µm.

E. A mossy-like GFP-negative presynaptic ending (Pre) containing round SVs is observed making asymmetric synaptic contacts (arrowheads) with a GFP+ (white arrowheads) and a GFP-negative (black arrowheads) dendrites (D). Scale bar: 0.5µm. Inset shows a higher magnification of the SVs within the white box.

F. Putative excitatory endings (Pre) are observed making asymmetric synaptic contacts (arrowheads) on a GFP+ (white arrowheads) and a GFP-negative (black arrowheads) distal dendrites (D). Scale bar: 0.5µm.

G. A putative excitatory ending (Pre; GFP-negative) containing round SVs makes synaptic contact (white arrowheads) with a GFP+ dendrite (D). Scale bar: 0.5µm.

H-I. Putative inhibitory presynaptic endings (Pre; GFP-negative) containing pleomorphic vesicles make symmetric synaptic contacts on GFP+ dendrites (D). Scales bar: 0.5µm. Inset in H, shows a higher magnification of the SVs and synaptic contact within the white box. White arrowheads in I point to the synaptic contact.

J. GFP+ and GFP-negative axons (Ax) are observed within the neuropile of the IC. Scale bar: 0.5µm.

3.3.3 Acoustic stimulation increases the percentage of endogenous inhibitory cells that express c-fos, but has no effect on the percentage of transplanted MGE cells that express c-fos.

Auditory stimulation increases the number of c-fos expressing neurons in the IC and thus can be used as an indirect marker of neural activity (Brown and Liu, 1995; Ehret and Fischer, 1991; Friauf, 1992). We quantified the percentage of endogenous inhibitory cells expressing c-fos in control (non-NE, non-injected) VGAT-dT mice (Figure 16A, B) and in transplanted MGE cells in both non-NE (Figure 16C) and NE subjects. A small percentage of endogenous inhibitory cells expressed c-fos under quiescent conditions (median=1.2%, IQR=1.4, n=4 IC) and this percentage increased almost fivefold (median=5.5%, IQR=4, n=6 IC, p=0.0095, Figure 16D) with acoustic stimulation (500ms, 90dB SPL white noise pulses delivered at 1Hz for 2 hours). Interestingly, a higher percentage of transplanted MGE cells expressed c-fos compared to endogenous inhibitory cells. However, the percentage of MGE cells that express c-fos did not significantly change after acoustic stimulation. In non-NE subjects, 24.5% of transplanted MGE cells expressed c-fos under quiescent conditions with an increase to 39.4% in the presence of acoustic stimulation (Figure 16E). Similarly, in NE subjects, 25.4% and 32.9% of transplanted MGE cells expressed c-fos under quiescent and stimulated conditions, respectively (Figure 16E). Neither noise exposure (p=0.1) or acoustic stimulation (p=1.58) had a significant effect on the percentage of c-fos expressing MGE cells (Table 8). These data suggest that while acoustic stimulation significantly increases the percentage of endogenous inhibitory cells that express c-fos, it has no effect on the percentage of c-fos expressing MGE cells.

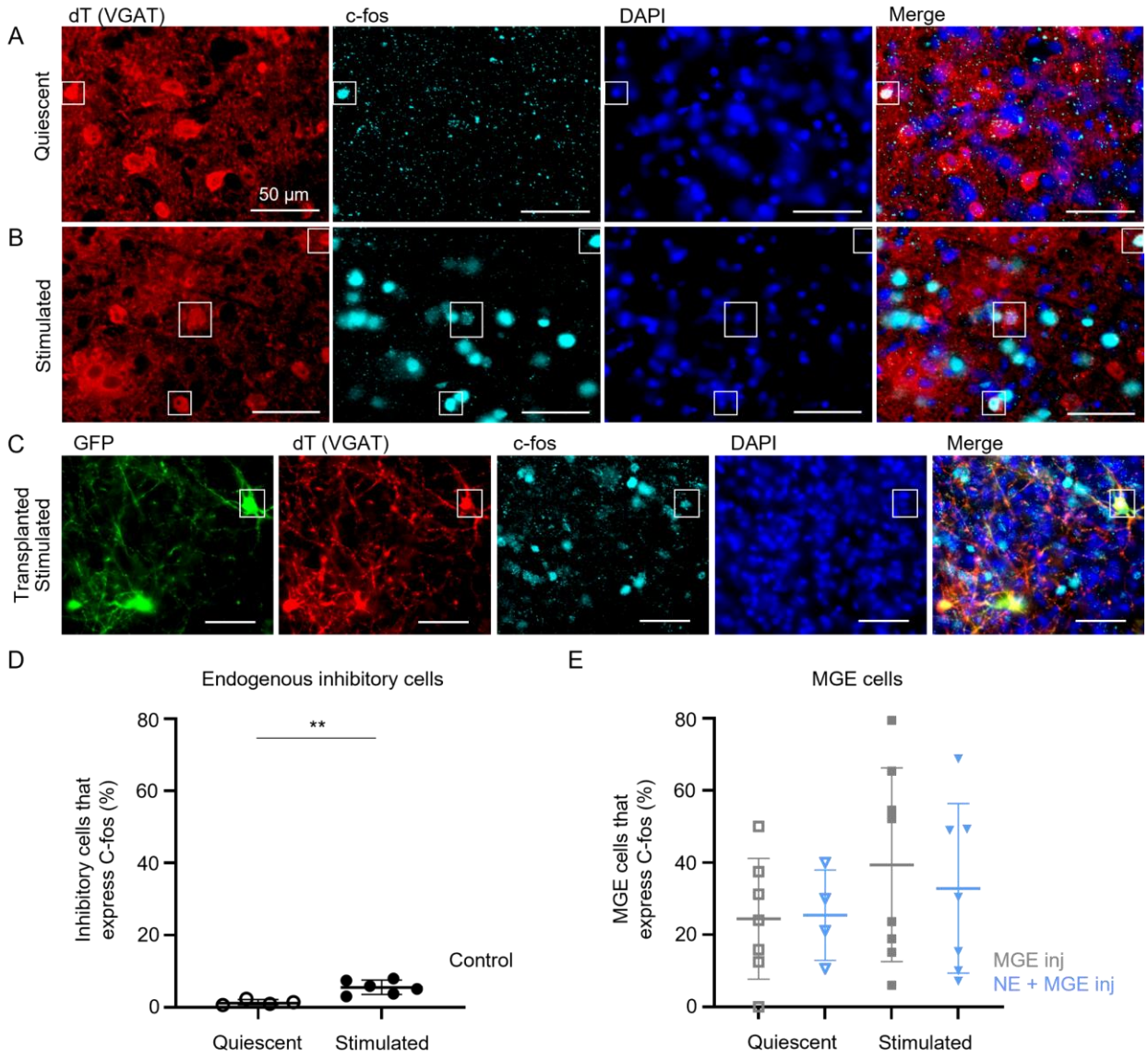

Figure 16. Acoustic stimulation increases c-fos expression in endogenous inhibitory cells but not transplanted MGE cells

A-B. Inhibitory cells in the IC of VGAT-dT (dT+, red) mice demonstrate c-fos expression (cyan) under stimulation (A) and quiescence (B, white boxes surround c-fos positive inhibitory cells). In figure A is quiescent and B is stimulated.

C. Transplanted MGE cells (GFP+, green) that differentiated into inhibitory neurons (dT+, red) also expressed c-fos (cyan, white box surrounds a c-fos positive inhibitory MGE cell).

Scale bars in all images are 50µm in length.

D. Acoustic stimulation significantly increased the percentage of endogenous inhibitory cells that express c-fos (quiescent median=1.18%, stimulated=5.51%, p=0.0095, Mann Whitney test). Individual data points represent data from a single IC and are plotted with the median and interquartile range. Asterisks denote statistical significance (**p<0.01).

E. Individual data points represent data from a single IC and are plotted with the mean and standard deviation. Data from non-noise exposed injected IC (MGE inj) are plotted as grey squares and noise exposed injected IC (NE + MGE inj) as light blue inverted triangles. Neither noise exposure (p=0.1) or acoustic stimulation (p=1.58) had a significant effect on the percentage of MGE cells that express c-fos.

Table 8. The effects of acoustic stimulation and noise exposure on the percentage of transplanted MGE cells that express c-fos

Two-way ANOVA table

	SS (Type III)	DF	MS	F (DFn, DFd)	P value
Interaction	85.61	1	85.61	F (1, 22) = 0.18	0.68
Acoustic stimulation	756.9	1	756.9	F (1, 22) = 1.58	0.22
Noise exposure	46.51	1	46.51	F (1, 22) = 0.10	0.76
Residual	10509	22	477.7		

Tukey's multiple comparisons test

	Mean 1 (% MGE cells)	Mean 2 (% MGE cells)	Mean Diff.	95.00% CI of diff.	Adjusted P Value
Quiet : MGE inj vs. Quiet : NE+MGE inj	24.45	25.44	-0.99	-39.03 to 37.05	1
Quiet: MGE inj vs. Sound: MGE inj	24.45	39.39	-14.94	-46.35 to 16.47	0.56
Quiet: MGE inj vs. Sound: NE+MGE inj	24.45	32.86	-8.41	-40.85 to 24.03	0.89
Quiet: NE+MGE inj vs. Sound: MGE inj	25.44	39.39	-13.95	-51.12 to 23.21	0.73
Quiet : NE+MGE inj vs. Sound : NE+MGE inj	25.44	32.86	-7.42	-45.46 to 30.62	0.95
Sound: MGE inj vs. Sound: NE+MGE inj	39.39	32.86	6.53	-24.88 to 37.94	0.94

3.3.4 Transplantation of MGE cells does not decrease the number of endogenous IC neurons that express c-fos

In addition to c-fos expression in GABAergic cells, we investigated whether transplanted MGE cells influence the number of c-fos expressing cells in the IC. It is well established that acoustic stimulation leads to a robust increase in c-fos expression in the IC (Brown and Liu, 1995; Ehret and Fischer, 1991; Friauf, 1992). In accordance with this, we observed a robust increase in the number of c-fos expressing cells in the IC following acoustic stimulation (500ms, 90dB SPL white noise pulses delivered at 1Hz for 2 hours) in both non-NE (Figure 17A) and NE mice. Acoustic stimulation and noise exposure, but not the presence of MGE cells, influenced the number of c-fos expressing cells in the IC (Table 9). Acoustic stimulation significantly increased the number of c-fos expressing cells in all groups (control: $p=0.0002$, MGE injected: $p=0.0153$, NE: $p<0.0001$, and NE + MGE injected: $p<0.0001$, Figure 17B). Additionally, in the presence of acoustic stimulation, the number of c-fos expressing cells was significantly increased in NE and MGE injected subjects compared to non-NE MGE injected subjects ($p=0.0034$, Figure 17B). Interestingly, there was no corresponding increase in the number of c-fos expressing cells between control and NE subjects in the presence of acoustic stimulation ($p=0.46$, Figure 17B). Given that there was no significant difference in the number of c-fos expressing cells between non-injected and injected subjects (Table 9), the increased c-fos expression in NE and MGE injected subjects compared to non-injected MGE injected subjects is unlikely to be due to the presence of MGE cells. This is supported by our finding that acoustic stimulation ($p<0.0001$) and noise exposure ($p=0.002$) had significant, independent effects on the number of c-fos expressing cells while the presence of MGE cells did not ($p=0.17$, Table 9).

Given the variability in the percentage of c-fos expressing MGE cells (Figure 16E), their influence on the number of c-fos expressing cells in the IC may not be well captured by the mean values. Furthermore, detectable levels of c-fos are not present in all activated neurons (Bullitt, 1990) and may underrepresent the activity of transplanted MGE cells. Thus, we investigated 1) the relationship between the number of c-fos expressing MGE cells and the number of c-fos expressing cells in the IC and 2) the MGE cell survival rate and the number of c-fos expressing cells in the IC. There was no significant correlation between the percentage of transplanted MGE cells that expressed c-fos and the total number of c-fos+ cells in the IC of non-NE or NE subjects in quiescent (MGE inj $r=-0.50$, $p=0.27$; NE+MGE inj $r=-0.60$, $p=0.42$) or stimulated conditions (MGE inj $r=0.57$, $p=0.15$; NE+MGE inj $r=0.29$, $p=0.56$). Furthermore, there was no significant correlation between the MGE cell survival rate and the total number of c-fos+ cells in the IC of non-NE or NE subjects in quiescent (MGE inj $r=0.50$, $p=0.27$; NE+MGE inj $r=0.80$, $p=0.33$) or stimulated conditions (MGE inj $r=0.40$, $p=0.33$; NE+MGE inj $r=0.04$, $p=0.96$). These data further support the conclusion that transplantation of MGE cells does not significantly affect the number of c-fos expressing cells in the IC.

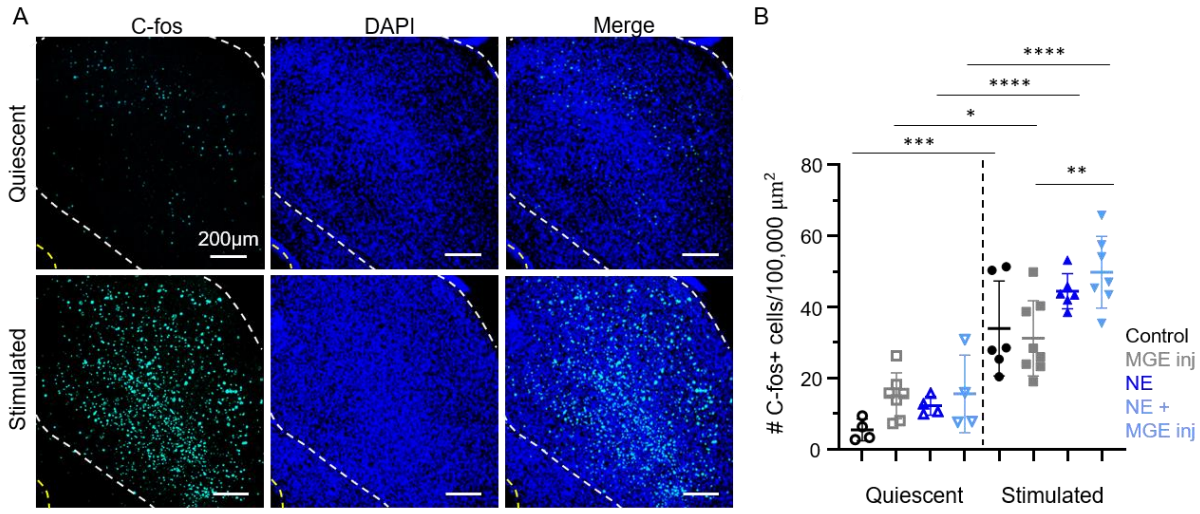

Figure 17. Transplanted MGE cells do not alter total c-fos expression in the IC.

A. The IC (outlined in white) shows scattered c-fos positive cells in quiescence (cyan, top row). Acoustic stimulation (bottom row) causes a robust increase in the number of c-fos positive cells (cyan). Scale bars are 200µm in length in all images. The aqueduct is outlined in yellow. DAPI (blue) is shown to verify nuclear labeling with c-fos.

B. Individual data points represent data from a single IC and are plotted with the mean and standard deviation. Data from non-noise exposed non-injected IC (Control) are plotted as black circles, non-noise exposed injected IC (MGE inj) are plotted as grey squares, non-injected noise exposed IC (NE) are plotted as dark blue triangles, and noise exposed injected IC (NE+MGE inj) are plotted as light blue inverted triangles. Acoustic stimulation significantly increased c-fos expression in all groups (control: $p=0.0002$, MGE injected: $p=0.0153$, NE: $p<0.0001$, and NE+MGE injected: $p<0.0001$). Additionally, c-fos expression was significantly increased in NE+MGE injected subjects compared to non-NE injected subjects ($p=0.0034$). Asterisks denote statistical significance (* $p<0.05$, ** $p<0.01$, *** $p<0.001$, **** $p<0.0001$).

Table 9. Three-way ANOVA: The effects of noise exposure, acoustic stimulation, and MGE injection on c-fos expression in the IC

Three-way ANOVA table

	SS	DF	MS	F (DFn, DFd)	P value
Acoustic stimulation	8264	1	8264	F (1, 38) = 102.4	<0.0001
MGE injection	160.5	1	160.5	F (1, 38) = 1.99	0.17
Noise exposure	887.9	1	887.9	F (1, 38) = 11.00	0.002
Acoustic stimulation x MGE injection	71.5	1	71.5	F (1, 38) = 0.89	0.35
Acoustic stimulation x Noise exposure	316.8	1	316.8	F (1, 38) = 3.92	0.05
MGE injection x Noise exposure	2.329	1	2.329	F (1, 38) = 0.03	0.87
Acoustic stimulation x MGE injection x Noise exposure	137.6	1	137.6	F (1, 38) = 1.71	0.20
Residual	3067	38	80.71		

Sidak's multiple comparisons test

	Mean 1	Mean 2	Mean Diff.	95.00% CI of diff.	Adjusted P Value
quiescent: Control vs. stimulated: Control	5.485	33.99	-28.51	-46.14 to -10.88	0.0002
quiescent: MGE inj vs. stimulated: MGE inj	15.06	31.23	-16.17	-30.31 to -2.036	0.02
quiescent: NE vs. stimulated: NE	12.27	44.49	-32.22	-49.85 to -14.59	<0.0001
quiescent: NE+MGE inj vs. stimulated: NE+MGE inj	15.61	49.83	-34.22	-51.34 to -17.10	<0.0001
quiescent: MGE inj vs. quiescent: NE+MGE inj	15.06	15.61	-0.55	-17.67 to 16.57	>1
quiescent: Control vs. quiescent: NE	5.485	12.27	-6.79	-26.10 to 12.53	0.98
stimulated: MGE inj vs. stimulated: NE+MGE inj	31.23	49.83	-18.6	-32.73 to -4.459	0.003
stimulated: Control vs. stimulated: NE	33.99	44.49	-10.49	-26.26 to 5.276	0.46
quiescent: MGE inj vs. quiescent: Control	15.06	5.485	9.57	-7.546 to 26.69	0.71
quiescent: NE+MGE inj vs. quiescent: NE	15.61	12.27	3.34	-15.98 to 22.65	>1
stimulated: MGE inj vs. stimulated: Control	31.23	33.99	-2.76	-17.51 to 11.99	>1
stimulated: NE+MGE inj vs. stimulated: NE	49.83	44.49	5.34	-9.858 to 20.53	0.98

Red p-values indicate statistical significance.

3.4 Discussion

Our study demonstrates that transplanted MGE cells survive, migrate, and differentiate into primarily inhibitory neurons in the IC of adult mice. Importantly, transplanted MGE cells integrate into the IC, forming synapses with and receiving synapses from endogenous IC neurons. Furthermore, the transplanted cells are active, with a high percentage of the MGE cells expressing c-fos in quiescent and stimulated conditions. However, the presence of inhibitory MGE cells does not decrease the number of c-fos expressing cells in the host IC.

The long-term survival rate of transplanted MGE cells in the non-NE and NE IC was relatively low, at 1.6% and 1.2%, respectively. While this survival rate is lower than has been observed in some areas (e.g. 20% survival in the postnatal cortex (Alvarez-Dolado et al., 2006), 9.8% in the young adult amygdala (Yang et al., 2016), 2.7% survival in the adult spinal cord (Bráz et al., 2012)), it is similar to that seen in the injured adult striatum (1% (Martínez-Cerdeño et al., 2010)) and injured adult spinal cord (1.3% (Bráz et al., 2012)). Even in the presence of modest survival rates, MGE cell transplantation has proven to be a viable option to drive behavioral change (Bráz et al., 2012; Hammad et al., 2015; Martínez-Cerdeño et al., 2010; Yang et al., 2016). Indeed, in the mouse spinal cord a MGE survival rate of 1.3% (667$\pm$ 267 MGE cells/subject) is sufficient to reverse mechanical hypersensitivity following peripheral nerve injury (Bráz et al., 2012). Interestingly, unlike the spinal cord, our results show that NE does not influence MGE cells survival in the IC. While the cause of decreased MGE survival in the injured spinal cord is unknown, it may be related to local, pro-inflammatory changes in the tissue environment following injury (Sun et al., 2021). While the pro-inflammatory effects of NE in the IC remain unknown, cochlear ablation does not appear to increase the proliferation of phagocytic microglia in the IC (Janz and Illing, 2014). This could suggest that the changes in the IC following the loss of

peripheral input are not directly mediated by an inflammatory process. If true, this might indicate that the tissue environment of the NE IC remains equally hospitable to transplanted MGE cells and could explain the similar survival rates we see in the non-NE and NE IC.

There is evidence that a homeostatic mechanism regulates the degree to which MGE cells increase inhibition in the host. For example, in the uninjured mouse spinal cord, the survival rate is 2.6%, twice that of the injured spinal cord (Bráz et al., 2012). However, despite demonstrating increased survival, transplanted MGE cells have no effect on the mechanical pain threshold in control mice (Bráz et al., 2012). Conversely, transplantation of MGE cells into the adult striatum leads to increased stride length in both naïve and injured rats (Martínez-Cerdeño et al., 2010); although MGE survival rate was only reported in the injured striatum. One possibility is that the host brain is capable of maintaining homeostasis with a limited number of MGE cells, but once a threshold is reached the transplanted cells are able to override this mechanism. The ability to maintain homeostasis may also be a function of the host environment leading to region-specific differences. Further research is necessary to understand the relationship between MGE cell survival and behavioral changes in both normal and pathologic states, particularly in the IC. However, if a homeostatic mechanism does indeed regulate inhibition from MGE cells at low survival rates, this would make MGE cell transplantation an ideal candidate therapy to mitigate the hyperexcitable changes observed in the IC following NE.

The utility of transplanted MGE cells as a technique to investigate the effects of increased inhibition in the IC following NE hinges on not only long-term survival, but integration and maturation into inhibitory neurons. Our results indicate that long-term survival is achieved in both the non-NE and NE exposed IC, with comparable survival rates and migration distances between non-NE and NE subjects. Of note, the survival rate in NE mice after 14 weeks post transplantation

was significantly lower than the survival rate in non-NE mice at 5 weeks post transplantation. While not significant, there was also a trend towards decreased survival rate in non-NE mice after 14 weeks post transplantation compared to 5 weeks, suggesting that the survival rate may not stabilize in the IC by 4 weeks post transplantation, as has been suggested in other brain areas (Alvarez-Dolado et al., 2006; Yang et al., 2016). Decreased MGE survival after 5 weeks post transplantation likely indicates cell loss after migration, as the transplanted cells have achieved a mature appearance by this time and there was no difference in the migration distance between 5- and 14-weeks post transplantation. One possible explanation for loss of MGE cells after migration is that cells who fail to make functional synapses and integrate into the IC are lost. The survival rates observed after fourteen weeks post transplantation may thus represent the functional survival rate or integration rate. Indeed, while we observed MGE cells with a mature morphology and axons with boutons containing the inhibitory vesicular transporter VGAT by 5 weeks post transplantation, we did not quantify the percentage of surviving MGE cells that formed synaptic structures at either 5 weeks or after 14 weeks post transplantation. However, we did determine that the vast majority (over 96% in both non-NE and NE subjects) of MGE cells after 14 weeks post transplantation were indeed GABAergic and that the transplanted MGE cells formed inhibitory synapses onto dendrites and cell bodies of endogenous IC neurons.

In addition to forming inhibitory synapses onto endogenous IC neurons, transplanted MGE cells are the target of pre-synaptic excitatory and inhibitory endings derived from endogenous IC neurons. Previous studies in the cortex reported that transplanted MGE cells preferentially receive excitatory input from host pyramidal neurons (Alvarez-Dolado et al., 2006; Derek G Southwell et al., 2010). Conversely, MGE cells in the striatum receive synaptic inputs from both local inhibitory neurons as well as excitatory projection neurons from the cortex and/or thalamus (Martínez-

Cerdeño et al., 2010). In the spinal cord, synaptic contacts were observed between both excitatory and inhibitory host neurons and transplanted MGE cells (Llewellyn-Smith et al., 2016). Despite representing a small portion of cells in the spinal cord, synaptic contacts between transplanted MGE cells were also observed (Llewellyn-Smith et al., 2016). This variability in connectivity may be an example of region-specific differences in MGE cell synaptic integration but importantly all of these studies demonstrate that MGE cells form synaptic contacts with host neurons.

About 25-40% of the transplanted MGE cells expressed c-fos, providing indirect evidence of cellular activity in MGE cells during both quiescent and stimulated conditions. While not compared directly in this study, a higher, but more variable, percentage of transplanted MGE cells appear to express c-fos in both quiescent and stimulated conditions compared to endogenous inhibitory cells in the IC. Additionally, while only a small percentage of endogenous inhibitory cells expressed c-fos under quiescent conditions, there was a dramatic increase in the percentage of c-fos expressing inhibitory cells following acoustic stimulation, suggesting that they are driven by sound. To our knowledge, this is the first study to show an increase in c-fos expression in identified GABAergic cells in the IC following acoustic stimulation.

Unlike endogenous inhibitory cells, the percentage of c-fos expressing MGE cells did not increase following acoustic stimulation. While this data does not rule out the possibility that MGE cells are driven by acoustic stimulation, it could indicate that the transplanted MGE cells integrate into the IC differently than endogenous inhibitory cells or that their activity more closely resembles that of cortical interneurons. Indeed, in layer II/III of primary visual cortex 35% of endogenous GAD+ neurons express c-fos following an hour of visual stimulation (Van der Gucht et al., 2002); similar to our finding that 39% of transplanted MGE cells express c-fos following acoustic stimulation. If transplanted MGE cells retain features of cortical interneurons it is possible that

their constitutive activity is higher than that of endogenous inhibitory cells of the IC. Alternatively, it is possible that the synaptic strength of inputs to transplanted MGE cells differs from that of endogenous inhibitory neurons in the IC, resulting in weaker sound evoked activity. Indeed, in the visual cortex, transplanted MGE cells form numerous, but weaker, interactions than endogenous inhibitory cells (Derek G Southwell et al., 2010). A higher number of synaptic connections may thus result in higher spontaneous activity in transplanted MGE cells as they integrate input from numerous endogenous IC neurons. Any resulting increase in activity due to sound evoked activity may be modest in comparison to this already elevated constitutive activity.

Several studies showed increased c-fos expression in central auditory structures after noise exposure (Liu et al., 2020; Zhang et al., 2003), consistent with the central gain hypothesis. In the present study, we observed a trend towards increased c-fos expression in the IC of NE subjects compared to control subjects, however, this increase did not achieve statistical significance. Interestingly, c-fos expression was significantly higher in NE + MGE injected subjects compared to non-NE MGE injected subjects. Given the comparable levels of c-fos expression observed between control and MGE injected subjects and NE and NE+MGE injected subjects, we do not believe that the transplantation of MGE cells influenced c-fos expression in the IC. This is supported by our statistical analysis (3-way ANOVA) which revealed that acoustic stimulation and noise exposure influenced c-fos expression, while MGE transplantation did not.

Given the elaborate network of processes we saw originating from transplanted MGE cells, we were surprised to find that the presence of MGE cells did not impact the percentage of c-fos expressing cells in the IC. However, these results do not rule out the possibility that transplanted MGE cells may still have a subtle effect on neural response properties in the IC. Indeed, while c-fos expression in neurons is believed to be related to membrane depolarization and calcium influx

(Sheng et al., 1990), detectable levels of c-fos are not found in all neurons (Bullitt, 1990) and expression does not directly correlate with synaptic activity or strength. Furthermore, while c-fos expression allows us to indirectly determine single cell activity, and could potentially reveal an increase in spontaneous or sound evoked activity, it does not have the ability to discern other response properties such as bursting activity or increased tuning broadness, which are known to increase following NE (Berger et al., 2014; Coomber et al., 2014; Longenecker and Galazyuk, 2016; Ma et al., 2006; Mulders and Robertson, 2013, 2009). Given the complex impact noise exposure has on auditory response properties, we cannot rule out the possibility that MGE cells impact the response properties of endogenous IC neurons and could therefore mitigate the effects of noise exposure.

The data presented herein provide the first evidence that transplantation of MGE cells is viable in the brainstem. The finding that MGE cells demonstrate long-term integration in the IC provides a promising foundation for their potential use as a local, targeted treatment to restore the excitatory/inhibitory balance following NE. Additionally, by providing a means to increase synaptic inhibition in very defined brainstem regions *in vivo* this technique could be used to investigate basic mechanisms underlying the development, plasticity, and function of defined auditory areas.

4.0 Transplantation of embryonic medial ganglionic eminence cells into the inferior colliculus of adult mice mitigates the effects of noise exposure on the acoustic startle response

4.1 Introduction

In addition to increasing hearing thresholds, noise exposure can lead the development of tinnitus and hyperacusis. Tinnitus is often described as "ringing in the ears" and is characterized by the perception of sound in the absence of an external source. Hyperacusis is characterized by increased sound sensitivity and decreased sound level tolerance; as a result, moderate intensity sounds are perceived as uncomfortably loud (Gu et al., 2010; Katzenell and Segal, 2001; Vernon, 1987). Many patients co-report tinnitus and hyperacusis (Aazh and Moore, 2018; Cederroth et al., 2020; Fournier and Hébert, 2013; Katzenell and Segal, 2001; Schecklmann et al., 2014) which can be present with (Aazh and Moore, 2018; König et al., 2006; Sheldrake et al., 2015) or without (Aazh and Moore, 2018; Gu et al., 2010; Schaette and McAlpine, 2011; Sheldrake et al., 2015) concomitant hearing loss. The presence of tinnitus and hyperacusis in the absence of auditory threshold shifts suggests that subtle, but clinically significant changes in hearing are occurring (Gu et al., 2010; Roberts et al., 2010; Schaette and McAlpine, 2011; Weisz et al., 2006). Even in the absence of hearing loss, tinnitus and hyperacusis can have a detrimental effect on quality of life (Aazh et al., 2017; Aazh and Mooreb, 2017; Ayodele et al., 2020; Bartels et al., 2008; Reynolds et al., 2004; Weidt et al., 2016). Despite ongoing research efforts, the etiology of these otologic conditions remains elusive and as a result, few treatment options are available.

Given the subjective nature of tinnitus and hyperacusis, determining the presence of these pathologies in animal models has relied on behavioral evidence (Hayes et al., 2014). The acoustic startle response (ASR) is an innate reflexive response to loud sounds (Davis et al., 1982; Yeomans et al., 2002). Variations of the ASR are thus an attractive behavioral model for tinnitus and hyperacusis as they require no training. The ASR became a viable tool for studying temporal processing when it was discovered that a silent gap inserted in a continuous background sound suppresses the ASR in naïve mice, but fails to do so in a subset of noise exposed animals (Turner et al., 2006). The decreased ability to detect silent gaps in sound (gap detection) following noise exposure is commonly used as a model for tinnitus (Berger et al., 2014; Chen et al., 2013; Hayes et al., 2014; Sturm et al., 2017; Turner et al., 2006). This model is based on the assumption that in animals with tinnitus, the tinnitus fills the silent gap, preventing the expected reduction in the ASR following a gap (Turner et al., 2006). The absence of gap detection deficits in human subjects (Campolo et al., 2013) has led to some debate as to whether gap detection deficits in animals are truly indicative of tinnitus or are instead representative of hyperacusis (Chen et al., 2013; Hickox and Liberman, 2014).

Increases in the ASR following noise exposure have been suggested to result from increased central gain and thus believed to represent the decreased sound tolerance reported by patients with hyperacusis (Berger and Coomber, 2015; Chen et al., 2013; Coomber et al., 2014; Hickox and Liberman, 2014; Sturm et al., 2017). The effects of noise exposure on the ASR are highly variable though, and appear to be dependent on the noise exposure conditions, subsequent degree of hearing loss, and time since noise exposure (Salloum et al., 2014). Similarly, changes in the magnitude of pre-pulse inhibition (PPI), a measure of sensorimotor gating, following noise exposure are correlated with the degree of hearing loss and associated plasticity (Carlson and

Willott, 1996; Willott and Turner, 2000). In cases of severe high frequency hearing loss, the inferior colliculus (IC) can undergo tonotopic reorganization, in which ventral neurons, which normally respond to high frequency sounds, respond to low and mid frequencies (Carlson and Willott, 1996; Willott and Turner, 2000). The percentage of IC cells that respond to a particular frequency is correlated with the degree of PPI at that frequency (Carlson and Willott, 1996; Willott and Turner, 2000). Thus, in animals with severe high frequency hearing loss, PPI is reduced at high pre-pulse stimulus frequencies but increased at mid and low pre-pulse stimulus frequencies (Carlson and Willott, 1996; Willott and Turner, 2000). Together, these findings suggest that when using these behavioral models it is important to consider the results in conjunction with hearing thresholds, which can be obtained via the auditory brainstem response (ABR). The ABR is an auditory evoked potential that produces a characteristic waveform with peaks that correspond to defined auditory areas (Henry and Haythorn, 1978; Jewett and Romano, 1972; Jewett and Williston, 1971). In addition to providing information about hearing thresholds, the latency and amplitude of the peaks provide information on the speed of transmission and synchronicity of neural firing (Henry and Haythorn, 1978; Jewett and Romano, 1972).

The IC is a prominent auditory midbrain structure and a major site of subcortical auditory integration (Chandrasekaran et al., 2013; Frisina et al., 1998; Ito and Oliver, 2014; Malmierca et al., 2003, 1995; Miller et al., 2005; Oliver et al., 1991; Rees and Orton, 2019; Saldaña et al., 1996; Saldaña and Merchán, 1992; Sturm et al., 2014, 2017; Wallace et al., 2012; Winer, 2006) that has been implicated in mediating auditory behavior (Auerbach et al., 2019; Berger et al., 2014; Chen et al., 2013; Hayes et al., 2014; Koch and Schnitzler, 1997; L. Li et al., 1998; Sturm et al., 2017; Turner et al., 2006; Willott and Turner, 2000). Indeed, the IC is critical for PPI, as lesioning the IC abolishes this behavior in naïve mice (Koch and Schnitzler, 1997; L. Li et al., 1998).

Furthermore, the emergence of hyper-excitable response properties of neurons in the IC following noise exposure is associated with the development of gap-detection deficits (Berger et al., 2014; Chen et al., 2013; Hayes et al., 2014; Sturm et al., 2017; Turner et al., 2006). Thus, it is hypothesized that a disruption in excitatory/inhibitory balance in central auditory structures, such as the IC, mediates the development of auditory pathologies such as tinnitus (Coomber et al., 2014; Middleton et al., 2011; Sturm et al., 2017; Wang et al., 2009; Yang et al., 2011) and hyperacusis (Knipper et al., 2013; Manohar et al., 2017). Attempts to correct noise exposure induced excitation have focused on increasing GABAergic tone systemically, with some success in animal models (Brozoski et al., 2010, 2007; Yang et al., 2011) but without clear clinical efficacy in humans (Bauer and Brozoski, 2006; Piccirillo et al., 2007). A more targeted approach to increasing inhibition could provide valuable insight into the extent to which local increases in excitation contribute to the development of tinnitus and hyperacusis and aid in the development of novel treatment strategies.

One approach to locally increase inhibition is through transplantation of cells harvested from the embryonic medial ganglionic eminence (MGE), the birthplace of cortical inhibitory interneurons (Lavdas et al., 1999). While naturally destined for the cerebral cortex, these inhibitory neuron precursors survive, mature, and integrate into a variety of structures within the adult central nervous system (Alvarez-Dolado et al., 2006; Baraban et al., 2009; Bráz et al., 2012; Hammad et al., 2015; Derek G Southwell et al., 2010; Southwell et al., 2014; Wichterle et al., 1999; Yang et al., 2016). The data presented in chapter 3, confirm that transplanted MGE cells are equally viable in the non-noise exposed and noise exposed IC and primarily differentiate into inhibitory neurons. While the majority of the transplanted MGE cells remained clustered at the injection site, approximately 1-2% of the transplanted MGE cells migrated away from the injection site and

formed elaborate branching processes capable of forming synapses with endogenous IC neurons. While the survival rate, defined as the percentage of transplanted MGE cells that migrated away from the injection site, in the IC is low, previous studies in the adult spinal cord and striatum demonstrate that survival rates as low as 1% are sufficient to affect behavioral change (Bráz et al., 2012; Martínez-Cerdeño et al., 2010).

In the present study, we investigated the effects of transplanted MGE cells on the ABR, ASR, and PPI in non-noise exposed and noise exposed mice. We found that transplantation of MGE cells into the IC led to decreases in the ABR wave 1 latency and amplitude, suggesting that increasing inhibition in the IC led to an increase in the speed of neural transmission but at the expense of synchrony. Additionally, we found that transplantation of MGE cells into the IC mitigated the noise-induced shift in the ASR curve. Together, these data suggest that the effects of transplanted MGE cells extend beyond the IC and may be useful in mitigating the effects of noise exposure.

4.2 Methods

Experimental procedures were performed in accordance with National Institutes of Health guidelines and were approved by the Institutional Animal Care and Use Committee at the University of Pittsburgh.

4.2.1 Animals

All experiments were performed in mice. Transplanted MGE cells were derived from embryonic green x VGAT-dT mice (see chapter 3 for details). Thus, MGE cells carried a single gene of VGAT-ires-cre, tdTomato, and green fluorescent protein (GFP), allowing for identification of transplanted MGE cells (GFP+) as well as identification of which transplanted cells were GABAergic (tdTomato+). Host mice were wild type CBA/CaJ mice (Jax 000654). Non-injected CBA/CaJ mice, with or without noise exposure served as behavioral controls.

4.2.2 MGE cell collection and stereotaxic injection

Collection, dissociation, and transplantation of MGE tissue explants into the IC was performed using previously described methods (see chapter 3 for details). Intracranial injection of MGE cells into the IC was performed between 5 and 9 weeks of age.

4.2.3 Noise exposure

Mice of either sex (3.7-5.3 weeks old) were randomly selected for noise-exposure. Noise exposure was performed using previously described methods (see chapter 3 for details).

4.2.4 Auditory Brainstem Response

In subjects injected with MGE cells (MGE inj), auditory brainstem response (ABR) thresholds were measured at baseline and at the time of behavioral testing (Figure 18A). Noise

exposed (NE) and MGE injected subjects (NE+MGE inj) were additionally tested at one-week post noise exposure (Figure 18A). NE subjects (non-injected) were tested before and one-week post noise exposure and at the time of behavioral testing (Figure 18A). Control (non-noise exposed, non-injected) subjects were only tested at the time of behavioral testing (Figure 18A).

Measurements were made using previously described methods (Sturm et al., 2017). Briefly, subjects were anesthetized with vaporized isoflurane and their body temperature maintained between 36-38˚C with a heating pad (FHC DC temperature controller). The subjects were placed in a sound-attenuating chamber (Medical Associates) and subdermal electrodes were placed at the vertex and ventral to each pinna, as reference and ground. Measurements were made using the Z-series 3-DSP Bioacoustic System (Tucker Davis Technologies) and stimuli were delivered open field (System 3 Software Package, Tucker Davis Technologies). ABR thresholds were obtained for 1ms clicks presented at various sound intensities (20-80dB SPL) at a rate of 18.56/s. Evoked potentials were averaged 1024 times and filtered using a 300-3000Hz band-pass filter. ABR waveforms were visualized using BioSigRZ software (Tucker-Davis Technologies) and stacked in ascending order. Threshold was determined by visual analysis and defined as the lowest level at which a reproducible wave or trough appeared. Wave 1 latency was defined as the time from stimulus onset to the wave 1 peak. Wave 1 amplitude was defined as the amplitude difference between the wave 1 peak and trough.

4.2.5 Behavioral testing and analysis

Behavioral tests were performed between 24 and 27 weeks of age (20-21 weeks post noise exposure, 19 weeks post MGE injection). Variations of the acoustic startle response (ASR) were

used to evaluate central auditory gain (amplitude varied acoustic startle response, AmpVar-ASR) and sensorimotor gating (pre-pulse inhibition, PPI) in control, MGE injected, NE, and NE+MGE injected subjects. Sessions were repeated three times, consecutively. AmpVar-ASR trials consisted of startle stimuli (20ms white noise pulses) presented at varying loudness (70-115dB SPL, Figure 19A). Each session contained 20 trials of each stimulus type presented pseudo-randomly. In PPI trials, 50ms, 30dB SPL tones pips (10, 20, or 32 kHz) were presented 50ms before the startle stimulus (20ms, 115dB SPL white noise pulse, Figure 19A). Prior to the start of the first session, an acclimation period of 5-minutes of silence followed by 20 startle only (115dB SPL) trials was given

The ASR, defined as the absolute value of the maximum force exerted by the mouse onto a piezoelectric platform (Clause et al., 2011) in response to the startle stimulus, was determined for each trial. Trials in which the ASR was less than two standard deviations above the average root means squared of the baseline activity were excluded.

For AmpVar-ASR trials, the ASR in response to each stimulus amplitude was fit to a psychometric curve of the form:

$$y = \frac{3 - P_1}{1 + e^{-\left(\frac{x - P_2}{P_3}\right)}}$$

This formula was optimized to fit the AmpVar-ASR data, where $3\text{-}P_1$ represents the maximal height of the psychometric curve. P_2 and P_3 were obtained for each subject, with P_2 representing

the startle stimulus amplitude that elicited a startle response that was fifty percent of the maximum startle response (a measure of shift) and P_3 representing the steepness of the psychometric curve.

For PPI trials, the percent decrease was calculated to characterize the degree to which a pre-pulse decreases the startle amplitude.

$$Percentdecrease = \frac{ASR\ at\ 115dB\ SPL - ASR\ following\ a\ prepulse}{ASR\ at\ 115dB\ SPL} \times 100$$

Therefore, the higher the percent decrease, the more the ASR was decreased by the presence of a pre-pulse.

4.2.6 Statistical analysis

Statistical analysis was performed using GraphPad Prism software. Mann Whitney tests were used to compare two independent groups. Wilcoxon matched-pairs signed rank tests were used to compare two paired groups. Kruskal-Wallis tests were used to compare three or more groups, multiple comparisons were corrected for using the Dunn pairwise method. Two-way ANOVA was used for comparisons in which there were two independent variables, multiple comparisons were corrected for using Tukey's test. Statistical significance for all tests was set to $p<0.05$ and corrected for in cases of multiple comparisons.

4.3 Results

MGE cells were injected bilaterally into the IC of 17 subjects. Seven subjects were excluded, of whom 5 demonstrated unilateral MGE survival and 2 were near misses. After confirming bilateral MGE cell survival and migration, 6 MGE injected subjects and 4 NE+MGE injected subjects were included. Six control and 5 NE subjects were included for comparison.

4.3.1 Transplantation of MGE cells into the IC does not affect hearing thresholds, but may increase spiral ganglion recruitment at the expense of synchronicity

Our noise exposure protocol (8-16kHz bandpass noise at 100dB SPL for 2hrs) resulted in an approximately 20dB SPL threshold shift at one-week post noise exposure (Figure 18B). Click ABR thresholds were not significantly increased in either NE subjects (pre-NE median=40 dB SPL, post-NE median=60dB SPL, p=0.06, Wilcoxon test) or NE subjects who would subsequently be injected with MGE cells (pre-NE median=45dB SPL, post-NE median=65dB SPL, p=0.13, Wilcoxon test). Furthermore, there was no significant difference in the change in click ABR thresholds between NE subjects (median=20dB SPL) and NE subjects who would subsequently be injected with MGE cells (NE+MGE inj, median=17.5dB SPL, p=0.4, Figure 18B). At the time of behavioral testing (20-21 weeks post noise exposure), both NE and NE+MGE injected subjects demonstrated a permanent threshold shift. NE subjects maintained a median permanent threshold shift of 20dB SPL (IQR=12.5, n=5) while NE+MGE injected subjects demonstrated a median permanent threshold shift of 10dB SPL (IQR=10, n=4). We also observed a slight increase in click ABR thresholds following MGE injection in non-noise exposed subjects (MGE inj, median=5dB SPL, IQR=21.3, n=6). The change in click ABR thresholds from baseline to the time of behavioral

testing was not significantly different between MGE injected, NE, and NE+MGE injected subjects (Table 10).

In addition to the change in hearing thresholds, we were interested in whether the absolute value of hearing thresholds varied between the groups at the time of behavioral testing. We found that noise exposed subjects, regardless of MGE cell injection, had higher hearing thresholds than non-noise exposed subjects (Figure 18D). Click ABR thresholds in NE subjects (mean=61dB SPL) were significantly higher than control (mean= 52dB SPL, p=0.04) and MGE injected (52dB SPL, p=0.04) subjects (Table 11). There was no significant difference in the click ABR thresholds NE+MGE injected subjects (mean=56dB SPL) compared to control (p=0.53), MGE injected (p=0.53), or NE (p=0.53, Table 11). Simple main effects analysis revealed that noise exposure (p=0.01) but not MGE injection (p=0.31) had a significant effect on click ABR thresholds at the time of behavioral testing (Table 11). Together, these results suggest that our noise exposure protocol resulted in mild, sustained hearing loss that was unaffected by transplantation of MGE cells into the IC.

In addition to hearing thresholds, we examined the latency and amplitude of wave 1 of the ABR in response to 80dB SPL clicks at the time of behavioral testing. The latency and amplitude of wave 1 provide information about the speed and synchronicity of action potentials in the spiral ganglion neurons of the auditory nerve (Henry and Haythorn, 1978; Jewett and Romano, 1972) and thus provide information on cochlear gain. Noise exposure resulted in increased wave 1 latency, indicating a delayed response at the level of the auditory nerve, while MGE injection decreased wave 1 latency in both non-noise exposed and noise exposed subjects. We observed an increased wave 1 latency in NE subjects (mean=1.8ms) compared to control (mean=1.6ms), MGE injected (mean=1.5ms), and NE+MGE injected subjects (mean=1.6ms, Figure 18E). However, the

only comparison to reach statistical significance was between NE and MGE injected subjects (p=0.01, Table 12). We found that noise exposure (p=0.01), but not MGE injection (p=0.06), contributed to the variability in wave 1 latency (Table 12). Despite not reaching statistical significance, there was a trend towards decreased wave 1 latency in MGE injected subjects. Indeed, we observed shorter wave 1 latency times in MGE injected subjects compared to control (p=0.63, Table 12) and in NE+MGE injected subjects compared to NE subjects (p=0.42, Table 12). Given that we found no significant interaction between the effects of noise exposure and MGE injection (p=0.69, Table 12), it is likely that any possible contribution to wave 1 latency from MGE injection is similar in both non-noise exposed and noise exposed subjects.

Wave 1 amplitude was decreased in NE, MGE injected, and NE+MGE injected subjects, indicating a more asynchronous response at the level of the auditory nerve. The mean wave 1 amplitude was twice as large in control subjects (mean=1.29μV) than in MGE injected (mean=0.65μV), NE (mean=0.52μV), and NE+MGE injected subjects (mean=0.66μV, Figure 18F). Compared to control, both NE (p=0.02) and MGE injected subjects (p=0.05) had significantly lower wave 1 amplitudes (Table 13). Noise exposure had a significant, independent effect on wave 1 amplitude (p=0.04, Table 13). Interestingly, MGE injection alone did not account for a significant source of variation (p=0.18), but there was a significant interaction between MGE injection and noise exposure (p=0.03, Table 13). This interaction suggests that effects of transplanted MGE cells on wave 1 amplitude is variable between non-noise exposed and noise exposed subjects. This explains our finding that NE+MGE injected subjects had similar wave 1 amplitudes as both MGE injected and NE subjects. Had the effects of NE and MGE injection been independent, we would have expected the cumulative effect to result in much lower wave 1 amplitudes in NE+MGE injected subjects than in NE animals of MGE animals.

Together, these data demonstrate that even in the presence of mild threshold shifts, noise exposure led to increased wave 1 latency and decreased wave 1 amplitude, suggesting that there was less recruitment and less synchrony in the activation of spiral ganglion neurons in response to sound. Wave 1 latency and amplitude was evaluated in response to 80dB SPL clicks, which were roughly 30dB above the average hearing threshold for control and MGE injected subjects, 25dB above the average threshold for NE+MGE injected subjects and 20dB above the average hearing threshold in NE subjects. Thus, it is possible that the difference in the stimulus level relative to threshold contributed to the increased wave 1 latency and decreased waved 1 amplitude in NE subjects. However, this would not explain the decreased wave 1 latency and amplitude in MGE injected subjects, who had hearing thresholds that were similar to control subjects. As such, transplantation of MGE cells into the IC likely led to decreased wave 1 latency and amplitude, suggesting that the spiral ganglion neurons were activated more quickly, but less synchronously. The finding that transplantation of MGE cells into the IC effected spiral ganglion activity was surprising and suggests that the effects of MGE cells are not limited to local IC circuits.

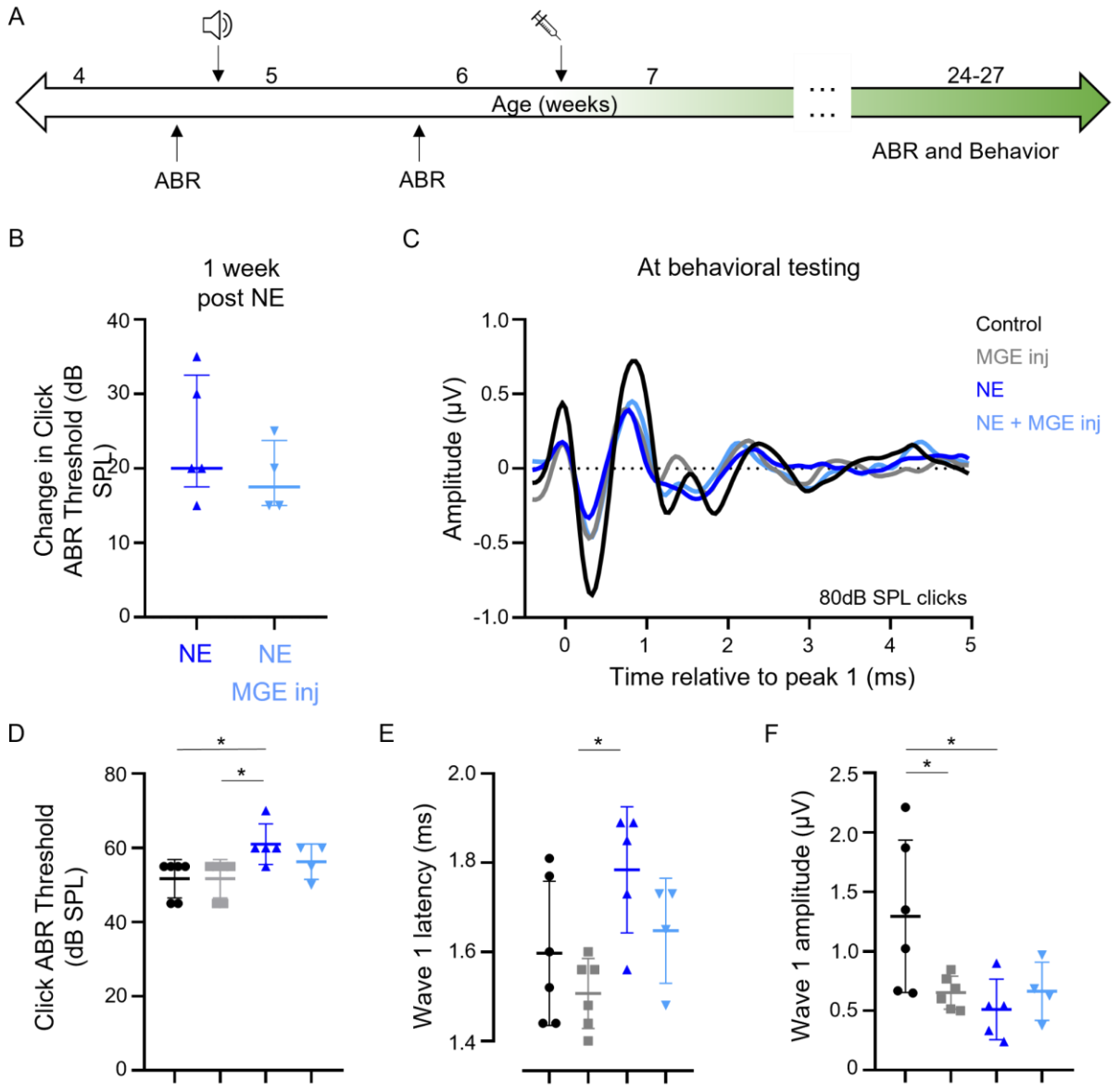

Figure 18. Transplanted MGE cells do not affect click ABR thresholds, but decrease wave 1 latency and amplitude.

A. Methods schematic: Arrow represents time with age in weeks noted above.

Approximate time at which auditory brainstem responses (ABRs) were recorded is noted. ABRs were measured in MGE injected, NE, and NE+MGE injected subjects at approximately 4 to 5 weeks old. Repeat ABRs were performed in NE and NE+MGE injected subjects one week following noise exposure. ABRs were recorded in all subjects (Control, MGE inj, NE, and NE+MGE inj) at the time of behavioral testing.

The speaker icon indicates the approximate time of noise exposure for NE and NE+MGE inj subjects.

The syringe icon indicated the approximate time of MGE injection for MGE inj and NE+MGE inj subjects.

The green shading in the arrow roughly indicates the expected degree of integration of the transplanted MGE cells. Dark green indicated that migration and maturation of transplanted MGE cells has stabilized.

B. Change in click ABR thresholds at 1-week post noise exposure. NE subjects (dark blue triangles, n=5) experienced a median threshold shift of 20dB. NE+MGE subjects (light blue inverted triangles, n=4) experienced a median threshold shift of 17.5dB SPL. There was no significant difference in the threshold shift of NE or NE+MGE injected subjects at 1-week post noise exposure ($p=0.39$, Mann-Whitney test).

C-F. Average ABR waveforms at 80dB SPL, click ABR thresholds, and wave 1 amplitude and latency in control (black circles, n=6 mice), MGE injected (grey squares, n=6 mice), noise exposed (NE, dark blue triangles, n=5 mice), and NE and MGE injected (NE+MGE inj, light blue inverted triangles, n=4 mice) subjects at the time of behavioral testing. D-F, individual data with mean and standard deviation. Asterisks denote statistical significance (*$p<0.05$).

C. The average click ABR waveform at 80dB for control, MGE inj, NE, and NE+MGE inj subjects. Wave 1 amplitude is decreased in MGE inj, NE, and NE+MGE inj subjects. Individual waveforms were aligned by peak wave 1 latency before averaging. Group waveforms are also aligned by peak wave 1 latency.

D. Click ABR thresholds were significantly increased in NE subjects (61dB SPL) compared to control (52dB SPL, $p=0.04$) and MGE injected (52dB SPL, $p=0.04$) subjects. There was no significant difference in the click ABR thresholds of NE+MGE injected subjects (56dB SPL) compared to NE, control, or MGE injected subjects.

E. Wave 1 latency was increased in NE subjects (1.78ms) compared to control (1.60ms), MGE injected (1.51ms), and NE+MGE injected subjects (1.65ms). MGE injected subjects had the shortest wave 1 latency, while NE+MGE injected subjects had a similar wave 1 latency to control subjects. Wave 1 latency was significantly lower in MGE injected subjects compared to NE subjects ($p=0.01$).

F. Wave 1 amplitude was decreased in NE (0.51μV), MGE injected (0.65μV), and NE+MGE injected (0.66μV) subjects compared to control (1.29μV). Wave 1 amplitude was significantly lower in MGE inj subjects compared to control subjects ($p=0.05$) and in NE subjects compared to control subjects ($p=0.02$).

Table 10. Change in click ABR thresholds from baseline to the time of behavioral testing

Descriptive Statistics

	Median (dB)	IQR	n
MGE injected	5	21.25	6
Noise exposed	20	12.5	5
Noise exposed and MGE injected	10	10	4

Kruskal-Wallis table

Kruskal-Wallis H	3.02
degrees of freedom	2
p value	0.22

Dunn's multiple comparisons test

	Mean rank 1	Mean rank 2	Mean rank diff.	Adjusted P Value
MGE inj vs. NE	6.3	10.7	-4.5	0.27
NE+MGE inj vs MGE inj	7.3	6.3	1	>1
NE+MGE inj vs NE	7.3	10.7	-3.5	0.71

Table 11. Click ABR thresholds at the time of behavioral testing

Two-way ANOVA table

	SS (Type III)	DF	MS	F (DFn, DFd)	P value
Interaction	28.8	1	28.8	F (1, 17) = 1.075	0.31
MGE Injection	28.8	1	28.8	F (1, 17) = 1.075	0.31
Noise exposure	247.2	1	247.2	F (1, 17) = 9.229	0.01
Residual	455.4	17	26.79		

Tukey's multiple comparisons test

	Mean 1 (dB SPL)	Mean 2 (dB SPL)	Mean Diff.	95.00% CI of diff.	Adjusted P Value
Control vs. NE	51.67	61	-9.33	-18.24 to -0.42	0.04
Control vs. MGE inj	51.67	51.67	0.00	-8.49 to 8.49	>1
Control vs. NE+MGE inj	51.67	56.25	-4.58	-14.08 to 4.91	0.53
NE vs. MGE inj	61	51.67	9.33	0.42 to 18.24	0.04
NE vs. NE+MGE inj	61	56.25	4.75	-5.12 to 14.62	0.53
MGE inj vs. NE+MGE inj	51.67	56.25	-4.58	-14.08 to 4.91	0.53

Red p-values indicate statistical significance.

Table 12. The effects of MGE injection and noise exposure on click ABR wave 1 latency at 80dB SPL

Two-way ANOVA table

	SS (Type III)	DF	MS	F (DFn, DFd)	P value
Interaction	0.003	1	0.003	F (1, 17) = 0.1658	0.69
MGE Injection	0.065	1	0.065	F (1, 17) = 3.933	0.06
Noise exposure	0.138	1	0.138	F (1, 17) = 8.257	0.01
Residual	0.283	17	0.017		

Tukey's multiple comparisons test

	Mean 1 (ms)	Mean 2 (ms)	Mean Diff.	95.00% CI of diff.	Adjusted P Value
Control vs. NE	1.60	1.78	-0.19	-0.41 to 0.03	0.12
Control vs. MGE inj	1.60	1.51	0.09	-0.12 to 0.31	0.63
Control vs. NE+MGE inj	1.60	1.65	-0.05	-0.29 to 0.19	0.93
NE vs. MGE inj	1.78	1.51	0.28	0.063 to 0.50	0.01
NE vs. NE+MGE inj	1.78	1.65	0.14	-0.11 to 0.38	0.42
MGE inj vs. NE+MGE inj	1.51	1.65	-0.14	-0.38 to 0.10	0.36

Red p-values indicate statistical significance.

Table 13. The effects of MGE injection and noise exposure on click ABR wave 1 amplitude at 80dB SPL

Two-way ANOVA table

	SS (Type III)	DF	MS	F (DFn, DFd)	P value
Interaction	0.81	1	0.81	F (1, 17) = 5.285	0.03
MGE Injection	0.31	1	0.31	F (1, 17) = 2.001	0.18
Noise exposure	0.76	1	0.76	F (1, 17) = 5.009	0.04
Residual	2.59	17	0.15		

Tukey's multiple comparisons test

	Mean 1 (µV)	Mean 2 (µV)	Mean Diff.	95.00% CI of diff.	Adjusted P Value
Control vs. NE	1.29	0.51	0.78	0.12 to 1.46	0.02
Control vs. MGE inj	1.29	0.65	0.64	0.0009 to 1.28	0.05
Control vs. NE+MGE inj	1.29	0.66	0.63	-0.09 to 1.35	0.10
NE vs. MGE inj	0.51	0.65	-0.14	-0.81 to 0.53	0.93
NE vs. NE+MGE inj	0.51	0.66	-0.15	-0.90 to 0.59	0.94
MGE inj vs. NE+MGE inj	0.65	0.66	-0.01	-0.73 to 0.71	>1

Red p-values indicate statistical significance.

4.3.2 Noise exposure decreases the ASR at moderate stimulus levels, but transplantation of MGE cells into the IC of noise exposed mice mitigates this effect

Knowing that transplantation of MGE cells into the IC has implications beyond local IC circuits, we were interested in 1) if transplantation of MGE cells would disrupt normal IC function, leading to changes in PPI or the AmpVar-ASR of non-NE mice and 2) whether transplantation of MGE cells could mitigate any effects of noise exposure on PPI and the AmpVar-ASR.

We found that PPI was robustly maintained with pre-pulse stimulus frequencies of 10 (Table 14), 20 (Table 15), and 32kHz (Table 16, Figure 19B), regardless of whether subjects were previously noise exposed or injected with MGE cells. In all subjects, higher frequency pre-pulses elicited higher PPI (Figure 19B). A 10kHz pre-pulse was associated with an approximately 30% decrease in the startle response (Table 14), while 20 and 32kHz pre-pulses resulted in 50-60% decrease in the startle response (Table 15 and 16, respectively). No significant differences were observed between control, MGE injected, NE, or NE+MGE injected subjects at any of the pre-pulse frequencies (Tables 14-16). Neither noise exposure or MGE injection alone were a significant source of variability in PPI at any frequency (Tables 14-16). Interestingly, we did see a significant interaction between noise exposure and MGE injection for 32kHz pre-pulses ($p=0.01$, Table 16), suggesting that PPI in response to high frequency pre-pulses may be affected by the combination of noise exposure and MGE injection. Given that we saw no significant difference in PPI between the groups at 32kHz, further research is necessary to understand the behavioral relevance of this interaction. Together, these data suggest that PPI was unaffected by either noise exposure or MGE injection.

Next, we investigated the effects of noise exposure on the AmpVar-ASR. Our noise exposure protocol (8-16kHz bandpass noise at 100dB SPL for 2hrs) resulted in a decrease in the

ASR of NE subjects in response to 80-115dB SPL startle stimuli, leading to a psychometric AmpVar-ASR curve that was right-shifted and shorter (Figure 19C). MGE injection had no effect on the AmpVar-ASR in non-NE subjects (Figure 19C). However, in NE+MGE injected subjects, transplantation of MGE cells appeared to rescue the ASR, particularly in response to moderate to high amplitude startle stimuli (90-115dB SPL, Figure 19C). As a result, the psychometric AmpVar-ASR curve of NE+MGE injected subjects was similar in shape to that of control and MGE injected subjects, suggesting that transplantation of MGE cells mitigated the decreased startle amplitudes caused by noise exposure.

To characterize the shape of the psychometric curve, we examined the position of the half-maximum ASR (P2, a measure of shift) and the steepness (P3). Noise exposure primarily effected the shift of the psychometric curve (P2), with a higher startle stimulus amplitude required to elicit the half-maximum ASR amplitude in NE subjects compared to control, MGE injected, or NE+MGE injected subjects (Figure 19C, middle). Indeed, the startle stimulus amplitude required to elicit the half-maximum ASR amplitude of NE subjects was significantly higher at 97dB SPL, compared to control subjects at 87dB SPL ($p=0.01$) and MGE injected subjects at 86dB SPL ($p=0.005$, Table 17). While not significant, the startle stimulus amplitude required to elicit the half-maximum ASR in NE+MGE injected subjects (89dB SPL) was also lower than that of NE subjects ($p=0.08$, Table 17). These data suggest that transplantation of MGE cells into the IC of NE subjects mitigates the noise-induced shift in the psychometric AmpVar-ASR curve. Consistent with this, there was no significant difference in startle stimulus amplitude required to elicit the half-maximum ASR of NE+MGE injected subjects compared to control ($p=0.84$) and MGE injected ($p=0.73$, Table 17) subjects. We found that both noise exposure ($p=0.004$) and MGE injection ($p=0.05$) had significant, independent effects on the ASR. While the interaction between noise

exposure and MGE injection did not reach statistical significance (p=0.08), the increase in the ASR associated with MGE injection was greater in NE+MGE injected subjects than MGE injected subjects. Together, these results suggest that our noise exposure protocol led to a right-shift in the AmpVar-ASR curve, which was mitigated by the transplantation of MGE cells.

Subjectively, we noticed a decrease in the growth and maximum value of the ASR in NE subjects. However, when comparing the steepness of the psychometric curve (P3), we found that NE subjects (mean=7.4) actually exhibited a slight increase in the steepness of the AmpVar-ASR curve compared to control (mean=5.8), MGE injected (mean=5.9), and NE+MGE injected subjects (mean=5.4, Figure 19C, right). This slight increase in steepness, however, was not statistically significant (Table 18). Consistent with this, we found that neither noise exposure (p=0.47) or MGE injection (p=0.22) had a significant effect on the steepness of the AmpVar-ASR curve (Table 18). These results suggest that the of the steepness of the AmpVar-ASR curve was maintained, regardless of whether subjects had a history of noise exposure or were injected with MGE cells.

This led us to wonder whether noise exposure decreased the maximum value of the ASR but preserved the growth of the AmpVar-ASR curve, which might explain our subjective observation that the AmpVar-ASR curve was both right shifted and shorter in NE subjects compared to control subjects. However, we found no significant difference in the maximum ASR between the groups (Table 19). Consistent with this, we found that neither noise exposure (p=0.38) or MGE injection (p=0.13) had a significant effect on the maximum ASR (Table 19). Thus, the maximum value of the ASR was also unaffected by noise exposure and MGE injection.

Together, these results suggest that the effects of transplanted MGE cells may differ between non-noise exposed and noise exposed subjects. While the interaction between noise exposure and MGE injection on the half-maximum ASR did not achieve statistical significance,

transplanted MGE cells appeared to increase the ASR of noise exposed subjects (NE+MGE inj vs NE) more than that of non-noise exposed subjects (MGE inj vs control). Transplantation of MGE cells into the noise exposed IC mitigated the noise induced shift in the AmpVar-ASR curve but had no effect on PPI. This suggests that while transplanted MGE cells mitigated the observed behavioral effect of noise exposure, they did not do so at the expense of normal IC function, at least as it pertains to PPI. Consistent with this, we saw no change in PPI or the AmpVar-ASR curve of non-noise exposed, MGE injected subjects. Thus, the effect of transplanted MGE cells on behavior may be influenced by prior noise exposure. As a result, MGE cells may be useful in mitigating the effects of noise exposure while preserving IC function.

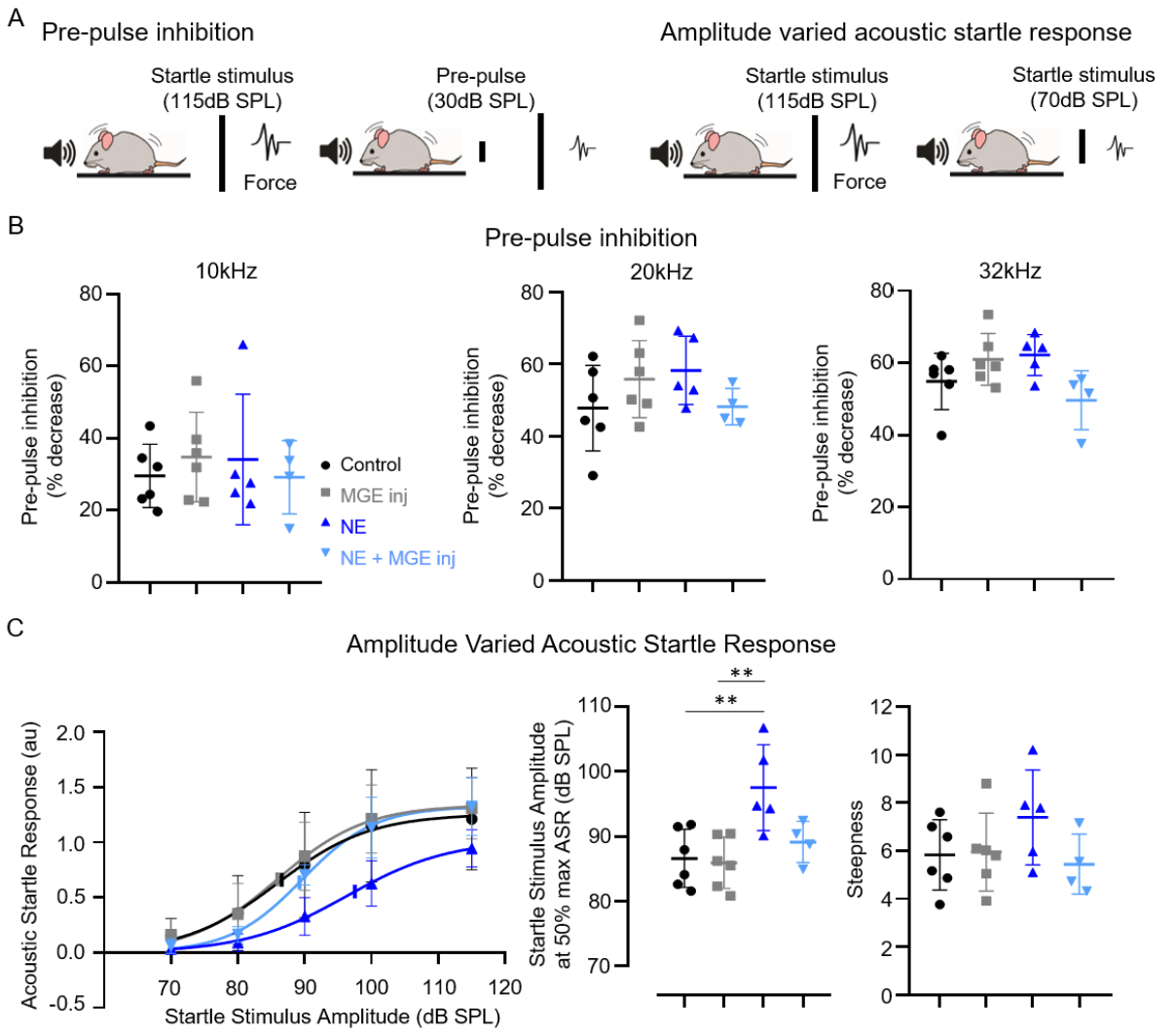

Figure 19. Transplantation of MGE cells mitigates the effects of noise exposure on the amplitude varied ASR curve but has no effect on PPI

A. Schematic representation of behavioral tests and expected outcomes. Mice were placed on a piezoelectric platform that recorded the force exerted on the platform, the acoustic startle response (ASR), following the startle stimulus. Trials with and without a pre-pulse were pseudo randomly presented. Pre-pulse inhibition (PPI, left) was measured as the percent decrease in the ASR when the startle stimulus (20 ms, 115dB SPL white noise pulse) was preceded by a pre-pulse of 10, 20, or 32kHz (30dB SPL). The presence of a pre-pulse is expected to lead to a decrease in the ASR. The amplitude varied acoustic startle response (AmpVar-ASR, right) was evaluated by measuring the ASR in response to startle stimuli (20ms white noise pulse) at various intensities (70-115dB SPL). The ASR is expected to increase with increasing startle stimulus amplitude.

B and C, PPI and Amp-Var ASR responses for control (black circles, n=6 mice), MGE injected (grey squares, n=6 mice), noise exposed (NE, dark blue triangles, n=5 mice), and NE and MGE injected (NE+MGE inj, light blue inverted triangles, n=4 mice) subjects. Individual subject data is plotted with mean and standard deviation, unless otherwise noted. Asterisks denote statistical significance (**$p<0.01$).

B. Pre-pulse inhibition at 10 (left), 20 (middle), and 32kHz (right). PPI improved with increasing frequency. A 10kHz pre-pulse reduced the ASR by roughly 30%, while 20 and 32kHz pre-pulses reduced the ASR by roughly 50-60%. There were no significant differences in PPI between the groups at any pre-pulse frequency.

C. The average ASR at each startle stimulus amplitude is plotted with the average psychometric curve for each group (left). Vertical lines represent the half-maximum ASR. NE subjects had a decreased ASR at moderate and high intensities (80-115dB SPL). NE+MGE inj subjects had a decreased ASR at 80dB SPL but achieve values similar to control subjects in response to higher amplitude stimuli. MGE injected and control subjects have similar ASR curves. The startle stimulus amplitude required to elicit the half-maximum ASR (middle) was significantly higher in NE mice (98dB SPL) compared to control (87dB SPL, $p=0.001$), MGE inj (86dB SPL, $p=0.005$) subjects. The startle stimulus amplitude at the half maximum ASR in NE+MGE inj (89dB SPL) subjects was similar to control and MGE inj subjects.

That steepness of the psychometric curve (right) was slightly higher in NE subjects (7.4) compared to control (5.8), MGE inj (5.9), and NE+MGE inj (5.4) subjects. There were no significant differences in the steepness of the psychometric curve between the groups.

Table 14. Effects of MGE injection and noise exposure on PPI at 10kHz

Two-way ANOVA table

	SS (Type III)	DF	MS	F (DFn, DFd)	P value
Interaction	132.9	1	132.9	F (1, 17) = 0.81	0.38
MGE Injection	0.08	1	0.08	F (1, 17) = 0.0005	0.98
Noise exposure	1.40	1	1.40	F (1, 17) = 0.01	0.93
Residual	2780	17	163.5		

Tukey's multiple comparisons test

	Mean 1 (% decrease)	Mean 2 (% decrease)	Mean Diff.	95.00% CI of diff.	Adjusted P Value
Control vs. NE	29.55	34.13	-4.58	-26.59 to 17.43	0.93
Control vs. MGE inj	29.55	34.78	-5.23	-26.22 to 15.76	0.89
Control vs. NE+MGE inj	29.55	29.15	0.40	-23.07 to 23.86	>1
NE vs. MGE inj	34.13	34.78	-0.65	-22.67 to 21.36	1
NE vs. NE+MGE inj	34.13	29.15	4.97	-19.41 to 29.36	0.94
MGE inj vs. NE+MGE inj	34.78	29.15	5.63	-17.84 to 29.09	0.90

Table 15. Effects of MGE injection and noise exposure on PPI at 20kHz

Two-way ANOVA table

	SS (Type III)	DF	MS	F (DFn, DFd)	P value
Interaction	418.4	1	418.4	F (1, 17) = 4.14	0.06
MGE Injection	5.13	1	5.13	F (1, 17) = 0.05	0.82
Noise exposure	10.48	1	10.48	F (1, 17) = 0.10	0.75
Residual	1717	17	101		

Tukey's multiple comparisons test

	Mean 1 (% decrease)	Mean 2 (% decrease)	Mean Diff.	95.00% CI of diff.	Adjusted P Value
Control vs. NE	47.79	58.28	-10.48	-27.78 to 6.81	0.34
Control vs. MGE inj	47.79	55.84	-8.05	-24.54 to 8.44	0.52
Control vs. NE+MGE inj	47.79	48.22	-0.43	-18.87 to 18.01	1
NE vs. MGE inj	58.28	55.84	2.44	-14.86 to 19.73	0.98
NE vs. NE+MGE inj	58.28	48.22	10.05	-9.11 to 29.22	0.46
MGE inj vs. NE+MGE inj	55.84	48.22	7.62	-10.82 to 26.06	0.65

Table 16. Effects of MGE injection and noise exposure on PPI at 32kHz

Two-way ANOVA table

	SS (Type III)	DF	MS	F (DFn, DFd)	P value
Interaction	442.8	1	442.8	F (1, 17) = 8.45	0.001
MGE Injection	52.16	1	52.16	F (1, 17) = 1.00	0.33
Noise exposure	20.90	1	20.90	F (1, 17) = 0.40	0.54
Residual	891.2	17	52.42		

Tukey's multiple comparisons test

	Mean 1 (% decrease)	Mean 2 (% decrease)	Mean Diff.	95.00% CI of diff.	Adjusted P Value
Control vs. NE	54.87	62.16	-7.30	-19.75 to 5.17	0.37
Control vs. MGE inj	54.87	60.99	-6.12	-18.00 to 5.77	0.48
Control vs. NE+MGE inj	54.87	49.65	5.22	-8.07 to 18.50	0.68
NE vs. MGE inj	62.16	60.99	1.17	-11.29 to 13.64	0.99
NE vs. NE+MGE inj	62.16	49.65	12.51	-1.30 to 26.31	0.08
MGE inj vs. NE+MGE inj	60.99	49.65	11.33	-1.95 to 24.62	0.11

Red p-values indicate statistical significance.

Table 17. The effects of MGE injection and noise exposure on the startle stimulus amplitude corresponding to the half-maximum ASR

Two-way ANOVA table

	SS (Type III)	DF	MS	F (DFn, DFd)	P value
Interaction	76.05	1	76.05	F (1, 17) = 3.36	0.08
MGE Injection	104.1	1	104.1	F (1, 17) = 4.60	0.05
Noise exposure	253.9	1	253.9	F (1, 17) = 11.22	0.003
Residual	384.5	17	22.62		

Tukey's multiple comparisons test

	Mean 1 (dB SPL)	Mean 2 (dB SPL)	Mean Diff.	95.00% CI of diff.	Adjusted P Value
Control vs. NE	86.59	97.5	-10.91	-19.10 to -2.72	0.01
Control vs. MGE inj	86.59	85.93	0.66	-7.15 to 8.46	1
Control vs. NE+MGE inj	86.59	89.12	-2.54	-11.26 to 6.19	0.84
NE vs. MGE inj	97.5	85.93	11.57	3.38 to 19.75	0.005
NE vs. NE+MGE inj	97.5	89.12	8.38	-0.69 to 17.44	0.08
MGE inj vs. NE+MGE inj	85.93	89.12	-3.19	-11.92 to 5.54	0.73

Red p-values indicate statistical significance.

Table 18. Effects of MGE injection and noise exposure on the slope of the psychometric AmpVar-ASR curve

Two-way ANOVA table

	SS (Type III)	DF	MS	F (DFn, DFd)	P value
Interaction	5.45	1	5.45	F (1, 17) = 2.10	0.17
MGE Injection	4.30	1	4.30	F (1, 17) = 1.66	0.22
Noise exposure	1.43	1	1.43	F (1, 17) = 0.55	0.47
Residual	44.08	17	2.59		

Tukey's multiple comparisons test

	Mean 1	Mean 2	Mean Diff.	95.00% CI of diff.	Adjusted P Value
Control vs. NE	5.83	7.39	-1.56	-4.33 to 1.21	0.40
Control vs. MGE inj	5.83	5.95	-0.12	-2.76 to 2.53	1
Control vs. NE+MGE inj	5.83	5.44	0.39	-2.57 to 3.34	0.98
NE vs. MGE inj	7.39	5.95	1.45	-1.33 to 4.22	0.47
NE vs. NE+MGE inj	7.39	5.44	1.95	-1.12 to 5.02	0.30
MGE inj vs. NE+MGE inj	5.95	5.44	0.50	-2.45 to 3.46	0.96

Table 19. Effects of MGE injection and noise exposure on the maximum ASR

Two-way ANOVA table

	SS (Type III)	DF	MS	F (DFn, DFd)	P value
Interaction	0.11	1	0.11	F (1, 17) = 0.99	0.33
MGE Injection	0.28	1	0.28	F (1, 17) = 2.51	0.13
Noise exposure	0.09	1	0.09	F (1, 17) = 0.80	0.38
Residual	1.88	17	0.11		

Tukey's multiple comparisons test

	Mean 1	Mean 2	Mean Diff.	95.00% CI of diff.	Adjusted P Value
Control vs. NE	1.22	0.94	0.28	-0.29 to 0.85	0.53
Control vs. MGE inj	1.22	1.31	-0.09	-0.63 to 0.46	0.97
Control vs. NE+MGE inj	1.22	1.32	-0.10	-0.71 to 0.51	0.96
NE vs. MGE inj	0.94	1.31	-0.36	-0.94 to 0.21	0.30
NE vs. NE+MGE inj	0.94	1.32	-0.38	-1.01 to 0.25	0.35
MGE inj vs. NE+MGE inj	1.31	1.32	-0.01	-0.62 to 0.59	1.00

4.4 Discussion

Our results provide the first evidence that the effects of transplanted MGE cells extend beyond the IC and may be useful in mitigating behavioral effects of noise exposure. We found that transplantation of MGE cells into the IC led to a decrease in the wave 1 amplitude and latency of the click ABR waveform. These results suggest that increasing inhibition in the IC led to increased cochlear gain, as evidenced by increased recruitment of spiral ganglion neurons (decreased wave 1 latency), but at the expense of synchrony (decreased wave 1 amplitude). In noise exposed mice, transplantation of MGE cells into the IC mitigated the noise induced shift in the AmpVar-ASR curve without effecting PPI. Furthermore, we found that transplantation of MGE cells into the non-noise exposed IC had no effect on PPI or the AmpVar-ASR curve. Thus, the behavioral effects of transplanted MGE cells appear to be state dependent and vary based on a prior history of noise exposure. Importantly, transplanted MGE cells appear to mitigate the behavioral effects of noise exposure while maintaining normal IC function in at least two auditory behaviors to which the IC contributes.

4.4.1 Transplanted MGE cells do not disrupt PPI

In chapter 3 we showed that the majority of transplanted MGE cells remain clustered at the injection site, with roughly 1-2% of MGE cells migrating away. Our results suggest that the MGE cells that migrate from the injection site are largely inhibitory and are capable of forming synaptic connections with endogenous IC neurons. However, the differentiation and impact of the MGE cells clustered at the injection site was difficult to evaluate. While the high clustering prevented the visualization of neuronal processes that might have originated from the aggregated cells, we

wondered whether the mere existence of a cellular aggregate in the IC could disrupt normal IC activity. The IC is critical for PPI and lesioning the IC has been shown to abolish this behavior in naïve mice (Koch and Schnitzler, 1997; L. Li et al., 1998). Thus, if MGE cells were to disrupt IC activity, we would expect to see a small change in the PPI of injected mice. Our finding that PPI was maintained in MGE injected subjects indicates that transplantation of MGE cells does not negatively impact the IC's role in sensorimotor gaiting and suggests that at least this particular function is preserved.

4.4.2 The effects of noise exposure on PPI and the AmpVar-ASR may be related to the degree of hearing loss

The behavioral consequences of noise exposure are highly variable and, in the case of PPI and the ASR, appear to be related to the noise exposure conditions and subsequent degree of hearing loss (Carlson and Willott, 1996; Hickox and Liberman, 2014; Salloum et al., 2014; Sturm et al., 2017; Willott and Turner, 2000). Our results demonstrate that PPI was maintained in all subjects, regardless of prior noise exposure or MGE injection. While several previous studies suggest that the magnitude of the PPI is negatively correlated with the hearing threshold at the pre-pulse frequency (i.e. higher thresholds correspond to decreased PPI) (Carlson and Willott, 1996; Willott and Turner, 2000)(Carlson and Willott, 1996; Willott and Turner, 2000), others suggest that noise exposure does not negatively impact PPI (Hickox and Liberman, 2014; Sturm et al., 2017). One possible explanation for these differences is the degree of hearing loss following noise exposure. Indeed, in subjects with minimal to no permanent threshold shifts, PPI appears to be preserved (Hickox and Liberman, 2014; Sturm et al., 2017). This is consistent with our findings, as our NE subjects demonstrated a mild permanent threshold shift. Similar to PPI, the impact of

noise exposure on the ASR amplitude appears to be highly variable. Some studies suggest that noise exposure can lead to an increase in the ASR at high intensities (≥105dB SPL) (Chen et al., 2013; Salloum et al., 2014). Conversely, others demonstrate transient increases in the ASR (Sun et al., 2012) or even a decreased ASR (Salloum et al., 2014) following noise exposure. Again, this variability might be explained by methodological differences leading to variable degrees of hearing loss. Indeed, the magnitude of the maximal ASR appears to have an inverted "U" shaped relationship with hearing thresholds, with enhancement of the ASR most prominent in the presence of moderate hearing loss (thresholds=50-70dB SPL) (Salloum et al., 2014). However, when comparing across studies the change in hearing thresholds after noise exposure may be more relevant than the absolute value of hearing thresholds, as some anesthetics (e.g. vaporized isoflurane) increase ABR thresholds more than others (e.g. intraperitoneal injection of ketamine and xylazine) (Cederholm et al., 2012; Ruebhausen et al., 2012). While these methodological differences make it difficult to compare the results across studies, they suggest that a complicated relationship exists between noise exposure, hearing loss, and the ASR.

4.4.3 The relationship between hearing loss and the ASR might be explained by the medial olivocochlear reflex

The proposed ASR circuit suggests that the cochlear nucleus (CN) and lateral superior olivary complex (LSO) are the primary auditory structures involved in generating the ASR in the absence of a pre-pulse (Koch and Schnitzler, 1997). This circuit primarily focuses on the afferent auditory pathway, but it is important to also consider how incoming acoustic information is shaped by efferent activity at the level of the cochlea. Medial olivocochlear (MOC) efferent activity is mediated, in part, by the IC which makes direct glutamatergic synapses onto MOC cells in the

medial superior olive which then make cholinergic synapses onto outer hair cells in the cochlea (Art et al., 1984; Goutman et al., 2015; Guinan, 2006; Rasmussen, 1953). MOC activity results in decreased basilar membrane motion, which transiently decreases auditory nerve sensitivity (Guinan, 2006). Spontaneous activity in MOC cells is believed to be driven by spontaneous synaptic activity (Fujino et al., 1997), and thus potentially correlated with spontaneous activity in the IC. Given the potential tonic role of the IC in mediating cochlear gain, the IC may be an important mediator of the ASR. While untested, we propose a hypothetical circuit in which the IC plays a role in mediating the ASR (Figure 20) that might explain the various consequences of noise exposure on the ASR (Table 20).

Under the current model, hyperexcitability in the CN is proposed to lead to increases in the ASR. However, we believe this is only part of the story. In our hypothetical circuit, the magnitude of the ASR is affected by the number of outer and inner hair cells, the excitatory tone of the IC and subsequent effect on MOC activity, and the excitatory tone of the CN (Table 20). We think that hyperexcitability in the IC may lead to a tonic increase in MOC activity and thus a decrease in cochlear gain in response to mild hearing loss. Consistent with this, MOC activity is increased in patients with tinnitus and decreased sound level tolerance in the setting of clinically normal hearing thresholds (Knudson et al., 2014). While this relationship has yet to be investigated in animal models, we expect that the net effect of mild hearing loss would be a decrease in the ASR. This would explain our finding that the ASR is decreased in NE subjects with a permanent threshold shift of 20dB SPL. As the degree of hearing loss increases to moderate levels, the number of outer hair cells decreases (Chen and Fechter, 2003). Despite hyperexcitability in the IC, the MOC reflex would be decreased because of outer hair cell loss, leading to increased cochlear gain. Increased cochlear gain coupled with hyperexcitability in the CN would result in an increase in

the ASR. In support of this, the greatest increases in maximum ASR are observed in subjects with moderate hearing loss (thresholds=50-70dB SPL) (Chen et al., 2013; Salloum et al., 2014). Finally, in cases of severe hearing loss, both inner and outer hair cells are lost. The ASR requires detection of acoustic input, and the loss of inner hair cells would result in decreased transmission of auditory information from the periphery to central structures, leading to a decreased ASR. This is supported by evidence that severe hearing loss (thresholds >70dB SPL) is associated with a chronic decrease in the ASR (Salloum et al., 2014). It is important to reiterate that while our hypothetical circuit could explain the relationship between the degree of hearing loss and the long-term consequences on the ASR, it remains to be tested.

The commercial availability of transgenic mouse lines with modified nicotinic α9 and/or α10 subunits, which are the post synaptic receptor subunits present on OHCs that mediate the MOC reflex, may provide an opportunity to investigate the role of the MOC on the ASR. Indeed, comparison of the ASR in CBACaJ;129S-Chrna9^{tm1Bedv}/J (alpha9-KO) mice (Jax #005696) and Chrna9$^{L9'T/L9'T}$ mice (Taranda et al., 2009), which demonstrate lost or enhanced MOC function, respectively, would be helpful in elucidating the effects of MOC activation on the ASR. If our hypothetical circuit is true, we would expect alpha9-KO mice to demonstrate an increased ASR and Chrna9$^{L9'T/L9'T}$ mice to demonstrate a decreased ASR compared to control mice.

The relationship between excitation in the IC and the strength of the MOC reflex also requires further investigation. Studies have demonstrated that stimulation of the IC leads to MOC activation (Groff and Liberman, 2003; Mulders and Robertson, 2000) but the relationship between spontaneous firing rates in the IC and MOC cells and whether MOC cells exhibit hyperexcitable response properties following noise exposure have yet to be explored. One possibility would be to use optogenetics to modulate activity in the IC while measuring the ASR and distortion product

otoacoustic emissions (DPOAEs), a measure of outer hair cell function (Brownell, 1990). We would expect that increasing activity in the IC would lead to an increase in the ASR and decreased DPOAEs and vice versa for decreasing activity in the IC. Another important experiment would be to expose mice to various levels of noise exposure and record from the IC and MOC cells in vivo to determine whether there is an increase in the spontaneous firing rate of MOC cells following noise exposure and if this increase correlates with hyper-excitable response properties in IC neurons.

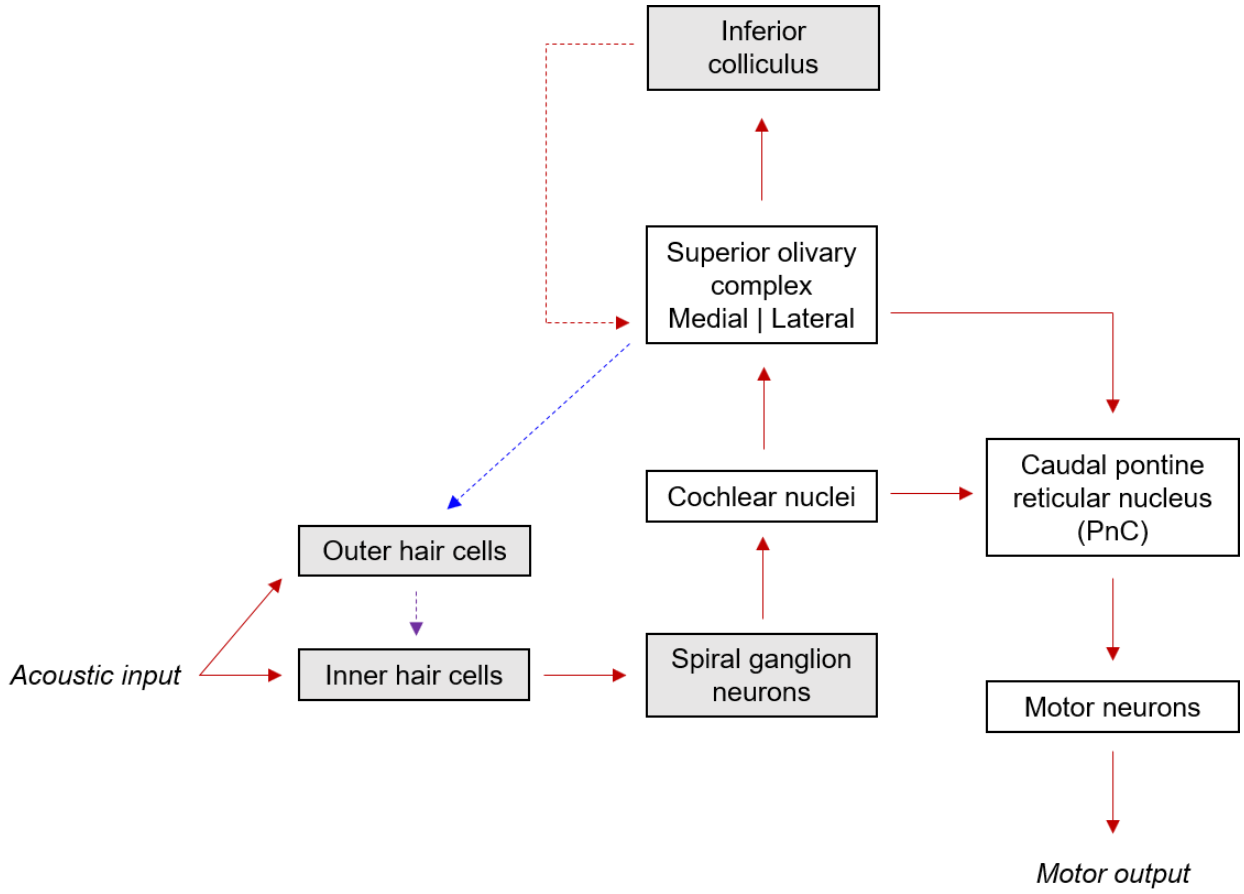

Figure 20. A modified ASR circuit that accounts for possible efferent activity

The proposed ASR circuit postulates that ASR is primarily mediated by the cochlear nucleus and lateral superior olivary complex, which send excitatory input to the caudal pontine reticular nucleus which in turn activates motor neurons leading to the ASR (Koch and Schnitzler, 1997). This circuit, however, does not account for efferent influence from the inferior colliculus (IC). Thus, we propose a modified circuit that includes the possible influence of the IC on medial olivocochlear (MOC) neurons in the medial superior olivary complex which synapse onto outer hair cells. Outer hair cells modulate cochlear gain by amplifying or dampening basilar membrane motion which influences inner hair cell activity.

Grey boxes and dashed arrows represent additions we have made to the current startle circuit. Red arrows indicate excitatory input. Blue arrows indicate inhibitory input. The purple arrow indicates that either increased excitation or inhibition is possible.

Table 20. Potential impact of variable degrees of hearing loss on the ASR

Degree of hearing loss	Outer hair cells (#)	Inner hair cells (#)	IC excitation	MOC activity	CN excitation	Startle response
Mild	—	—	↑	↑	↑	↓
Moderate	↓	—	↑	↓	↑	↑
Severe	↓	↓	↑	↓	↑	↓

We believe that the effect of noise exposure on the ASR may be dependent on the degree of hearing loss. For each degree of hearing loss we have indicated the expected effect on the number of outer and inner hair cells, excitation in the IC and subsequent MOC activity, and excitation in the cochlear nucleus. At each level of hearing loss, we indicate which effect we believe will most impact the ASR in red.

4.4.4 Changes in ABR wave 1 latency and amplitude following MGE cell injection are likely mediated via efferent projections from the IC

The influence of the IC on MOC cells may also explain our finding that transplantation of MGE cells into the IC influenced the shape of the ABR waveform. MGE injected subjects showed decreased wave 1 latency and amplitude compared to control subjects. Since wave 1 of the ABR corresponds to the spiral ganglion neurons, any change to wave 1 following manipulations in the IC likely reflects MOC activity. The majority of transplanted MGE cells mature into inhibitory neurons and could therefore decrease activity in the IC, leading to an increase in outer hair cell function and increased cochlear gain. Increased cochlear gain could explain the shorter wave 1 latency observed in MGE injected subjects, as an increase in basilar membrane motion would facilitate excitation in inner hair cells and subsequently in spiral ganglion neurons. While we would expect increased cochlear gain to also led to increased wave 1 amplitude, the impact of the MGE

cells in the IC may not be uniform, leading to variable impact on the outer hair cells and asynchrony.

The ABR waveform can also be affected by noise exposure, even in the absence of threshold shifts (Kujawa and Liberman, 2009). Our noise exposure protocol led to a mild threshold shift with a decrease in wave 1 amplitude and an increase in wave 1 latency, however the increase in latency was not significantly different from control. A decrease in wave 1 amplitude following noise exposure has been suggested to be due to loss of synapses between inner hair cells and spiral ganglion neurons (Hickox and Liberman, 2014; Jensen et al., 2015; Lin et al., 2011). In addition to the loss of peripheral input, an increase in the MOC activity might also contribute to an increase in wave 1 latency and decrease in wave 1 amplitude. Indeed, a decrease in outer hair cell activity would mean less amplification of basilar membrane motion and thus less excitation in the inner hair cells and spiral ganglion neurons. If increased MOC activity does indeed contribute to decreased activity in spiral ganglion neurons following noise exposure, transplantation of MGE cells in the IC might be able to compensate for the loss of synapses between inner hair cells and spiral ganglion neurons by decreasing MOC activity. Indeed, we found that wave 1 latency in NE+MGE injected subjects was similar to that of control subjects. The introduction of MGE cells into the IC of noise exposed mice might therefore mitigate the effects of noise exposure by decreasing the MOC reflex.

4.4.5 Conclusions and Future directions

To our knowledge, these data provide the first evidence that local increases in inhibition in the IC may be useful in mitigating the behavioral effects of noise exposure and provides a new strategy to explore treatment options for central hearing dysfunction following noise exposure.

Comparing our results to previously published findings on the effects of noise exposure on the ASR also brought up questions regarding a potential role of the MOC on the ASR and auditory function following noise exposure. While there is some clinical evidence supporting our hypothesis that increased MOC activity can occur in the setting of tinnitus and hyperacusis (Knudson et al., 2014), the effects of increased MOC activity on the ASR remain to be explored. Further investigation into the mechanism by which transplanted MGE cells impact the ASR and cochlear gain would be helpful in understanding the role of the efferent pathway in the development of auditory pathologies following noise exposure. Nevertheless, the finding that local increases in inhibition mitigate some of the behavioral changes observed after NE provides a promising foundation for local, targeted treatment.

5.0 General Discussion

5.1 Summary of results

The aims of this dissertation were to 1) to characterize the spontaneous and sound evoked response properties of neurons in the central nucleus of the inferior colliculus (CNIC) and cortex of the inferior colliculus (CtxIC) in mice, and 2) to investigate the role of inhibition in mitigating the effects of noise exposure.

In chapter 2, we used array recordings in anesthetized mice to characterize the spontaneous and sound evoked response properties of neurons in the CNIC and CtxIC. Consistent with the different inputs received by neurons in these regions, we observed differences in basic tuning properties (frequency response areas, FRAs, and spectro-temporal receptive fields, STRFs). We found that neurons in the CNIC had lower and less variable spontaneous firing rates, delayed onset, higher thresholds, were more consistently and selectively tuned, and had a higher incidence of non-monotonic rate-level functions. However, we found no significant differences in other response properties, such as gap detection thresholds, distribution of the best synchrony or rate-based modulation frequencies, or the degree of lateral inhibition. To determine whether differences in the response properties of CNIC and CtxIC neurons to simple pure tone stimuli were sufficient for reliable classification, we trained logistic regression (LR), support vector machine (SVM), and random forest (RF) algorithms on parameters extracted from the FRA. We found that all three algorithms performed well, with the random forest algorithm achieving the highest performance, with an accuracy of 84% and area under the ROC curve of 90%. In summary, these data suggest

that the CNIC and CtxIC neurons have distinct receptive fields and these differences, when combined, allow for robust, reliable discrimination.

In chapters 3 and 4, we used transplantation of inhibitory precursor cells to investigate the role of inhibition in noise-induced pathology in the inferior colliculus (IC). We found that transplanted medial ganglionic eminence (MGE) cells survive, migrate, and differentiate into primarily inhibitory neurons in the IC of adult mice, regardless of prior noise exposure. Importantly, transplanted MGE cells integrated into the IC and formed synapses with and received synaptic endings from endogenous IC neurons. Furthermore, we observed that a high percentage of transplanted MGE cells expressed c-fos, suggesting that they were active. Interestingly, the effects of transplanted MGE cells extended beyond the IC. We found that transplantation of MGE cells into the IC led to decreases in the auditory brainstem response (ABR) wave 1 latency and amplitude, suggesting that increasing inhibition in the IC led to increased cochlear gain. Additionally, we found that transplantation of MGE cells into the IC mitigated the noise induced shift in the amplitude varied acoustic startle response (AmpVar-ASR) curve. Our data provide the first evidence that transplantation of MGE cells is viable in the brainstem and that local increases in inhibition are sufficient to mitigate at least some of the behavioral effects of noise exposure. These findings encourage further investigation into treatments that provide local, targeted increases in inhibition to restore auditory function following noise exposure.

5.2 Advantages and limitations

5.2.1 High-density multielectrode array recordings

We used a high-density multielectrode array to record from the CNIC and CtxIC. This approach allowed us to simultaneously record from many neurons and across multiple depths. While multielectrode recordings can be a powerful tool for data collection, they limit the ability to perform on-line analyses, thus limiting the ability to perform closed-loop experiments by obtaining real-time feedback and generating neuron-specific stimuli. Without real-time feedback, multielectrode recordings rely on a pre-defined stimulus set, which is appropriate when the goal is to understand how neural populations encode a given stimulus set (for example, sets of natural sounds), but is not suitable when the goal is to derive mechanistic explanations of neural activity. For example, broadband stimuli that were used to characterize the response field (e.g. FRA and STRF) were well-suited to multielectrode array recordings. However, for stimuli that required a center or carrier frequency based on neural responses (e.g. two-tone, gap detection, and amplitude modulated tones), we had to present each stimulus set at a limited number of frequencies, as we did not have access to individual neural BFs until after the experiment. This approach may have potentially masked differences in lateral inhibition and temporal processing of neurons in the CNIC and CtxIC. A technical limitation was a trade-off between the number of sortable units and hold times. Our complete stimulus set (especially because we presented each stimulus set at multiple frequencies due to the limitation described above) was 3-4 hours long, and if the same units were to be isolated over this entire time period, we would have obtained much lower yields. To counter this, we sorted units for each stimulus set separately, which increased yield but

decreased interpretability, as we could not directly relate single-unit responses across stimulus sets.

5.2.2 Machine learning algorithms to discriminate between neural populations

Although the receptive fields of neurons in the CNIC and CtxIC demonstrate subtle but significant differences, distinguishing neurons based on their response properties alone has been challenging. Rather than relying on a single response feature for discrimination, machine learning algorithms allow us to determine whether a combination of response features are sufficient for reliable discrimination. We trained logistic regression (LR) models, support vector machine (SVM) classifiers, and random forest (RF) algorithms on pure-tone responses to determine whether neurons from the CNIC and CtxIC could be reliably separated based on simple response properties. When interpreting the performance of these algorithms, we must consider the features of the model itself and the quality of the training data.

LR and linear SVM algorithms construct a single classification model with a linear decision boundary. Conversely, RF algorithms construct an ensemble of decision trees, which are non-linear classifiers, using random subsets of variables from a single training data set and aggregates the outputs from the ensemble to classify the sample (Breiman, 2001). Thus, LR and SVM algorithms are well suited for linear data while RF classifiers can better handle non-linear data. Additionally, ensemble approaches, such as the RF, tend to outperform single models, such as LR and SVM. Given the differences in these algorithms, it is difficult to discern whether the superior performance of the RF was due to non-linearities in the data or to an ensemble approach.

The training data itself is also critically important. Our training data was small in size and missing values for several variables, requiring imputation. The missing values were related to the

high thresholds we saw and most effected neurons in the CNIC, which had significantly higher thresholds than CtxIC neurons. Imputation may have introduced bias into the training data set, which would impact performance. Thus, future work should aim to address the causes of data loss (i.e. high thresholds) in a larger dataset. Repeating these experiments in awake mice would likely result in decreased data loss, as we believe the high thresholds were due to the use of isoflurane anesthesia. Furthermore, these experiments would provide a better understanding of the response properties of these neurons under more natural listening conditions.

5.2.3 Increasing inhibition in the IC using transplanted MGE cells

Transplanted MGE cells demonstrate elaborate arborization and form synaptic connections with endogenous neurons, allowing them to increase inhibition and potentially modify underlying disease processes in the spinal cord (Basbaum and Bráz, 2016; Bráz et al., 2012; Etlin et al., 2016). Unlike, other methods to increase inhibition locally, such as intrathecal injection of baclofen or muscimol, which result in unregulated increases in inhibition, the increase in inhibition from transplanted MGE cells appears to be regulated by an unknown homeostatic mechanism (Basbaum and Bráz, 2016). As such, transplanted MGE cells act as more than a GABAergic pump and may provide a unique opportunity to increase inhibition without compromising normal function.

Our results suggest that transplanted MGE cells are equally viable in the non-noise exposed and noise exposed IC, with similar survival rates, migration distances, and differentiation into inhibitory neurons. Transplantation of MGE cells into noise exposed mice mitigated the noise induced shift in the AmpVar-ASR curve but had no effect on the AmpVar-ASR curve of non-noise exposed mice. These results are consistent with the hypothesis that a homeostatic mechanism regulates that degree to which transplanted MGE cells increase inhibition in the host. However,

these experiments were performed in small cohort of animals and requires verification with a larger sample size. Furthermore, our ABR results suggest that the transplanted MGE cells increased cochlear gain in non-noise exposed mice, as evidenced by decreased wave 1 latencies. Thus, transplantation of MGE cells in non-noise exposed mice was not without consequence. This finding is not necessarily contrary to the hypothesis that a homeostatic mechanism regulates MGE function, as the effect of MGE cells may vary in non-noise exposed and noise exposed mice. Thus, further research into the interaction between noise exposure and MGE cell transplantation and the mechanism by which MGE cell activity is regulated by the host is warranted. These results would be helpful in determining the degree to which MGE cells are able to modify disease process without impacting normal function.

5.3 Implications for future research

5.3.1 Synaptic connectivity of transplanted MGE cells

The development and maintenance of central auditory pathologies following noise exposure is believed to be the result of increased gain, or hyper-excitable response properties, in central auditory structures (Asokan et al., 2018; Auerbach et al., 2019, 2014; Mulders and Robertson, 2009). Our finding that transplantation of MGE cells into the IC mitigates the noise-induced shift in the AmpVar-ASR curve is consistent with this hypothesis. However, the mechanism by which transplanted MGE cells restore IC function requires further investigation.

Previous research has shown that noise exposure can lead to hyper-excitable response patterns in IC neurons (Berger et al., 2014; Coomber et al., 2014; Longenecker and Galazyuk,

2016; Ma et al., 2006; Mulders and Robertson, 2013, 2009). Interestingly, synaptic reorganization of local IC circuits appears to vary between mice with and without gap-detection deficits (Sturm et al., 2017), a commonly used behavioral indicator of tinnitus (Berger et al., 2014; Chen et al., 2013; Hayes et al., 2014; Sturm et al., 2017; Turner et al., 2006). Animals with gap detection deficits experience increased excitation in the IC due to synaptic reorganization and loss of excitatory inputs onto Type I GABAergic neurons (Sturm et al., 2017). Conversely, animals without gap detection deficits maintain an excitatory/inhibitory balance similar to that of control subjects, despite undergoing synaptic reorganization (Sturm et al., 2017). These findings implicate excitatory/inhibitory imbalance in local IC circuits in the maintenance of tinnitus. Transplanted MGE cells may, therefore, mitigate the effects of noise exposure by acting as a replacement for the lost inhibition from Type I GABAergic neurons, which are believed to form local connections (Sturm et al., 2017). While we did not thoroughly investigate the projections of MGE cells, we did observe that the majority of the cell bodies, and their processes, remained within the boundaries of the IC; suggesting that transplanted MGE cells form local synaptic connections.

Intrinsic connections in the IC are responsible for shaping the response properties of neurons to spectral and temporal cues (see Chapter 1.5). Intrinsic inputs are derived from both disc cells, which are oriented within an isofrequency laminae, and stellate cells, which are unoriented or orthogonal to the isofrequency laminae (Oliver et al., 1991). Morphologically, MGE cells appear to resemble stellate cells and may possess processes that span several tonotopic bands within the IC. Thus, transplanted MGE cells may mitigate the effects of noise exposure by integrating inputs across tonotopic bands, leading to increased specificity in target neurons. Future research investigating the source of inputs to transplanted MGE cells as well as their synaptic

targets will be helpful in determining whether transplanted MGE cells increase specificity in target neurons and the mechanism by which such effects occur.

Synaptic input maps of transplanted MGE cells could be characterized using laser-scanning photostimulation (LSPS) with caged glutamate (Callaway and Katz, 1993; Sturm et al., 2014, 2017). LSPS is a robust method by which to measure the strength and spatial distribution of synaptic inputs over large areas (Callaway and Katz, 1993). Additionally, this technique has been used to characterize the input maps of endogenous IC neurons (Sturm et al., 2014, 2017) and could therefore provide insight into whether transplanted MGE cells have synaptic input maps that resemble endogenous GABAergic IC neurons. Transplanting MGE cells from Tg(act-EGFP)Y01Osb (green) mice (Jax #006567) into the IC of non-noise exposed and noise exposed mice would provide insight into any potential differences in the source and strength of synaptic inputs onto transplanted MGE cells in these environments. This data could help determine whether regulation of MGE cell activity arises from differences in synaptic connectivity.

Also of interest, would be whether transplantation of MGE cells into the IC induces a period of plasticity and synaptic reorganization of endogenous IC neurons. Previous research has shown that transplanting MGE cells into the visual cortex induces ocular dominance plasticity after the critical period (Derek G. Southwell et al., 2010). To determine whether transplantation of MGE cells into the IC induces plasticity and synaptic reorganization in endogenous IC neurons, MGE cells from green mice could be transplanted into the IC of non-noise exposed and noise exposed mice. Synaptic reorganization of endogenous GABAergic and glutamatergic neurons could be characterized by crossing VGAT-ires-cre mice (Jax 016962, 129S6/SvEvTac background) or Vglut2-ires-Cre mice (Jax #016963) with the Ai9/tdTomato cre reporter line (Jax 007909, C57BL/6J background), respectively. These experiments would provide valuable

information on the synaptic connectivity of MGE cells and reveal any effects on synaptic reorganization following MGE cell transplantation.

Characterizing the effect of transplanted MGE cells on the sound evoked response properties of target neurons may be challenging. Given the relative sparsity of transplanted MGE cells compared to endogenous IC neurons, in vivo recordings using either a single electrode or probe could miss transplanted MGE cells and their target neurons completely. However, it is possible that the presence of MGE cells induces changes in the population response of the IC. Machine learning algorithms, such as those described in chapter 2, may be useful in characterizing the population response of neurons in noise exposed subjects with and without transplanted MGE cells. In addition to determining if the population response differs between subjects with and without transplanted MGE cells, pairing these experiments with behavioral testing could provide useful information about the response properties that contribute to the development of tinnitus and hyperacusis. Indeed, one of the original goals of this thesis was to investigate the relationship between auditory behavior and spontaneous and sound evoked response properties in the IC of MGE injected subjects, with and without noise exposure. Thus, an immediate next step could be to combine the methods we developed in aims 1 and 2 of this thesis to investigate functional changes in the IC following MGE injection. The RF classifier may be a particularly apt model for this type of investigation, as it is able to rank variables or combinations of variables by importance (Breiman, 2001). Of particular interest, might be the response properties of the CNIC and lateral CtxIC, which project to the MOC neurons.

Calcium imaging may also be a useful tool to investigate the effects of transplanted MGE cells on the spontaneous and sound evoked activity of endogenous IC neurons. Previous studies have used two photon calcium imaging to characterize the sound evoked response properties of

neurons in the CtxIC (Barnstedt et al., 2015; Wong and Borst, 2019). But the restricted depth of two-photon imaging has limited its utility in the deeper layers of the IC. The recent development of hybrid multiplexed sculpted light microscopy (HyMS), which uses a hybrid of two-photon-three-photon excitation (Weisenburger et al., 2019) could make calcium imaging a viable approach to studying the deeper portions of the IC. Using the HyMS approach, Weisenburger et al. (2019) were able to record from several thousand (~4,121) neurons from a ~690 x 675 x 1,000µm volume. While this would not reach the deepest portions of the mouse CNIC (~1,500µm from the tissue surface), it would provide greater imaging depth that conventional two- or three-photon imaging. Furthermore, this technique would allow for visualization of fluorescently tagged transplanted MGE cells and allow the investigator to perform recordings in these target areas.

Combining the HyMS approach with optogenetic approaches that allow for hyperpolarization of the transplanted MGE cells would provide an opportunity to characterize the sound evoked responses of neurons in the IC with and without the MGE cell activity. One way to optically drive MGE cells would be through transgenic expression of Halorhodopsin, a light-gated chloride ion pump. VGAT driven expression of Halorhodopsin in transplanted MGE cells could be achieved by crossing Ai39 mice (Jax 014539, B6 background) (Madisen et al., 2012) with VGAT-ires-cre mice (Jax 016962, 129S6/SvEvTac background). This line could then be crossed with Tg(act-EGFP)Y01Osb (green) mice (Jax #006567) to create a VGAT-Ai39-Green line. MGE cells derived from VGAT-Ai39-Green embryos would thus express GFP, allowing for identification in the IC, and be hyperpolarized in the presence of yellow light stimulation. MGE cells from VGAT-Ai39-Green embryos could be transplanted into the IC of mice with a GCaMP reporter in excitatory or inhibitory neurons. Host mice could be Ai95(RCL-GCaMP6f)-D mice (Jax #028865) crossed with either VGAT-ires-cre or Vglut2-ires-Cre mice (Jax #016963), which

would induce fluorescent calcium indication in inhibitory or excitatory neurons, respectively. This approach would allow for the characterization of the sound evoked response properties of endogenous IC neurons with and without activity of transplanted MGE cells.

Together, these experiments would improve our understanding off the effect of transplanted MGE cells on local IC circuits and the potential mechanism by which they affect the ASR following noise exposure. These results would not only be beneficial in the development of novel treatment strategies for tinnitus and hyperacusis, but they would also provide insight into the disease process itself.

5.3.2 A proposed role for the MOC reflex in mediating the ASR

Our behavioral results, in combination with previously published data, suggest that changes in the ASR following noise exposure may be related to the degree of concomitant hearing loss. In chapter 3 we propose a hypothetical circuit by which the IC may mediate the ASR via the MOC reflex. Several transgenic mouse lines with modified nicotinic α9 and/or α10 subunits, which are the post synaptic receptor subunits present on OHCs that mediate the MOC reflex, exist and provide an opportunity to investigate the role of the MOC on the ASR. If our hypothetical circuit is true, we would expect alpha9-KO mice (CBACaJ;129S-Chrna9^{tm1Bedv}/J (alpha9-KO), Jax #005696), which demonstrate loss of MOC function due to loss of the nicotinic α9 subunit, to demonstrate an increased ASR; and Chrna9$^{L9'T/L9'T}$ mice (Taranda et al., 2009), which have enhanced MOC function due to an overactive nicotinic α9 subunit, to demonstrate a decreased ASR compared to control mice. While the effects of the MOC on the AmpVar-ASR have yet to be investigated, there is some data on the relationship between MOC activity and PPI. Alpha9-KO mice demonstrate decreased 50% PPI thresholds (i.e. the pre-pulse level required to inhibit the

startle response 50% of the time was lower) while Chrna9$^{L9'T/L9'T}$ mice demonstrate increased 50% PPI thresholds (Allen and Luebke, 2017). Lower PPI thresholds in the setting of decreased MOC function could represent increased cochlear gain, which would increase the effect of lower amplitude pre-pulses. However, we would also expect increased gain to also affect the response to the startle stimulus. Without data on the magnitude of the ASR and the percent inhibition at each pre-pulse level it is difficult to interpret this PPI threshold shift. Thus, future research investigating the relationship between MOC activity, and the AmpVar-ASR and PPI is needed to confirm or refute our hypothetical circuit.

Additionally, the effects of noise exposure on the MOC reflex requires further investigation. Spontaneous activity in MOC cells is believed to be driven by spontaneous synaptic activity (Fujino et al., 1997), which could arise from activity in the IC. Noise exposure is known to increase spontaneous firing rates in the IC (Berger et al., 2014; Coomber et al., 2014; Longenecker and Galazyuk, 2016; Ma et al., 2006; Mulders and Robertson, 2013, 2009) and thus may result in increased spontaneous firing rates in MOC cells as well. The effects of noise exposure on the spontaneous and sound evoked activity in MOC neurons could be characterized using in vivo recordings of the periolivary region of the superior olivary complex, which contains the MOC cells. Additional recordings in the IC of the same mice would be helpful in determining whether hyperexcitable response properties in MOC neurons correlates with hyper-excitable response properties in the IC. IC recordings could target the CNIC and lateral CtxIC, which are the primary source of efferent projections to MOC neurons.

The behavioral consequences of noise exposure are highly variable and, in the case of PPI and the AmpVar-ASR, appear to be related to the noise exposure conditions and subsequent degree of hearing loss (Carlson and Willott, 1996; Hickox and Liberman, 2014; Salloum et al., 2014;

Sturm et al., 2017; Willott and Turner, 2000). Understanding the relationship between the excitatory/inhibitory tone of the IC and the ASR could provide the necessary context to the explain the different effects of noise exposure on the ASR that are reported in the literature. Furthermore, these experiments could provide valuable insight into the mechanism by which transplanted MGE cells mitigate the noise induced shift in the AmpVar-ASR curve. Understanding the effects of noise exposure on the MOC reflex could thus improve our understanding of the impact of central gain on shaping peripheral input and the potential mechanism by which local increases in inhibition may be useful in mitigating the effects of noise exposure.

5.3.3 Using machine learning models to characterize neural populations

The ability to reliably discriminate neural populations based on their response properties alone has broad implications for future research. In our experiments, the RF classifier achieved the highest performance. While this could be a feature of the model itself or the training data, the RF classifier has many benefits. One of which is its ability to rank variables or combinations of variables by importance (Breiman, 2001). This feature is most helpful when there are a high number of variables. As such, the RF classifier may be a useful tool in providing insight into the response properties that are most salient for auditory processing in different neural population or across different conditions or pathological states.

One potential application for the RF algorithm could be in determining which response properties contribute to auditory processing disorders following noise exposure. For example, hyper-excitable response patterns have been observed in animals with and without gap-detection deficits (Berger et al., 2014). While synaptic input maps have revealed differences in synaptic reorganization in the IC of animals with and without gap detection deficits (Sturm et al., 2017),

there appears to be no clear distinction in the response properties of neurons between these groups (Berger et al., 2014). The response properties of neurons in the IC alone are thus insufficient to predict whether a subject will also demonstrate gap-detection deficits. One possible explanation for this is that subtle differences exist in the response properties of these neurons that, when combined, could potentially predict the likelihood of an animal experiencing gap detection deficits. Given that a RF classifier can rank variables and combination of variables according to importance, this would be a particularly apt approach to answer this type of question.

5.4 Clinical relevance of dissertation research

To our knowledge, our data provide the first evidence that neurons in the CNIC and CtxIC can be reliably discriminated based on their response properties to simple stimuli and that local increases in inhibition may be useful in mitigating a behavioral effect of noise exposure. The finding that MGE cells demonstrate long-term integration in the IC provides a promising foundation for their use as a local, targeted treatment to restore excitatory/inhibitory balance following noise exposure. Furthermore, this technique can be used to investigate the mechanisms underlying the development, plasticity, and function of defined auditory areas. Similarly, the ability to reliably discriminate between CNIC and CtxIC neurons may provide valuable insight into the response properties that contribute to auditory processing under normal conditions as well as how those responses change in different listening conditions or in the pathologic state. Future research using these techniques could be useful in the treatment of tinnitus and hyperacusis, as discussed throughout this dissertation, but could also be applied to other auditory processing disorders.

References

Aazh, H., Lammaing, K., Moore, B.C.J., 2017. Factors related to tinnitus and hyperacusis handicap in older people. Int. J. Audiol. 56, 677–684.

Aazh, H., Moore, B.C.J., 2018. Prevalence and characteristics of patients with severe hyperacusis among patients seen in a tinnitus and hyperacusis clinic. J. Am. Acad. Audiol. 29, 626–633.

Aazh, H., Mooreb, B.C.J., 2017. Factors associated with depression in patients with tinnitus and hyperacusis. Am. J. Audiol. 26, 562–569.

Aitkin, L., Schuck, D., 1985. Low frequency neurons in the lateral central nucleus of the cat inferior colliculus receive their input predominantly from the medial superior olive. Hear. Res. 17, 87–93.

Aitkin, L., Tran, L., Syka, J., 1994. The responses of neurons in subdivisions of the inferior colliculus of cats to tonal, noise and vocal stimuli. Exp Brain Res. 1, 53–64.

Aitkin, L.M., Dickhaus, H., Schult, W., Zimmermann, M., 1978. External nucleus of inferior colliculus: auditory and spinal somatosensory afferents and their interactions. J. Neurophysiol. 41, 837–847.

Aitkin, L.M., Kenyon, C.E., Philpott, P., 1981. The representation of the auditory and somatosensory systems in the external nucleus of the cat inferior colliculus. J. Comp. Neurol. 196, 25–40.

Aitkin, L.M., Webster, W.R., Veale, J.L., Crosby, D.C., 1975. Inferior colliculus. I. Comparison of response properties of neurons in central, pericentral, and external nuclei of adult cat. J. Neurophysiol. 38, 1196–1207.

Allen, P.D., Luebke, A.E., 2017. Reflex modification audiometry reveals dual roles for olivocochlear neurotransmission. Front. Cell. Neurosci. 11.

Alvarez-Dolado, M., Calcagnotto, M.E., Karkar, K.M., Southwell, D.G., Jones-Davis, D.M., Estrada, R.C., Rubenstein, J.L.R., Alvarez-Buylla, A., Baraban, S.C., 2006. Cortical Inhibition Modified by Embryonic Neural Precursors Grafted into the Postnatal Brain. J. Neurosci. 26, 7380–7389.

Andersen, R.A., Snyder, R.L., Merzenich, M.M., 1980. The topographic organization of

corticocollicular projections from physiologically identified loci in the AI, AII, and anterior auditory cortical fields of the cat. J. Comp. Neurol. 191, 479–494.

Andoni, S., Li, N., Pollak, G.D., 2007. Spectrotemporal receptive fields in the inferior colliculus revealing selectivity for spectral motion in conspecific vocalizations. J. Neurosci. 27, 4882–4893.

Art, J.J., Fettiplace, R., Fuchs, P.A., 1984. Synaptic hyperpolarization and inhibition of turtle cochlear hair cells. J. Physiol. 356, 525–550.

Asokan, M.M., Williamson, R.S., Hancock, K.E., Polley, D.B., 2018. Sensory overamplification in layer 5 auditory corticofugal projection neurons following cochlear nerve synaptic damage. Nat. Commun. 9, 1–10.

Auerbach, B.D., Radziwon, K., Salvi, R., 2019. Testing the Central Gain Model: Loudness Growth Correlates with Central Auditory Gain Enhancement in a Rodent Model of Hyperacusis. Neuroscience 407, 93–107.

Auerbach, B.D., Rodrigues, P. V., Salvi, R.J., 2014. Central gain control in tinnitus and hyperacusis. Front. Neurol. 5.

Ayodele, O.S., Segun-Busari, S.S.-B., Omokanye, K.H., Dunmade, D.A., Ologe, E.F., 2020. Quality of life of tinnitus patients with and without hearing loss. Int. J. Otorhinolaryngol. Head Neck Surg. 7, 11.

Baraban, S.C., Southwell, D.G., Estrada, R.C., Jones, D.L., Sebe, J.Y., Alfaro-Cervello, C., Garcia-Verdugo, J.M., Rubenstein, J.L.R., Alvarez-Buylla, A., 2009. Reduction of seizures by transplantation of cortical GABAergic interneuron precursors into Kv1.1 mutant mice. Proc. Natl. Acad. Sci. 106, 15472–15477.

Barnstedt, O., Keating, P., Weissenberger, Y., King, A.J., Dahmen, J.C., 2015. Functional microarchitecture of the mouse dorsal inferior colliculus revealed through in vivo two-photon calcium imaging. J. Neurosci. 35, 10927–10939.

Bartels, H., Middel, B.L., Van Der Laan, B.F.A.M., Staal, M.J., Albers, F.W.J., 2008. The additive effect of co-occurring anxiety and depression on health status, quality of life and coping strategies in help-seeking tinnitus sufferers. Ear Hear. 29, 947–956.

Basbaum, A.I., Bráz, J.M., 2016. Cell transplants to treat the “disease” of neuropathic pain and itch. Pain 157, S42–S47.

Bauer, C.A., Brozoski, T.J., 2006. Effect of Gabapentin on the Sensation and Impact of Tinnitus.

Laryngoscope 116, 675–681.

Beebe, N.L., Young, J.W., Mellott, J.G., Schofield, B.R., 2016. Extracellular molecular markers and soma size of inhibitory neurons: Evidence for four subtypes of GABAergic cells in the inferior colliculus. J. Neurosci. 36, 3988–3999.

Berger, J.I., Coomber, B., 2015. Tinnitus-related changes in the inferior colliculus. Front. Neurol. 6, 1–12.

Berger, J.I., Coomber, B., Wells, T.T., Wallace, M.N., Palmer, A.R., 2014. Changes in the response properties of inferior colliculus neurons relating to tinnitus. Front. Neurol. 5, 1–13.

Bernstein, L.R., Trahiotis, C., 2012. Lateralization produced by interaural temporal and intensitive disparities of high-frequency, raised-sine stimuli: Data and modeling. J. Acoust. Soc. Am. 131, 409–415.

Bernstein, L.R., Trahiotis, C., 2008. Discrimination of interaural temporal disparities conveyed by high-frequency sinusoidally amplitude-modulated tones and high-frequency transposed tones: Effects of spectrally flanking noises. J. Acoust. Soc. Am. 124, 3088–3094.

Bernstein, L.R., Trahiotis, C., 1994. Detection of interaural delay in high-frequency sinusoidally amplitude-modulated tones, two-tone complexes, and bands of noise. J. Acoust. Soc. Am. 95, 3561–3567.

Beyerl, B.D., 1978. Afferent projections to the central nucleus of the inferior colliculus in the rat. Brain Res. 145, 209–223.

Biebel, U.W., Langner, G., 2002. Evidence for interactions across frequency channels in the inferior colliculus of awake chinchilla. Hear. Res. 169, 151–168.

Bledsoe, S.C., Nagase, S., Miller, J.M., Altschuler, R.A., 1995. Deafness-induced plasticity in the mature central auditory system. Neuroreport.

Bráz, J.M., Sharif-Naeini, R., Vogt, D., Kriegstein, A., Alvarez-Buylla, A., Rubenstein, J.L., Basbaum, A.I., 2012. Forebrain GABAergic Neuron Precursors Integrate into Adult Spinal Cord and Reduce Injury-Induced Neuropathic Pain. Neuron 74, 663–675.

Breiman, L., 2001. Random Forests. Mach. Learn. 45, 5–32.

Brimijoin, W.O., O'Neill, W.E., 2005. On the prediction of sweep rate and directional selectivity for FM sounds from two-tone interactions in the inferior colliculus. Hear. Res. 210, 63–79.

Brown, M.C., Liu, T.S., 1995. Fos-like immunoreactivity in central auditory neurons of the mouse. J. Comp. Neurol. 357, 85–97.

Brownell, W.E., 1990. Outer hair cell electromotility and otoacuostic emissions. Ear Hear. 11, 82–92.

Brozoski, T.J., Caspary, D.M., Bauer, C.A., Richardson, B.D., 2010. The effect of supplemental dietary Taurine on Tinnitus and auditory discrimination in an animal model. Hear. Res. 270, 71–80.

Brozoski, T.J., Spires, T.J.D., Bauer, C.A., 2007. Vigabatrin, a GABA transaminase inhibitor, reversibly eliminates tinnitus in an animal model. JARO - J. Assoc. Res. Otolaryngol. 8, 105–118.

Brunso-Bechtold, J.K., Thompson, G.C., Masterton, R.B., 1981. HRP study of the organization of auditory afferents ascending to central nucleus of inferior colliculus in cat. J. Comp. Neurol. 197, 705–722.

Bullitt, E., 1990. Expression of C-fos-like protein as a marker for neuronal activity following noxious stimulation in the rat. J. Comp. Neurol. 296, 517–530.

Caicedo, A., Herbert, H., 1993. Topography of descending projections from the inferior colliculus to auditory brainstem nuclei in the rat. J. Comp. Neurol. 328, 377–392.

Callaway, E.M., Katz, L.C., 1993. Photostimulation using caged glutamate reveals functional circuitry in living brain slices. Proc. Natl. Acad. Sci. U. S. A. 90, 7661–7665.

Campolo, J., Lobarinas, E., Salvi, R., 2013. Does tinnitus "fill in''' the silent gaps?" Noise Health 15, 398–405.

Cant, N.B., 2005. Projections from the cochlear nuclear complex to the inferior colliculus, in: Winer, J.A., Schreiner, C.E. (Eds.), The Inferior Colliculus. Springer Science+Business Media, Inc., New York, pp. 115–131.

Cant, N.B., Benson, C.G., 2005. An atlas of the inferior colliculus of the gerbil in three dimensions. Hear. Res. 206, 12–27.

Cant, N.B., Benson, C.G., 2003. Parallel auditory pathways: Projection patterns of the different neuronal populations in the dorsal and ventral cochlear nuclei. Brain Res. Bull. 60, 457–474.

Carlson, S., Willott, J.F., 1996. The behavioral salience of tones as indicated by prepulse inhibition of the startle response : relationship to hearing loss and central neural plasticity in C57BL / 6J mice. Hear. Res. 99, 168–175.

Cederholm, J.M.E., Froud, K.E., Wong, A.C.Y., Ko, M., Ryan, A.F., Housley, G.D., 2012. Differential actions of isoflurane and ketamine-based anaesthetics on cochlear function in the

mouse. Hear. Res. 292, 71–79.

Cederroth, C.R., Lugo, A., Edvall, N.K., Lazar, A., Lopez-Escamez, J.A., Bulla, J., Uhlen, I., Hoare, D.J., Baguley, D.M., Canlon, B., Gallus, S., 2020. Association between hyperacusis and tinnitus. J. Clin. Med. 9, 1–13.

Chandrasekaran, L., Xiao, Y., Sivaramakrishnan, S., 2013. Functional Architecture of the Inferior Colliculus Revealed with Voltage-Sensitive Dyes. Front. Neural Circuits 7, 1–23.

Chen, C., Rodriguez, F.C., Read, H.L., Escabí, M.A., 2012. Spectrotemporal sound preferences of neighboring inferior colliculus neurons: implications for local circuitry and processing. Front. Neural Circuits 6, 1–16.

Chen, G. Di, Fechter, L.D., 2003. The relationship between noise-induced hearing loss and hair cell loss in rats. Hear. Res. 177, 81–90.

Chen, G., Lee, C., Sandridge, S.A., Butler, H.M., Manzoor, N.F., Kaltenbach, J.A., 2013. Behavioral evidence for possible simultaneous induction of hyperacusis and tinnitus following intense sound exposure. JARO - J. Assoc. Res. Otolaryngol. 14, 413–424.

Clause, A., Nguyen, T., Kandler, K., 2011. An acoustic startle-based method of assessing frequency discrimination in mice. J. Neurosci. Methods 200, 63–67.

Coleman, J.R., Clerici, W.J., 1987. Sources of projections to subdivisions of the inferior colliculus in the rat. J. Comp. Neurol. 262, 215–226.

Coomber, B., Berger, J.I., Kowalkowski, V.L., Shackleton, T.M., Palmer, A.R., Wallace, M.N., 2014. Neural changes accompanying tinnitus following unilateral acoustic trauma in the guinea pig. Eur. J. Neurosci. 40, 2427–2441.

Covey, E., Kauer, J.A., Casseday, J.H., 1996. Whole-cell patch-clamp recording reveals subthreshold sound-evoked postsynaptic currents in the inferior colliculus of awake bats. J. Neurosci. 16, 3009–3018.

Czornik, M., Malekshahi, A., Mahmoud, W., Wolpert, S., Birbaumer, N., 2022. Psychophysiological Treatment of Chronic Tinnitus: A Review. Clin. Psychol. Psychother. 1–18.

Davis, M., Gendelman, D.S., Tischler, M.D., Gendelman, P.M., 1982. A Primary Acoustic Startle Circuit: Lesion and stimulation studies. J. Neurosci. 2, 791–805.

Dong, S., Mulders, W.H.A.M., Rodger, J., Robertson, D., 2009. Changes in neuronal activity and gene expression in guinea-pig auditory brainstem after unilateral partial hearing loss.

Neuroscience 159, 1164–1174.

Dong, S., Mulders, W.H.A.M., Rodger, J., Woo, S., Robertson, D., 2010. Acoustic trauma evokes hyperactivity and changes in gene expression in guinea-pig auditory brainstem. Eur. J. Neurosci. 31, 1616–1628.

Druga, R., Syka, J., 1993. NADPH-diaphorase activity in the central auditory structures of the rat. Neuroreport.

Druga, R., Syka, J., 1984. Neocortical projections to the inferior colliculus in the rat. (An experimental study using anterograde degeneration techniques). Physiol Bohemoslov 3, 251–3.

Druga, R., Syka, J., Rajkowska, G., 1997. rojections of auditory cortex onto the inferior colliculus in the rat. Physiol Res. 3, 215–22.

Du, J., Blanche, T.J., Harrison, R.R., Lester, H.A., Masmanidis, S.C., 2011. Multiplexed, high density electrophysiology with nanofabricated neural probes. PLoS One 6.

Egorova, M., Ehret, G., Vartanian, I., Esser, K.H., 2001. Frequency response areas of neurons in the mouse inferior colliculus. I. Threshold and tuning characteristics. Exp. Brain Res. 140, 145–161.

Egorova, M., Vartanyan, I., Ehret, G., 2006. Frequency response areas of mouse inferior colliculus neurons: II. Critical bands. Neuroreport 17, 1783–1786.

Egorova, M.A., Akimov, A.G., Khorunzhii, G.D., Ehret, G., 2020. Frequency response areas of neurons in the mouse inferior colliculus. III. Time-domain responses: Constancy, dynamics, and precision in relation to spectral resolution, and perception in the time domain. PLoS One 15, 1–30.

Ehret, G., Fischer, R., 1991. Neuronal activity and tonotopy in the auditory system visualized by c-fos gene expression. Brain Res. 567, 350–354.

Etlin, A., Bráz, J.M., Kuhn, J.A., Wang, X., Hamel, K.A., Llewellyn-Smith, I.J., Basbaum, A.I., 2016. Functional Synaptic Integration of Forebrain GABAergic Precursors into the Adult Spinal Cord. J. Neurosci. 36, 11634–11645.

Faye-Lund, H., 1985. The neocortical projection to the inferior colliculus in the albino rat. Anat Embryol 1, 53–70.

Feliciano, M., Potashner, S.J., 1995. Evidence for a Glutamatergic Pathway from the Guinea Pig Auditory Cortex to the Inferior Colliculus. J. Neurochem. 65, 1348–1357.

Foster, N.L., Mellott, J.G., Schofield, B.R., 2014. Perineuronal nets and GABAergic cells in the inferior colliculus of guinea pigs. Front. Neuroanat. 7, 1–11.

Fournier, P., Hébert, S., 2013. Gap detection deficits in humans with tinnitus as assessed with the acoustic startle paradigm: Does tinnitus fill in the gap? Hear. Res. 295, 16–23.

Friauf, E., 1992. Tonotopic Order in the Adult and Developing Auditory System of the Rat as Shown by c-fos Immunocytochemistry. Eur. J. Neurosci. 4, 798–812.

Frisina, R.D., Walton, J.P., Lynch-Armour, M.A., Byrd, J.D., 1998. Inputs to a physiologically characterized region of the inferior colliculus of the young adult CBA mouse. Hear. Res. 115, 61–81.

Fujino, K., Koyano, K., Ohmori, H., 1997. Lateral and medial olivocochlear neurons have distinct electrophysiological properties in the rat brain slice. J. Neurophysiol. 77, 2788–2804.

Fuzessery, Z.M., Hall, J.C., 1996. Role of GABA in shaping frequency tuning and creating FM sweep selectivity in the inferior colliculus. J. Neurophysiol. 76, 1059–1073.

Galazyuk, A. V., Voytenko, S. V., Longenecker, R.J., 2017. Long-Lasting forward Suppression of Spontaneous Firing in Auditory Neurons: Implication to the Residual Inhibition of Tinnitus. JARO - J. Assoc. Res. Otolaryngol. 18, 343–353.

Goldberg, J.M., Brown, P.B., 1969. Response of Binaural Neurons of Dog Superior Olivary Complex to Dichotic Tonal Stimuli: Some Physiological Mechanisms of Sound Localization. J. Physiol. 32, 613–636.

Goldberg, J.M., Brownell, W.E., 1973. Discharge charateristics of neurons in anteroventral and dorsal cochlear nuclei of cat. Brain Res. 64, 35–54.

Goutman, J.D., Elgoyhen, A.B., Gómez-casati, M.E., 2015. Cochlear hair cells : The sound-sensing machines 589, 3354–3361.

Grant, K.W., Kubli, L.R., Phatak, S.A., Galloza, H., Brungart, D.S., 2021. Estimated prevalence of functional hearing difficulties in blast-exposed service members with normal to near-normal-hearing thresholds. Ear Hear. 1615–1626.

Groff, J.A., Liberman, M.C., 2003. Modulation of Cochlear Afferent Response by the Lateral Olivocochlear System: Activation Via Electrical Stimulation of the Inferior Colliculus. J. Neurophysiol. 90, 3178–3200.

Gröschel, M., Ryll, J., Götze, R., Ernst, A., Basta, D., 2014. Acute and long-term effects of noise exposure on the neuronal spontaneous activity in cochlear nucleus and inferior colliculus

brain slices. Biomed Res. Int. 2014.

Gu, J.W., Halpin, C.F., Nam, E.C., Levine, R.A., Melcher, J.R., 2010. Tinnitus, diminished sound-level tolerance, and elevated auditory activity in humans with clinically normal hearing sensitivity. J. Neurophysiol. 104, 3361–3370.

Guinan, J.J., 2006. Olivocochlear efferents: Anatomy, physiology, function, and the measurement of efferent effects in humans. Ear Hear. 27, 589–607.

Guo, W., Chambers, A.R., Darrow, K.N., Hancock, K.E., Shinn-Cunningham, B.G., Polley, D.B., 2012. Robustness of cortical topography across fields, laminae, anesthetic states, and neurophysiological signal types. J. Neurosci. 32, 9159–9172.

Hammad, M., Schmidt, S.L., Zhang, X., Bray, R., Frohlich, F., Ghashghaei, H.T., 2015. Transplantation of GABAergic Interneurons into the neonatal primary visual cortex reduces absence seizures in stargazer mice. Cereb. Cortex 25, 2970–2979.

Hastie, T., Tibshirani, R., Freidman, J., 2009. The Elements of Statistical Learning: Data mining, inference, and prediction, 2nd ed, Springer Series in Statistics. Springer, New York.

Hattori, T., Suga, N., 1997. The inferior colliculus of the mustached bat has the frequency-vs-latency coordinates. J. Comp. Physiol. - A Sensory, Neural, Behav. Physiol. 180, 271–284.

Hayes, S.H., Radziwon, K.E., Stolzberg, D.J., Salvi, R.J., 2014. Behavioral models of tinnitus and hyperacusis in animals. Front. Neurol. 5, 1–15.

Henry, K.R., Haythorn, M.M., 1978. Effects of age and stimulus intensity of the far field auditory brain stem potentials in the laboratory mouse. Dev. Psychobiol. 11, 161–168.

Hickox, A.E., Liberman, M.C., 2014. Is noise-induced cochlear neuropathy key to the generation of hyperacusis or tinnitus? J. Neurophysiol. 111, 552–564.

Hurley, L.M., Thompson, A.M., 2001. Serotonergic innervation of the auditory brainstem of the Mexican free-tailed bat, Tadarida brasiliensis. J. Comp. Neurol. 435, 78–88.

Ito, T., Bishop, D.C., Oliver, D.L., 2009. Two classes of GABAergic neurons in the inferior colliculus. J. Neurosci. 29, 13860–13869.

Ito, T., Oliver, D.L., 2014. Local and commissural IC neurons make axosomatic inputs on large GABAergic tectothalamic neurons. J. Comp. Neurol. 522, 3539–3554.

Ito, T., Ono, M., Oliver, D.L., 2018. Neuron Types, Intrinsic Circuits, and Plasticity in the Inferior Colliculus. Oxford Handb. Audit. Brainstem 1–29.

Janz, P., Illing, R.B., 2014. A role for microglial cells in reshaping neuronal circuitry of the adult

rat auditory brainstem after its sensory deafferentation. J. Neurosci. Res. 92, 432–445.

Jenkins, W.M., Masterton, R.B., 1982. Sound localization: Effects of unilateral lesions in central auditory system. J. Neurophysiol. 47, 987–1016.

Jensen, J.B., Lysaght, A.C., Liberman, M.C., Qvortrup, K., Stankovic, K.M., 2015. Immediate and delayed cochlear neuropathy after noise exposure in pubescent mice. PLoS One 10, 1–17.

Jewett, D.L., Romano, M.N., 1972. Neonatal development of auditory system potentials averaged from the scalp of rat and cat. Brain Res. 36, 101–115.

Jewett, D.L., Williston, J.S., 1971. Auditory-evoked far fields averaged from the scalp of humans. Brain 94, 681–696.

Joris, P.X., Schreiner, C.E., Rees, A., 2004. Neural Processing of Amplitude-Modulated Sounds. Physiol Rev 84, 541–577.

Jun, J., Mitelut, C., Lai, C., Gratiy, S.L., Anastassiou, C.A., Harris, T.D., 2017. Real-time spike sorting platform for high-density extracellular probes with ground-truth validation and drift correction. bioRxiv 1–29.

Kane, E.S., Conlee, J.W., 1979. Descending inputs to the caudal cochlear nucleus of the cat: Degeneration and autoradiographic studies. J. Comp. Neurol. 187, 759–783.

Karetko, M., Skangiel-Kramska, J., 2009. Diverse functions of perineuronal nets. Acta Neurobiol Exp 69, 564–577.

Katzenell, U., Segal, S., 2001. Hyperacusis: Review and clinical guidelines. Otol. Neurotol. 22, 321–326.

Klein-Hennig, M., Dietz, M., Hohmann, V., Ewert, S.D., 2011. The influence of different segments of the ongoing envelope on sensitivity to interaural time delays. J. Acoust. Soc. Am. 129, 3856–3872.

Klug, A., Bauer, E.E., Hanson, J.T., Hurley, L., Meitzen, J., Pollak, G.D., 2002. Response selectivity for species-specific calls in the inferior colliculus of Mexican free-tailed bats is generated by inhibition. J. Neurophysiol. 88, 1941–1954.

Knipper, M., Van Dijk, P., Nunes, I., Rüttiger, L., Zimmermann, U., 2013. Advances in the neurobiology of hearing disorders: Recent developments regarding the basis of tinnitus and hyperacusis. Prog. Neurobiol. 111, 17–33.

Knudson, I.M., Shera, C.A., Melcher, J.R., 2014. Increased contralateral suppression of otoacoustic emissions indicates a hyperresponsive medial olivocochlear system in humans

with tinnitus and hyperacusis. J. Neurophysiol. 112, 3197–3208.

Koch, M., Schnitzler, H.-U., 1997. The acoustic startle response in rats—circuits mediating evocation, inhibition and potentiation. Behav. Brain Res. 89, 35–49.

König, O., Schaette, R., Kempter, R., Gross, M., 2006. Course of hearing loss and occurrence of tinnitus. Hear. Res. 221, 59–64.

Krishna, B.S., Semple, M.N., 2000. Auditory Temporal Processing: Responses to Sinusoidally Amplitude-Modulated Tones in the Inferior Colliculus. J. Neurophysiol. 84, 255–273.

Kujawa, S.G., Liberman, M.C., 2009. Adding Insult to Injury : Cochlear Nerve Degeneration after " Temporary " Noise-Induced Hearing Loss 29, 14077–14085.

Kulesza, R.J., Viñuela, A., Saldaña, E., Berrebi, A.S., 2002. Unbiased stereological estimates of neuron number in subcortical auditory nuclei of the rat. Hear. Res. 168, 12–24.

Langner, G., Schreiner, C.E., 1988. Periodicity coding in the inferior colliculus of the cat. I. Neuronal Mechanisms. J. Neurophysiol. 60, 1799–1821.

Lavdas, a a, Grigoriou, M., Pachnis, V., Parnavelas, J.G., 1999. The medial ganglionic eminence gives rise to a population of early neurons in the developing cerebral cortex. J. Neurosci. 19, 7881–7888.

Le Beau, F.E.N., Rees, A., Malmierca, M.S., 1996. Contribution of GABA- and glycine-mediated inhibition to the monaural temporal response properties of neurons in the inferior colliculus. J. Neurophysiol. 75, 902–919.

LeBeau, F.E.N., Malmierca, M.S., Rees, A., 2001. Iontophoresis in vivo demonstrates a key role for GABAA and glycinergic inhibition in shaping frequency response areas in the inferior colliculus of guinea pig. J. Neurosci. 21, 7303–7312.

Lee, J., Lin, J., Rabang, C., Wu, G.K., 2019. Differential Inhibitory Configurations Segregate Frequency Selectivity in the Mouse Inferior Colliculus. J. Neurosci. 39, 6905–6921.

Lesicko, A.M.H., Hristova, T.S., Maigler, K.C., Llano, D.A., 2016. Connectional modularity of top-down and bottom-up multimodal inputs to the lateral cortex of the mouse inferior colliculus. J. Neurosci. 36, 11037–11050.

Li, H., Mizuno, N., 1997. Single neurons in the spinal trigeminal and dorsal column nuclei project to both the cochlear nucleus and the inferior colliculus by way of axon collaterals: A fluorescent retrograde double-labeling study in the rat. Neurosci. Res. 29, 135–142.

Li, K., Chan, C.H.K., Rajendran, V.G., Meng, Q., Rosskothen-Kuhl, N., Schnupp, J.W.H., 2019.

Microsecond sensitivity to envelope interaural time differences in rats. J. Acoust. Soc. Am. 145, EL341–EL347.

Li, L., Korngut, L.M., Frost, B.J., Beninger, R.J., 1998. Prepulse inhibition following lesions of the inferior colliculus: Prepulse intensity functions. Physiol. Behav. 65, 133–139.

Li, Y., Evans, M.S., Faingold, C.L., 1998. In vitro electrophysiology of neurons in subnuclei of rat inferior colliculus. Hear. Res. 121, 1–10.

Liang, L., Lu, T., Wang, X., 2002. Neural representations of sinusoidal amplitude and frequency modulations in the primary auditory cortex of awake primates. J. Neurophysiol. 87, 2237–61.

Liberman, M.C., Dodds, L.W., 1984. Single-neuron labeling and chronic cochlear pathology. III. Stereocilia damage and alterations of threshold tuning curves. Hear. Res. 16, 55–74.

Lim, D.J., 1976. Ultrastructural cochlear changes following acoustic hyperstimulation and ototoxicity. Ann. Otol. Rhinol. Laryngol. 85, 740–751.

Lin, H.W., Furman, A.C., Kujawa, S.G., Liberman, M.C., 2011. Primary neural degeneration in the guinea pig cochlea after reversible noise-induced threshold shift. JARO - J. Assoc. Res. Otolaryngol. 12, 605–616.

Liu, Y., Alkharabsheh, A., Sun, W., 2020. Hyperexcitability of the nucleus accumbens is involved in noise-induced hyperacusis. Neural Plast. 2020.

Llewellyn-Smith, I.J., Basbaum, A.I., Braz, J., 2016. Long-term, dynamic synaptic reorganization after GABAergic precursos cell transplantation into adult mouse spinal cord. Physiol. Behav. 176, 139–148.

Loftus, W.C., Bishop, D.C., Oliver, D.L., 2010. Differential patterns of inputs create functional zones in central nucleus of inferior colliculus. J. Neurosci. 30, 13396–13408.

Loftus, W.C., Bishop, D.C., Saint Marie, R.L., Oliver, D.L., 2004. Organization of Binaural Excitatory and Inhibitory Inputs to the Inferior Colliculus from the Superior Olive. J. Comp. Neurol. 472, 330–344.

Loftus, W.C., Malmierca, M.S., Bishop, Deborah, C., Oliver, D.L., 2008. The cytoarchitecture of the inferior colliculus revisited: A common organization of the lateral cortex in rat and cat. Neuroscience 154, 196–205.

Longenecker, R.J., Galazyuk, A. V, 2016. Variable Effects of Acoustic Trauma on Behavioral and Neural Correlates of Tinnitus In Individual Animals 10, 1–14.

Ma, W.L.D., Hidaka, H., May, B.J., 2006. Spontaneous activity in the inferior colliculus of CBA/J

mice after manipulations that induce tinnitus. Hear. Res. 212, 9–21.

Madisen, L., Mao, T., Koch, H., Zhuo, J.M., Berenyi, A., Fujisawa, S., Hsu, Y.W.A., Garcia, A.J., Gu, X., Zanella, S., Kidney, J., Gu, H., Mao, Y., Hooks, B.M., Boyden, E.S., Buzsáki, G., Ramirez, J.M., Jones, A.R., Svoboda, K., Han, X., Turner, E.E., Zeng, H., 2012. A toolbox of Cre-dependent optogenetic transgenic mice for light-induced activation and silencing. Nat. Neurosci. 15, 793–802.

Maffi, C.L., Aitkin, L.M., 1987. Differential neural projections to regions of the inferior colliculus of the cat responsive to high frequency sounds. Hear. Res. 26, 211–219.

Malmierca, M.S., Blackstad, T.W., Osen, K.K., Karagülle, T., Molowny, R.L., 1993. The central nucleus of the inferior colliculus in rat: A Golgi and computer reconstruction study of neuronal and laminar structure. J. Comp. Neurol. 333, 1–27.

Malmierca, M.S., Hernández, O., Falconi, A., Lopez-Poveda, E.A., Merchán, M., Rees, A., 2003. The commissure of the inferior colliculus shapes frequency response areas in rat: An in vivo study using reversible blockade with microinjection of kynurenic acid. Exp. Brain Res. 153, 522–529.

Malmierca, M.S., Rees, A., Le Beau, F.E.N., Bjaalie, J.G., 1995. Laminar organization of frequency-defined local axons within and between the inferior colliculi of the guinea pig. J. Comp. Neurol. 357, 124–144.

Manohar, S., Spoth, J., Radziwon, K., Auerbach, B.D., Salvi, R., 2017. Noise-induced hearing loss induces loudness intolerance in a rat Active Sound Avoidance Paradigm (ASAP). Hear. Res. 353, 197–203.

Manzoor, N.F., Gao, Y., Licari, F., Kaltenbach, J.A., 2013. Comparison and contrast of noise-induced hyperactivity in the dorsal cochlear nucleus and inferior colliculus. Hear. Res. 295, 114–123.

Martínez-Cerdeño, V., Noctor, S.C., Espinosa, A., Ariza, J., Parker, P., Orasji, S., Daadi, M.M., Bankiewicz, K., Alvarez-Buylla, A., Kriegstein, A.R., 2010. Embryonic MGE Precursor Cells Grafted into Adult Rat Striatum Integrate and Ameliorate Motor Symptoms in 6-OHDA-Lesioned Rats. Cell Stem Cell 6, 238–250.

McFadden, D., Pasanen, E.G., 1976. Lateralization at high frequencies based on interaural time differences. J. Acoust. Soc. Am. 59, 634–639.

Meininger, V., Pol, D., Derer, P., 1986. The inferior colliculus of the mouse. A Nissl and Golgi

study. Neuroscience 17, 1159–1171.

Merchán, M., Aguilar, L.A., Lopez-Poveda, E.A., Malmierca, M.S., 2005. The inferior colliculus of the rat: Quantitative immunocytochemical study of GABA and glycine. Neuroscience 136, 907–925.

Middleton, J.W., Kiritani, T., Pedersen, C., Turner, J.G., Shepherd, G.M.G., Tzounopoulos, T., 2011. Mice with behavioral evidence of tinnitus exhibit dorsal cochlear nucleus hyperactivity because of decreased GABAergic inhibition. Proc. Natl. Acad. Sci. 108, 7601–7606.

Milbrandt, J.C., Holder, T.M., Wilson, M.C., Salvi, R.J., Caspary, D.M., 2000. GAD levels and muscimol binding in rat inferior colliculus following acoustic trauma. Hear. Res. 147, 251–260.

Miller, K.E., Casseday, J.H., Covey, E., 2005. Relation between intrinsic connections and isofrequency contours in the inferior colliculus of the big brown bat, Eptesicus fuscus. Neuroscience 136, 895–905.

Monaghan, J.J.M., Garcia-Lazaro, J.A., McAlpine, D., Schaette, R., 2020. Hidden Hearing Loss Impacts the Neural Representation of Speech in Background Noise. Curr. Biol. 30, 4710-4721.e4.

Montes-Lourido, P., Kar, M., David, S. V, Sadagopan, S., 2021. Neuronal selectivity to complex vocalization features emerges in the superficial layers of primary auditory cortex. PLoS Biol. 19, 1–30.

Moore, D.R., Kotak, V.C., Sanes, D.H., 1998. Commissural and lemniscal synaptic input to the gerbil inferior colliculus. J. Neurophysiol. 80, 2229–2236.

Morawski, M., Brückner, G., Arendt, T., Matthews, R.T., 2012. Aggrecan: Beyond cartilage and into the brain. Int. J. Biochem. Cell Biol. 44, 690–693.

Morest, D.K., Oliver, D.L., 1984. The neuronal architecture of the inferior colliculus in the cat: defining the functional anatomy of the auditory midbrain. J Comp Neurol. 222, 209–36.

Mossop, J.E., Wilson, M.J., Caspary, D.M., Moore, D.R., 2000. Down-regulation of inhibition following unilateral deafening. Hear. Res. 147, 183–187.

Mulders, W.H.A.M., Robertson, D., 2013. Development of hyperactivity after acoustic trauma in the guinea pig inferior colliculus. Hear. Res. 298, 104–108.

Mulders, W.H.A.M., Robertson, D., 2011. Progressive centralization of midbrain hyperactivity after acoustic trauma. Neuroscience 192, 753–760.

Mulders, W.H.A.M., Robertson, D., 2009. Hyperactivity in the auditory midbrain after acoustic trauma: dependence on cochlear activity. Neuroscience 164, 733–746.

Mulders, W.H.A.M., Robertson, D., 2000. Effects on cochlear responses of activation of descending pathways from the inferior colliculus. Hear. Res. 149, 11–23.

Nelson, P.G., Erulkar, S.D., 1963. Synaptic mechanisms of excitation and inhibition in the central auditory pathway. J. Neurophysiol. 26, 908–923.

Niu, Y., Kumaraguru, A., Wang, R., Sun, W., 2013. Hyperexcitability of inferior colliculus neurons caused by acute noise exposure. J. Neurosci. Res. 91, 292–299.

Nuetzel, J.M., Hafter, E.R., 1976. Lateralization of complex waveforms: Effects of fine structure, amplitude, and duration. J. Acoust. Soc. Am. 60, 1339–1346.

Ohlrogge, M., Doucet, J.R., Ryugo, D.K., 2001. Projections of the lateral reticular nucleus to the cochlear nucleus in rats. J. Comp. Neurol. 436, 290–303.

Oliver, D.L., 2005. Neuronal Organization in the Inferior Colliculus, in: Winer, J.A., Schreiner, C.E. (Eds.), The Inferior Colliculus. Springer Science+Business Media, Inc., New York, pp. 69–114.

Oliver, D.L., 1987. Projections to the inferior colliculus from the anteroventral cochlear nucleus in the cat: Possible substrates for binaural interaction. J. Comp. Neurol. 264, 24–46.

Oliver, D.L., Beckius, G.E., Bishop, D.C., Kuwada, S., 1997. Simultaneous anterograde labeling of axonal layers from lateral superior olive and dorsal cochlear nucleus in the inferior colliculus of cat. J. Comp. Neurol. 382, 215–229.

Oliver, D.L., Beckius, G.E., Shneiderman, A., 1995. Axonal projections from the lateral and medial superior olive to the inferior colliculus of the cat: A study using electron microscopic autoradiography. J. Comp. Neurol. 360, 17–32.

Oliver, D.L., Kuwada, S., Yin, T.C.T., Haberly, L.B., Henkel, C.K., 1991. Dendritic and axonal morphology of HRP-injected neurons in the inferior colliculus of the cat. J. Comp. Neurol. 303, 75–100.

Oliver, D.L., Morest, D.K., 1984. The central nucleus of the inferior colliculus in the cat. J. Comp. Neurol. 222, 237–264.

Oliver, D.L., Ostapoff, E.M., Beckius, G.E., 1999. Direct innervation of identified tectothalamic neurons in the inferior colliculus by axons from the cochlear nucleus. Neuroscience 93, 643–658.

Oliver, D.L., Winer, J.A., Beckius, G.E., Marie, R.L.S., 1994. Morphology of GABAergic neurons in the inferior colliculus of the cat. J. Comp. Neurol. 340, 27–42.

Ono, M., Bishop, D.C., Oliver, D.L., 2020. Neuronal sensitivity to the interaural time difference of the sound envelope in the mouse inferior colliculus. Hear. Res. 385, 107844.

Ono, M., Oliver, D.L., 2014. Asymmetric temporal interactions of sound-evoked excitatory and inhibitory inputs in the mouse auditory midbrain. J. Physiol. 592, 3647–3669.

Ono, M., Yanagawa, Y., Koyano, K., 2005. GABAergic neurons in inferior colliculus of the GAD67-GFP knock-in mouse: Electrophysiological and morphological properties. Neurosci. Res. 51, 475–492.

Palmer, A.R., Berger, J.I., 2018. Changes in the Inferior Colliculus Associated with Hearing Loss: Noise-Induced Hearing Loss, Age- Related Hearing Loss, Tinnitus and Hyperacusis 1, 1–26.

Palombi, Peggy Shadduck, Caspary, D.M., 1996. Physiology of the young adult Fischer 344 rat inferior colliculus: Responses to contralateral monaural stimuli. Hear. Res. 100, 41–58.

Palombi, Peggy S., Caspary, D.M., 1996. GABA inputs control discharge rate primarily within frequency receptive fields of inferior colliculus neurons. J. Neurophysiol. 75, 2211–2219.

Parnes, S.M., 1997. Current concepts in the clinical management of patients with tinnitus. Eur. Arch. Oto-Rhino-Laryngology 254, 406–409.

Patel, M.B., Sons, S., Yudintsev, G., Lesicko, A.M.H., Yang, L., Taha, G.A., Pierce, S.M., Llano, D.A., 2017. Anatomical characterization of subcortical descending projections to the inferior colliculus in mouse. J. Comp. Neurol. 525, 885–900.

Pedemonte, M., Torterolo, P., Velluti, R.A., 1997. In vivo intracellular characteristics of inferior colliculus neurons in guinea pigs. Brain Res. 759, 24–31.

Pedregosa, F., Varoquaux, G., Gramfort, A., Michel, V., Thirion, B., Grisel, O., Blondel, M., Prettenhofer, P., Weiss, R., Dubourg, V., Vanderplas, J., Passos, A., Cournapeau, D., Brucher, M., Perrot, M., Duchesnay, E., 2011. Scikit-learn: Machine Learning in Python. J. Mach. Learn. Res. 12, 2825–2830.

Pennington, J.R., David, S. V, 2020. Complementary Effects of Adaptation and Gain Control on Sound Encoding in Primary Auditory Cortex. eNeuro 7, 1–17.

Phillips, D.P., Rappaport, J.M., Gulliver, J.M., 1994. Impaired word recognition in noise by patients with noise-induced hearing loss: Contribution of temporal resolution defect. Am. J. Otol.

Piccirillo, J.F., Finnell, J., Vlahiotis, A., Chole, R.A., Spitznagel, E., 2007. Relief of Idiopathic Subjective Tinnitus. Arch. Otolaryngol. Neck Surg. 133, 390.

Pollak, G.D., Xie, R., Gittelman, J.X., Sari, A., Li, N., 2011. The dominance of inhibition in the inferior colliculus. Hear. Res. 274, 27–39.

Portfors, C. V., Felix, R.A., 2005. Spectral integration in the inferior colliculus of the CBA/CaJ mouse. Neuroscience 136, 1159–1170.

Quass, G.L., Rogalla, M.M., Ford, A.N., Apostolides, P.F., 2022. Neural population activity in the shell inferior colliculus predicts behavioral outcomes, in: ARO 45th Annual MidWinter Meeting. San Jose, CA, pp. 224–225.

Ramachandran, R., Davis, K.A., May, B.J., 1999. Single-unit responses in the inferior colliculus of decerebrate cats: I. Classification Based on Frequency Response Maps. J. Neurophysiol. 82, 152–63.

Rasmussen, G.L., 1953. Recurrent or "feed back" connections of the auditory system of the cat. Anat. Rec.

Rees, A., Langner, G., 2005. Temporal Coding in the Auditory Midbrain, in: Winer, J.A., Schreiner, C.E. (Eds.), The Inferior Colliculus. Springer Science+Business Media, Inc., New York, pp. 346–376.

Rees, A., Orton, Ll., 2019. Unifying the midbrain: The commissure of the Inferior Colliculus, in: Kandler, K. (Ed.), The Oxford Handbook of the Auditory Brainstem. Oxford University Press, New York, pp. 549–576.

Reetz, G., Ehret, G., 1999. Inputs from three brainstem sources to identified neurons of the mouse inferior colliculus slice. Brain Res. 816, 527–543.

Resnik, J., Polley, D.B., 2017. Fast-spiking GABA circuit dynamics in the auditory cortex predict recovery of sensory processing following peripheral nerve damage. Elife 6, 1–14.

Reynolds, P., Gardner, D., Lee, R., 2004. Tinnitus and psychological morbidity: A cross-sectional study to investigate psychological morbidity in tinnitus patients and its relationship with severity of symptoms and illness perceptions. Clin. Otolaryngol. Allied Sci. 29, 628–634.

Richardson, B.D., Brozoski, T.J., Ling, L.L., Caspary, D.M., 2012. Targeting inhibitory neurotransmission in tinnitus. Brain Res. 1485, 77–87.

Riquelme, R., Saldaña, E., Osen, K.K., Ottersen, O.P., Merchán, M.A., 2001. Colocalization of GABA and glycine in the ventral nucleus of the lateral lemniscus in rat: An in situ

hybridization and semiquantitative immunocytochemical study. J. Comp. Neurol. 432, 409–424.

Roberts, L.E., Eggermont, J.J., Caspary, D.M., Shore, S.E., Melcher, J.R., Kaltenbach, J.A., 2010. Ringing Ears: The Neuroscience of Tinnitus. J. Neurosci. 30, 14972–14979.

Rocchi, F., Ramachandran, R., 2018. Neuronal adaptation to sound statistics in the inferior colliculus of behaving macaques does not reduce the effectiveness of the masking noise. J. Neurophysiol. 120, 2819–2833.

Ruebhausen, M.R., Brozoski, T.J., Bauer, C.A., 2012. A comparison of the effects of isoflurane and ketamine anesthesia on auditory brainstem response (ABR) thresholds in rats. Hear. Res. 287, 25–29.

Ryugo, D.K., Willard, F.H., Fekete, D.M., 1981. Differential afferent projections to the inferior colliculus from the cochlear nucleus in the albino mouse. Brain Res. 210, 342–349.

Sadagopan, S., Wang, X., 2008. Level invariant representation of sounds by populations of neurons in primary auditory cortex. J. Neurosci. 28, 3415–3426.

Saint Marie, R.L., 1996. Glutamatergic connections of the auditory midbrain: Selective uptake and axonal transport of D-[3H]aspartate. J. Comp. Neurol. 373, 255–270.

Saldaña, E., Feliciano, M., Mugnaini, E., 1996. Distribution of descending projections from primary auditory neocortex to inferior colliculus mimics the topography of intracollicular projections. J. Comp. Neurol. 371, 15–40.

Saldana, E., Merchan, M.A., 2005. Intrinsic and Commissural Connections of the Inferior Colliculus, in: Winer, J.A., Schreiner, C.E. (Eds.), The Inferior Colliculus. Springer Science+Business Media, Inc., New York, pp. 155–181.

Saldaña, E., Merchán, M.A., 1992. Intrinsic and commissural connections of the inferior colliculus. J. Comp. Neurol. Neurol. 319, 417–437.

Salloum, R.H., Yurosko, C., Santiago, L., Sandridge, S.A., Kaltenbach, J.A., 2014. Induction of enhanced acoustic startle response by noise exposure: Dependence on exposure conditions and testing parameters and possible relevance to hyperacusis. PLoS One 9, 1–11.

Salvi, R., Lobarinas, E., Sun, W., 2009. Pharmacological Treatments for Tinnitus: New and Old. Drugs Futur. 34, 381–400.

Salvi, R.J., Wang, J., Ding, D., 2000. Auditory plasticity and hyperactivity following cochlear damage. Hear. Res. 147, 261–274.

Schaette, R., McAlpine, D., 2011. Tinnitus with a normal audiogram: Physiological evidence for hidden hearing loss and computational model. J. Neurosci. 31, 13452–13457.

Schecklmann, M., Landgrebe, M., Langguth, B., Vielsmeier, V., Kleinjung, T., Lehner, A., Kreuzer, P., Poeppl, T.B., Figueiredo, R., Azevedo, A., Binetti, A.C., Elgoyhen, A.B., Rates, M., Coelho, C., Vanneste, S., De Ridder, D., Van De Heyning, P., Zeman, F., Koller, M., 2014. Phenotypic characteristics of hyperacusis in tinnitus. PLoS One 9.

Schofield, B.R., 2001. Origins of projections from the inferior colliculus to the cochlear nucleus in guinea pigs. J. Comp. Neurol. 429, 206–220.

Schreiner, C.E., Langner, G., 1988. Periodicity coding in the inferior colliculus of the cat. II. Topographical organization. J. Neurophysiol. 60, 1823–1840.

Sheldrake, J., Diehl, P.U., Schaette, R., 2015. Audiometric characteristics of hyperacusis patients. Front. Neurol. 6, 1–7.

Sheng, M., McFadden, G., Greenberg, M.E., 1990. Membrane depolarization and calcium induce c-fos transcription via phosphorylation of transcription factor CREB. Neuron 4, 571–582.

Shneiderman, A., Henkel, C.K., 1987. Banding of lateral superior olivary nucleus afferents in the inferior colliculus: A possible substrate for sensory integration. J. Comp. Neurol. 266, 519–534.

Shneiderman, A., Oliver, D.L., Henkel, C.K., 1988. Connections of the dorsal nucleus of the lateral lemniscus: An inhibitory parallel pathway in the ascending auditory system? J. Comp. Neurol. 276, 188–208.

Slee, S.J., Young, E.D., 2011. Information conveyed by inferior colliculus neurons about stimuli with aligned and misaligned sound localization cues. J. Neurophysiol. 106, 974–985.

Smith, P.H., 1992. Anatomy and physiology of multipolar cells in the rat inferior collicular cortex using the in vitro brain slice technique. J. Neurosci. 12, 3700–3715.

Soleymani, T., Pieton, D., Pezeshkian, P., Miller, P., Gorgulho, A.A., Pouratian, N., De Salles, A.A.F., 2011. Surgical approaches to tinnitus treatment: A review and novel approaches. Surg. Neurol. Int. 2, 154.

Southwell, Derek G, Froemke, R.C., Alvarez-Buylla, A., Stryker, M.P., Gandhi, S.P., 2010. Cortical Plasticity Induced by Inhibiory Neuron Transplantation. Science (80-.). 327, 1145–1148.

Southwell, Derek G., Froemke, R.C., Alvarez-Buylla, A., Stryker, M.P., Gandhi, S.P., 2010.

Cortical Plasticity Induced by Inhibitory Neuron Transplantation. Science (80-.). 327, 1145–1148.

Southwell, D.G., Nicholas, C.R., Basbaum, A.I., Stryker, M.P., Kriegstein, A.R., Rubenstein, J.L., Alvarez-Buylla, A., 2014. Interneurons from Embryonic Development to Cell-Based Therapy. Science (80-.). 344, 1240622–1240622.

Southwell, D.G., Paredes, M.F., Galvao, R.P., Jones, D.L., Froemke, R.C., Sebe, J.Y., Alfaro-cervello, C., Tang, Y., Jose, M., Rubenstein, J.L., Baraban, S.C., Alvarez-buylla, A., 2012. Intrinsically determined cell death of developing cortical interneurons. Nature 491, 109–113.

Stiebler, I., Ehret, G., 1985. Inferior colliculus of the house mouse. I. A quantitative study of tonotopic organization, frequency representation, and tone-threshold distribution. J. Comp. Neurol. 238, 65–76.

Sturm, J., Nguyen, T., Kandler, K., 2014. Development of Intrinsic Connectivity in the Central Nucleus of the Mouse Inferior Colliculus. J. Neurosci. 34, 15032–15046.

Sturm, J.J., Zhang-Hooks, Y.-X., Roos, H., Nguyen, T., Kandler, K., 2017. Noise Trauma-Induced Behavioral Gap Detection Deficits Correlate with Reorganization of Excitatory and Inhibitory Local Circuits in the Inferior Colliculus and Are Prevented by Acoustic Enrichment. J. Neurosci. 37, 6314–6330.

Suga, N., Gao, E., Zhang, Y., Ma, X., Olsen, J.F., 2000. The corticofugal system for hearing: Recent progress. PNAS 97, 11807–11814.

Sun, J., Zhou, Y., Xu, B., Li, J., Zhang, L., Li, D., Zhang, S., Wu, J., Gao, S., Ye, D., Mei, W., 2021. STING/NF-κB/IL-6-Mediated Inflammation in Microglia Contributes to Spared Nerve Injury (SNI)-Induced Pain Initiation. J. Neuroimmune Pharmacol.

Sun, W., Deng, A., Jayaram, A., Gibson, B., 2012. Noise exposure enhances auditory cortex responses related to hyperacusis behavior. Brain Res. 1485, 108–116.

Syka, J., Popelář, J., Kvašňák, E., Astl, J., 2000. Response properties of neurons in the central nucleus and external and dorsal cortices of the inferior colliculus in guinea pig. Exp. Brain Res. 133, 254–266.

Tan, M.L., Theeuwes, H.P., Feenstra, L., Borst, J.G.G., 2007. Membrane Properties and Firing Patterns of Inferior Colliculus Neurons: An In Vivo Patch-Clamp Study in Rodents. J. Neurophysiol. 98, 443–453.

Taranda, J., Maison, S.F., Ballestero, J.A., Katz, E., Savino, J., Vetter, D.E., Boulter, J., Liberman,

M.C., Fuchs, P.A., Elgoyhen, A.B., 2009. A point mutation in the hair cell nicotinic cholinergic receptor prolongs cochlear inhibition and enhances noise protection. PLoS Biol. 7.

Thompson, A.M., 2005. Descending Connections of the Auditory Midbrain, in: Winer, J.A., Schreiner, C.E. (Eds.), The Inferior Colliculus. Springer Science+Business Media, Inc., New York, pp. 182–199.

Thorson, I.L., Liénard, J., David, S. V, 2015. The Essential Complexity of Auditory Receptive Fields. PLoS Comput. Biol. 11, 1–33.

Turner, J.G., Brozoski, T.J., Bauer, C.A., Parrish, J.L., Myers, K., Hughes, L.F., Caspary, D.M., 2006. Gap detection deficits in rats with tinnitus: A potential novel screening tool. Behav. Neurosci. 120, 188–195.

Van der Gucht, E., Clerens, S., Cromphout, K., Vandesande, F., Arckens, L., 2002. Differential expression of c-fos in subtypes of GABAergic cells following sensory stimulation in the cat primary visual cortex. Eur. J. Neurosci. 16, 1620–1626.

Vernon, J.A., 1987. Pathophysiology of tinnitus: A special case- Hyperacusis and a proposed treatment. Am. J. Otol. 8, 201–202.

Vogler, D.P., Robertson, D., Mulders, W.H.A.M., 2014. Hyperactivity following unilateral hearing loss in characterized cells in the inferior colliculus. Neuroscience 265, 28–36.

Wallace, M.N., Shackleton, T.M., Palmer, A.R., 2012. Morphological and physiological characteristics of laminar cells in the central nucleus of the inferior colliculus. Front. Neural Circuits 6, 1–16.

Walton, J.P., Frisina, R.D., Ison, J.R., O'Neill, W.E., 1997. Neural correlates of behavioral gap detection in the inferior colliculus of the young CBA mouse. J. Comp. Physiol. - A Sensory, Neural, Behav. Physiol. 181, 161–176.

Walton, J.P., Frisina, R.D., O'Neill, W.E., 1998. Age-related alteration in processing of temporal sound features in the auditory midbrain of the CBA mouse. J. Neurosci. 18, 2764–2776.

Wang, H., Brozoski, T.J., Turner, J.G., Ling, L., Parrish, J.L., Hughes, L.F., Caspary, D.M., 2009. Plasticity at glycinergic synapses in dorsal cochlear nucleus of rats with behavioral evidence of tinnitus. Neuroscience 164, 747–759.

Wang, J., Salvi, R.J., Powers, N., 1996. Plasticity of response properties of inferior colliculus neurons following acute cochlear damage. J. Neurophysiol. 75, 171–183.

Wang, X., Zhang, Y., Bai, S., Qi, R., Sun, H., Li, R., Zhu, L., Cao, X., Jia, G., Li, X., Gao, L., 2022. Corticofugal Modulation of Temporal and Rate Representations in the Inferior Colliculus of the Awake Marmoset. Cereb. Cortex 1–18.

Warr, B.W., 1972. Fiber degeneration following lesions in the multipolar and globular cell areas in the ventral cochlear nucleus of the cat. Brain Res. 40, 247–270.

Warr, W.B., 1980. Efferent components of the auditory system. Ann Otol Rhinol Laryngol Suppl 5, 114–20.

Weidt, S., Delsignore, A., Meyer, M., Rufer, M., Peter, N., Drabe, N., Kleinjung, T., 2016. Which tinnitus-related characteristics affect current health-related quality of life and depression? A cross-sectional cohort study. Psychiatry Res. 237, 114–121.

Weisenburger, S., Tejera, F., Demas, J., Zeng, H., Daigle, T., Zeng, H., Losonczy, A., Vaziri, A., 2019. Volumetric Ca 2 + Imaging in the Mouse Brain Using Hybrid Multiplexed Sculpted Light Microscopy 1050–1066.

Weisz, N., Hartmann, T., Dohrmann, K., Schlee, W., Norena, A., 2006. High-frequency tinnitus without hearing loss does not mean absence of deafferentation. Hear. Res. 222, 108–114.

Wenstrup, J.J., Ross, L.S., Pollak, G.D., 1986. Binaural response organization within a frequency-band representation of the inferior colliculus: Implications for sound localization. J. Neurosci. 6, 962–973.

Wichterle, H., Garcia-Verdugo, J.M., Herrera, D.G., Alvarez-Buylla, A., 1999. Young neurons from medial ganglionic eminence disperse in adult and embryonic brain. Nat. Neurosci. 2, 461–466.

Williamson, R.S., Polley, D.B., 2019. Parallel pathways for sound processing and functional connectivity among layer 5 and 6 auditory corticofugal neurons. Elife 8, 1–21.

Willott, J.F., 2005. Hearing loss and the inferior colliculus, in: Winer, J.A., Schreiner, C.E. (Eds.), The Inferior Colliculus. Springer Science+Business Media, Inc., New York, pp. 585–602.

Willott, J.F., Turner, J.G., 2000. Neural plasticity in the mouse inferior colliculus: Relationship to hearing loss, augmented acoustic stimulation, and prepulse inhibition. Hear. Res. 147, 275–281.

Winer, J.A., 2006. Decoding the auditory corticofugal systems. Hear. Res. 212, 1–8.

Winer, J.A., 2005. Three Systems of Descending Projections to the Inferior Colliculus, in: Winer, J.A., Schreiner, C.E. (Eds.), The Inferior Colliculus. Springer Science+Business Media, Inc.,

New York, pp. 231–247.

Winer, J.A., Chernock, M.L., Larue, D.T., Cheung, S.W., 2002. Descending projections to the inferior colliculus from the posterior thalamus and the auditory cortex in rat, cat, and monkey. Hear. Res. 168, 181–195.

Wise, S.P., Jones, E.G., 1977. Cells of origin and terminal distribution of descending projections of the rat somatic sensory cortex. J. Comp. Neurol. 175, 129–157.

Wong, A.B., Borst, J.G.G., 2019. Tonotopic and non-auditory organization of the mouse dorsal inferior colliculus revealed by two-photon imaging. Elife 1–31.

Wright, D.D., Ryugo, D.K., 1996. Mossy fiber projections from the cuneate nucleus to the cochlear nucleus in the rat. J. Comp. Neurol. 365, 159–172.

Xie, R., Meitzen, J., Pollak, G.D., 2005. Differing roles of inhibition in hierarchical processing of species-specific calls in auditory brainstem nuclei. J. Neurophysiol. 94, 4019–4037.

Yang, L., Pollak, G.D., Resler, C., 1992. GABAergic circuits sharpen tuning curves and modify response properties in the mustache bat inferior colliculus. J. Neurophysiol. 68, 1760–1774.

Yang, S., Weiner, B.D., Zhang, L.S., Cho, S.-J., Bao, S., 2011. Homeostatic plasticity drives tinnitus perception in an animal model. Proc. Natl. Acad. Sci. 108, 14974–14979.

Yang, W.Z., Liu, T.T., Cao, J.W., Chen, X.F., Liu, X., Wang, M., Su, X., Zhang, S.Q., Qiu, B.L., Hu, W.X., Liu, L.Y., Ma, L., Yu, Y.C., 2016. Fear Erasure Facilitated by Immature Inhibitory Neuron Transplantation. Neuron 92, 1352–1367.

Yeomans, J.S., Li, L., Scott, B.W., Frankland, P.W., 2002. Tactile, acoustic and vestibular systems sum to elicit the startle reflex. Neurosci. Biobehav. Rev. 26, 1–11.

Zacharek, M.A., Kaltenbach, J.A., Mathog, T.A., Zhang, J., 2002. Effects of cochlear ablation on noise induced hyperactivity in the hamster dorsal cochlear nucleus: Implications for the origin of noise induced tinnitus. Hear. Res. 172, 137–144.

Zhang, J.S., Kaltenbach, J.A., Wang, J., Kim, S.A., 2003. Fos-like immunoreactivity in auditory and nonauditory brain structures of hamsters previously exposed to intense sound. Exp. Brain Res. 153, 655–660.

Zhang, Y., Suga, N., 1997. Corticofugal amplification of subcortical responses to single tone stimuli in the mustached bat. J. Neurophysiol. 78, 3489–3492.

Zwislocki, J.J., Nguyen, M., 1999. Place code for pitch: A necessary revision. Acta Otolaryngol. 119, 140–5.